Faculty of Engineering and Information Technology

Design and Verification of Novel Powertrain Management for Multi-Geared Battery Electric Vehicles

A thesis submitted for degree of

Doctor of Philosophy

Jiageng RUAN

September 2016

CERTIFICATE OF ORIGINAL AUTHORSHIP

I certify that the work in this thesis has not previously been submitted for a degree nor has it been submitted as part of requirements for a degree except as fully acknowledged within the text.

I also certify that the thesis has been written by me. Any help that I have received in my research work and the preparation of the thesis itself has been acknowledged. In addition, I certify that all information sources and literature used are indicated in the thesis.

Signature of Student:

Date: 30 September 2016

ACKNOWLEDGEMENT

I'd like to take this opportunity to thank the following people and organizations for their assistance and support during my candidature.

My supervisor Professor Nong Zhang, his knowledge and guidance has been invaluable, and together with co-supervisors Professor Peter A. Watterson and Dr. Paul D. Walker have guided me through this research and supported my work.

My UTS colleagues, whose knowledge, advice, and experience have encouraged me to do better and better, Holger Roser, Luo Zhen, Zhu Bo, Zhou Xingxing, Jack Liang, Wu Jinglai, Zhu Sangzhi, Zhang Tianxiao, Fang Yuhong are along with me.

Most importantly my wife, Wang Jingyan, who is always by my side and help me through thick and thin, I couldn't have done this without you; and daughter, Xiran, my pride and joy. Of course, my parents' advice and encouragement are indispensable.

TABLE OF CONTENTS

LIST OF FIGURES

LIST OF TABLES

GLOSSARY OF TERMS AND NOTATIONS

ABBREVIATIONS USED IN THESIS

EV   -   Electric Vehicle

BEV - Battery Electric Vehicle

HEV - Hybrid Electric Vehicle

ICE   - Internal Combustion Engine

DCT - Dual Clutch Transmission

AT   - Automatic Transmission

AMT - Automated Manual Transmission

CVT - Continuously Variable Transmission

PM   - Permanent Magnet Motor

IM   - Induction Motor

SRM - Switched Reluctance Motor

DC   - Direct Current

VCU - Vehicle Control Unit

ABS - Anti-Lock Brake System

EBD - Electro Control Brake Distribution

BAS - Brake Assistance System

RBS - Regenerative Brake System

SOC - State of Charge

RSP - Relative selling price

ECE - United Nations Economic Commission for Europe (UNECE) urban driving cycle

NEDC - New European driving cycle

UDDS - Urban dynamometer driving schedule

LA-92 - Los Angeles 92 / Unified cycle driving schedule

HWFET- Highway fuel economic test

JP1015 - Japan 1015 emission test cycles model

KPK - Driving kilometres per kilowatt hour

MPC - Mileage per cycle

CPK - Consumed energy per km

RPK - Braking energy recovered per km

CHAPTER 4 NOTATIONS

m   - Vehicle mass

Rw   - Wheel radius

i_g   - Gear ratio

CR   - Coefficient of rolling resistance

g   - Gravity

φ - Road incline

Cd   - Drag coefficient

A   - Vehicle frontal area

u   - Vehicle speed

V_{bat} - Battery voltage

C_{bat} - Battery capacity

E_{bat} - Battery energy content

i_m - Main reduction ratio

i_{cvt} - CVT ratio varying range

$i_{converter}$	-	Torque converter ratio
η_{cvt}	-	CVT pulley-belt efficiency
$\eta_{converter}$	-	Torque converter efficiency
P_{loss}	-	Power losses in gearbox
$\sum P_{gear\_mesh}$	-	Power losses in all gear meshing
P_{con}	-	Power losses in concentric shaft
$P_{churning}$	-	Power losses in churning and windage
$\sum P_{Bearing}$	-	Drag torque in bearings
$P_{disengage\_gear}$	-	Power losses in disengaged gear set
T_{in}	-	Gearbox input torque
T_{con}	-	Torque lost in concentric shaft viscous shear resistance
$T_{bearing}$	-	Frag torque generated by bearings
i	-	Gear ratios of 1st, 2nd and final gear
$T_{1\_output\_outer}$	-	Output torque of the outer concentric shaft
$T_{gearmesh}$	-	Torque losses in gear pair meshing
$T_{disengage}$	-	Torque consumed in unengaged wet clutch pairs
$T_{churning}$	-	Drag torque generated by churning
P_m	-	Power losses in gear meshing
f_m	-	Friction coefficient
v^j	-	Temperature based kinematic viscosity of lubricant in transmission
V^h	-	Tangential velocity of pitch line
K^g	-	K-factor
T_1	-	pinion torque
n_1	-	Pinion rotational speed

β_w	-	Operating helix angle
r_{w1}	-	Outside pinion radius
α_ω	-	Transverse operating pressure angle
H_s	-	Sliding ratios at the beginning of approach action
H_t	-	Sliding ratios at the end of recess action
r	-	Ratio of currently meshed gear pair
$r_{o1/o2}$	-	Pinion outside radius
$r_{w1/w2}$	-	Pinion operating pitch radius
$z_{1/2}$	-	Gear teeth and pinion teeth.
R_f	-	Roughness factor
M_t	-	Transverse tooth module
f_g	-	Gear dip factor
D	-	Outside diameter of gear
F	-	Face width
L	-	Length of the gear in mm
β	-	Generated helix angle
R_{con_o}	-	Inner radius of the outer shaft
R_{con_i}	-	Outer radius of the inner shaft
$\Delta \omega$	-	Relative speed between two concentric shafts
$R_{i/o}$	-	Inner and outer oil firm radius;
μ	-	Viscosity of the lubricant oil
h_c	-	Clearance of clutch plate;
$v_n \uparrow$	-	Upshift speed threshold
$v_{n+1} \downarrow$	-	Downshift speed threshold.

CHAPTER 5 NOTATIONS

a_0 - Rolling coefficient in dynamometer

a_1 - Grading coefficient in dynamometer

a_2 - Acceleration coefficient in dynamometer

n - Dynamometer input speed

I - Coefficient of rotation parts translational equivalent inertia

G_f - Rolling resistance

G_i - Grading resistance

CHAPTER 6 NOTATIONS

$C_{capacity\_SR}$ - Required battery capacity for 158km range in single reduction powertrain

$C_{capacity\_DCT}$ - Required battery capacity for 158km range in single DCT powertrain

$C_{capacity\_CVT}$ - Required battery capacity for 158km range in single CVT powertrain

$E_{SR\_lifetime}$ - Lifetime electricity consumption for single reduction based BEV

$E_{DCT\_lifetime}$ - Lifetime electricity consumption for two-speed DCT based BEV

$E_{CVT\_lifetime}$ - Lifetime electricity consumption for simplified CVT based BEV

CHAPTER 7 NOTATIONS

$Brake_{\max\_1}$ - Maximum braking force on wheel when vehicle in 1st gear

$Brake_{\max\_2}$ - Maximum braking force on wheel when vehicle in 2nd gear

F_{bf} - Braking force on front axle

F_{br} - Braking force on rear axle

f_{regen} -   Regenerative braking force

$f_{caliper}$ -   Friction braking force

λ -   Wheel slip ratio

$Regen_{min}$ -   Minimum available motor braking force at full brake pedal

$Friction_{max}$ -   Maximum available friction braking force at full brake pedal

CHAPTER 8 NOTATIONS

Q_{re} -   Energy recovery rate

ABSTRACT

Despite the long-term benefit of battery electric vehicles (BEVs) to customers and the environment, the initial cost and limited driving range present the significant barriers for wide spread commercialization. The integration of multi-speed transmission to BEVs' powertrain systems, which is in place of fixed ratio reduction transmission, is considered as a feasible method to improve powertrain efficiency and extend limited driving range for a fixed battery size. Additionally, regenerative braking also extends the mileage by recapturing the vehicle's kinetic energy during braking, rather than dissipating it as heat. Both of these two methods reduce the requirement of battery pack capacity of BEVs without loss of performance. However, the motor-supplied braking torque is applied to the wheels in an entirely different way compared to the hydraulic friction braking systems. Drag torque and response delay may be introduced by transmitting the braking torque from the motor through a multi-speed transmission, axles and differential to the wheels. Furthermore, because the motor is usually only connected to one axle and the available torque is limited, the traditional friction brake is still necessary for supplementary braking, creating a blended braking system. Complicated effects such as wheel slip and locking, vehicle body bounce and braking distance variation, will inevitability impact on the performance and safety of braking. The aim of this thesis is to estimate if the multi-speed transmission and the mechanic-electric blended braking system are worthwhile for the customers, in terms of the price/performance relationship of others' design solutions;

To do so a generic battery electric vehicle is modelled in Matlab/Simulink® to predict motor efficiency, braking performance of different strategies, energy consumption and recovery for single reduction, two-speed Dual Clutch Transmission (DCT) and simplified Continuous Variable Transmission (CVT) equipped BEVs. Braking strategies for different purposes are proposed to achieve a balance between braking performance, driving comfort and energy recovery rate. Special measures are taken to avoid any effects of motor failure. All strategies are analysed in detail for various braking events. Advanced driver assistance systems (ADAS), such as Anti-Lock Brake System (ABS) and Electro Control Brake Distribution (EBD), are properly integrated to work harmoniously with the regenerative braking system (RBS). Different switching plans during braking are discussed. The braking energy recovery rates and brake force distribution details for different driving cycles are simulated.

A credible conclusion is gained, through experimental validation of single speed and two-speed DCT scenarios and reasonable assumptions to support the CVT scenario, that both two-speed DCT and simplified CVT improve the overall powertrain efficiency, save battery energy and reduce customer costs, although each of the configurations has unique cost and energy consumption related trade-offs. Results for two of the cycles in an 'Eco' mode are measured on a drive train testing rig and found to agree with the simulated results to within approximately 10%. Reliable conclusions can thus be gained on the economic and dynamic braking performance. The strategies proposed in this thesis are shown to not only achieve comfortable and safe driving during all conditions but also to significantly reduce cost in both the short and long terms.

CHAPTER 1 : INTRODUCTION

1.1 PROJECT STATEMENT

The development and verification of mathematical and experimental models of a Battery Electric Vehicle (BEV) equipped with regenerative braking and multi-speed transmissions for the prediction of motor performance, powertrain efficiency, braking energy recovery rate and manufacturing/maintenance cost under a wide range of operating conditions.

1.2 PROJECT OBJECTIVES

Considering the current development level of the battery, it is necessary to pursue every possible avenue for minor efficiency gains to prolong the one-charged mileage and reduce the charging times. A simple structure and optimized multi-speed transmission and high efficient regenerative braking strategy are two effective methods to remedy the deficiencies of the battery. In addition, motor, transmission system and braking system need an optimal algorithm to work cooperatively.

The characteristic of the motor is a decisive factor for the whole BEV's performance, e.g. acceleration, climbing, mileage and regenerative braking ability. Comprehensive investigations are necessary before determining the motor and transmission type applied to BEVs. According to the selected motor and gearbox, a fuel saving and high-performance shifting schedule can be designed. To recapture braking energy as much as possible, mechanical-friction and motor-electric blended braking is a beneficial choice.

This needs to work in conjunction with Anti-Lock Braking System (ABS) and Electronic Brake-Force Distribution (EBD) based on the requirements of braking performance and several safety regulations.

In summary, this thesis is focused on the investigation into multi-speed transmission based powertrain efficiency, braking performance and energy recovery rate under different braking blending strategies. The objectives of this project are:

1. Discussion and selection of traction motor, regarding to the performance, cost, efficiency, weight and robustness;

2. Modelling of electrified powertrains with single reduction, two-speed Dual Clutch Transmission (DCT), simplified Continuously Variable Transmission (CVT) respectively;

3. Design of economy-oriented shifting schedules for different multi-speed transmissions based on the selected motor characteristics;

4. Modelling of blended braking system, which includes mechanical friction brake and motor electric brake;

5. Design of blended braking strategies to achieve a balance between braking performance, driving comfort, energy recovery rate and cost saving;

6. Experimentally identify and study the performance and economic benefit of BEVs equipped with multi-speed transmissions and blended braking system in a variety of conditions.

1.3 PROJECT SCOPE

The optimization of powertrain design, including the selection of traction motor and transmission system, and the blended braking system on a battery electric vehicle is the primary goal of this thesis. The selected components are integrated into a completed BEV powertrain and tested on a testing bench.

In summary, the scope of this project is limited to the following:

1. Investigation of various motor types to select a proper traction motor, regarding to the characteristics and specific requirements;

2. Gear ratios investigation for motor based transmissions;

3. CVT optimization for electrified propulsion system;

4. Shifting schedules design for two-speed DCT and simplified CVT;

5. The dynamic and economic performance of BEVs equipped with multi-speed transmissions, i.e. CVT and two-speed DCT, are analysed, comparing to traditional widely adopted single reduction-BEV;

6. The potential and limitations of regenerative braking for specific BEV powertrain;

7. The purposes and principles of blended braking strategies;

8. The safety and economic benefit of three blended braking strategies;

9. The development and calibration of BEV powertrain testing bench;

10. The investigations of lifetime economic benefit for BEVs equipped with different transmissions under a variety of braking strategies and driving conditions.

1.4 PRESENTATION OF THIS THESIS

Chapter 2:

This chapter provides the framework for the research of this thesis. Initially the required background information on relevant aspects of multi-speed transmission and regenerative braking equipped BEVs is presented to introduce the topics for research. This is followed by a detailed literature review which identifies the state-of-the art in multi-speed BEVs and blended braking system design. To complement this work, a brief exploration of literature is performed in each relevant chapter to identify the important aspects of relevant research, as necessary.

Chapter 3:

Potential options of traction motors for battery electric vehicles are introduced. The principles, characteristics and applications of brushed DC motor, induction motor, switched reluctance motor and permanent magnetic synchronous motor are carefully analysed. A selection is made after the comparison of cost, reliability, controllability, efficiency and power density within above traction motor options.

Chapter 4:

The configurations of single reduction, two-speed DCT and simplified CVT based powertrains are demonstrated. The proper transmission gear ratios are calculated to meet the vehicle dynamic performance requirements. Correspondingly, the fuel saving-oriented shifting schedules for CVT and two-speed DCT are designed. Motor operating tracks with different transmissions are presented under a variety of driving conditions.

A general predictive backward-facing model, which includes battery, motor, transmission, vehicle body, blended braking system and driving cycles' profiles, is applied to MATLAB to investigate the economic benefit and dynamic performance achievement from multi-speed transmission based BEVs

Chapter 5:

The configuration of the lab powertrain testing rig is presented. Three wireless torque sensors are carefully calibrated to measure the transmission efficiency. Vehicle control unit comprising dSPACE prototyping system and self-designed electric control panel is demonstrated. Parameters are set in the dynamometer to provide the vehicle dynamic resistance on road.

Chapter 6:

This chapter is devoted to the analysis of experimental results, such as transmission operating temperature, two-speed DCT efficiencies and energy consumption of multi-speed transmission equipped BEVs in driving conditions. Additionally, the economic benefit for BEVs equipped with CVT and two-speed DCT is presented, regarding to the manufacturing and maintenance cost saving.

Chapter 7:

The maximum kinetic energy recovery potentials in a variety of driving cycles are calculated and shown in figures. Special testing manoeuvres are proposed based on a range of braking regulations and laws. The regenerative braking capability is restricted by regulations, motor performance and gear ratios. After the discussion of stability and

controllability in braking, three blended braking strategies are proposed to achieve the balance between braking performance and energy recovery ability, but with safety ensured by an automatic overriding control strategy.

Chapter 8:

This chapter is divided into four parts to test the performance of three blended braking strategies in simulation. Single straight line braking is tested in three; the cooperative actuation of regenerative braking, ABS and EBD; solutions of torque interruption in gear shifting during a blended braking; braking performance in several typical cycles. The energy recovery rates and braking force distribution are demonstrated.

Chapter 9:

In this chapter, the performance of the 'Eco' blended braking strategy has been experimentally verified in driving cycles by an integrated powertrain testing bench in the Lab. Specifically, 23.3% and 14.1% energy recovery rates, for NEDC and HWFET respectively, were achieved by the powertrain with regenerative braking in 'Eco' mode in experimental testing. Initial manufacture and daily-use cost savings by regenerative braking were analysed and compared to evaluate the three strategies. The outcomes show the vehicle equipped with RBS can achieve a longer driving range per charge, a lower 'fuel' cost and a lower battery pack price with the same target driving range, and lower maintenance cost.

Chapter 10:

The concluding chapter reviews and summaries each of the previous chapters, presenting significant and novel results of this thesis as well as identifying the important areas for further research.

1.5 PUBLICATIONS

Journals

Jiageng Ruan, Paul Walker, and Nong Zhang, "A Comparative Study Energy Consumption and Costs of Battery Electric Vehicle Transmissions," Applied Energy 165 (2016): 119–34, doi:10.1016/j.apenergy.2015.12.081.

Jiageng Ruan, Paul Walker, Nong Zhang, Guangzhong Xu, "The Safety and Dynamic Performance of Blended Brake System on a Two-Speed DCT Based Battery Electric Vehicle," SAE International Journal of Passenger Cars-Mechanical Systems 9 (2016): 143–53, doi:10.4271/2016-01-0468.

Jiageng Ruan, Nong Zhang, Paul Walker, Yuhong Fang, "Speed Ratio Design and Cost Analysis of Streamlined Continuously Variable Transmission Based on Pure Electric Vehicle," Automobile Technology, no. 6 (2015): 1–6.

Jiageng Ruan, Paul Walker, Nong Zhang, Peter Watterson, "The Performance and Economic Benefit of a Blended Braking System in a Multi-Speed Battery-Electric Vehicle", Applied Energy, **accepted in Sep/2016 and in process of publication**

Xingxing Zhou, Nong Zhang, Bo Zhu, Jiageng Ruan, "Numerical and Experimental Investigation of Drag Torque in a Two-Speed Dual Clutch Transmission," Mechanism and Machine Theory 79 (2014): 46–63.

Bo Zhu, Nong Zhang, Paul Walker, Wenzhang Zhan, Xingxing Zhou, Jiageng, "Two-Speed DCT Electric Powertrain Shifting Control and Rig Testing," Advances in Mechanical Engineering 2013 (2013): 1–10, doi:10.1155/2013/323917.

Conference Proceedings:

Jiageng Ruan, Paul Walker, and Nong Zhang, An Optimal Regenerative Braking Energy Recovery System for Two-Speed Dual Clutch Transmission-Based Electric Vehicles, April 1, 2014, doi:10.4271/2014-01-1740.

Jiageng Ruan, Walker Paul, and B. Zhu, "Experimental Verification of Regenerative Braking Energy Recovery System Based on Electric Vehicle Equipped with 2-Speed DCT," in 7th IET International Conference on Power Electronics, Machines and Drives (PEMD 2014) (Institution of Engineering and Technology, 2014), 0240–0240, doi:10.1049/cp.2014.0356.

Jiageng Ruan, Nong Zhang, and Paul Walker, "Comparing Of the Effects of CVT and DCT on the EVs Including Braking Energy Recovery," in 8TH AUSTRALASIAN CONGRESS ON APPLIED MECHANICS, 2014.

Jiageng Ruan, Nong Zhang, and Paul Walker, "Comparing of Single Reduction and CVT Based Transmissions on Battery Electric Vehicle," in The 14th IFToMM World Congress Proceeding, 2015.

Guangzhong Xu, Zhang Nong, Roser Holger, Jiageng Ruan, "Tyre Load Analysis of Hydro-Pneumatic Interconnected Suspension with Zero Warp Suspension Stiffness," 2016, doi:10.4271/2015-01-0630.

Xingxing Zhou, Paul Walker, Nong Zhang, Bo Zhu, Jiageng Ruan, "Study of Power Losses in a Two-Speed Dual Clutch Transmission" (SAE International , 2014), doi:10.4271/2014-01-1799 .

Xingxing Zhou, Paul Walker, Nong Zhang, Bo Zhu, Jiageng Ruan, "Simulation of Thermal Behavior of a Two-Speed Dual Clutch Transmission," in APCOM & ISCM 2013 Singapore, 2013, 1–5.

CHAPTER 2 : BACKGROUD INFORMATION AND LITERATURE REVIEW

2.1 BACKGROUD

Automobiles have made great contributions to the growth of modern society by satisfying many of the needs for mobility in everyday life. The rapid development of the automotive industry has prompted the progress of human beings from a primitive security to a highly developed industrial one.

At present, most vehicles rely on the combustion of hydrocarbon (HC) fuels to derive the energy necessary for their propulsion. Combustion is a reaction between the fuel and the air that releases heat and combustion products. Ideally, the combustion of an HC yields only carbon dioxide and water, which do not harm the environment. Indeed, green plants "digest" carbon dioxide by photosynthesis. Carbon dioxide is a necessary ingredient in vegetal life. Animals do not suffer from breathing carbon dioxide unless its concentration in air is such that oxygen is almost absent. However, the combustion of HC fuel in combustion engines is never ideal. Besides carbon dioxide and water, the combustion products contain a certain amount of nitrogen oxides (NO_x), carbon monoxide (CO), and unburned HCs, all of which are toxic to human health. You see it every time that smoke is expelled from your car's exhaust pipe, so there's no denying that vehicles are major contributors to air pollution and environment changing.

Therefore, the large number of automobiles in use around the world has caused and continues to cause serious problems for the environment and human life. Air pollution, global warming, and the rapid depletion of the Earth's petroleum resources are now problems of paramount concern. According to the Australian Greenhouse Office (AGO), transport currently accounts for 17% and 22% of greenhouse gas emission in Australia and the Organisation for Economic Co-operation and Development (OECD) countries respectively [1]. Specific to the individual household, the transport share of emission goes up to 34% [2]. Additionally, referring to the United States Environment Protection Agency (EPA), motor vehicles collectively cause 75 per cent of carbon monoxide pollution in the U.S [3]. The US Environmental Defence Fund (EDF) estimates that on-road vehicles cause one-third of the air pollution that produces smog in the U.S., and transportation causes 27 per cent of greenhouse gas emissions [4]. Motor vehicles also produce other pollutants like oil and petrol residues, which enter the storm water system and are a major source of waterway and ocean pollution. Passenger cars are our cities' biggest producers of carbon monoxide, oxides of nitrogen, sulphur oxides, ozone-forming substances, hydrocarbons and fine particulates.

As shown in Fig.2-1, about one third of the greenhouse gas emissions produced by an average Australian household each year are from transport [2].
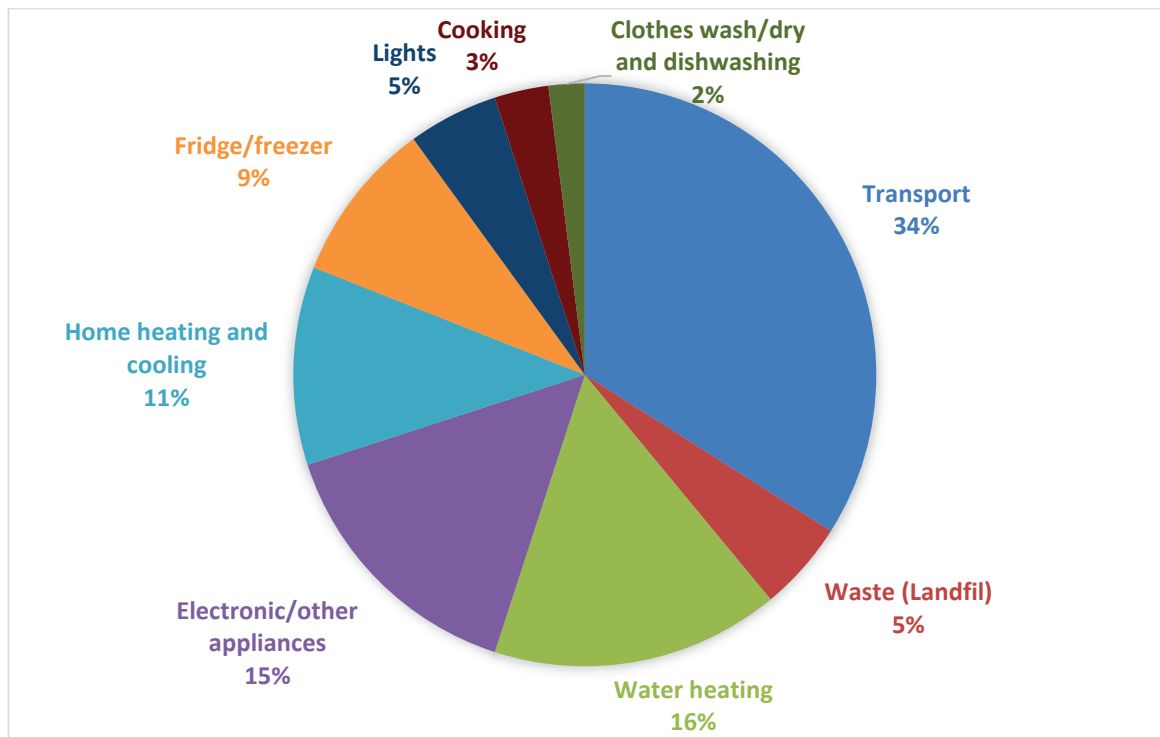
Figure 2-1: Greenhouse emissions per household application (tons per year)[2]

Historical data shows that the discovery of oil reserves grows slowly. On the other hand, the consumption shows a high growth rate. If oil discovery and consumption follow the current trends, the world oil resource will be used up in around forty years [5]. Transportation is the main sector for oil use, responsible for 59% of all oil use in 2011 (Fig.2-2 and Fig.2-3). This share is set to grow, with the Reference Case projecting a rise to 63% of all oil demand by 2040. These figures are based upon the calorific use of oil, not volumes. Given this number for transportation means that just over 40% of oil consumed in 2011 is in the other sectors. The petrochemical industry and other industrial usage accounted for one-quarter of all oil used in 2011, while residential and agriculture, together with some consumption in the commercial sector, contributed to 10% of the consumption. Little oil is used to produce electricity, with only 6% of total oil use

in this sector, although some OPEC countries use significant amounts of oil to produce electricity [6].
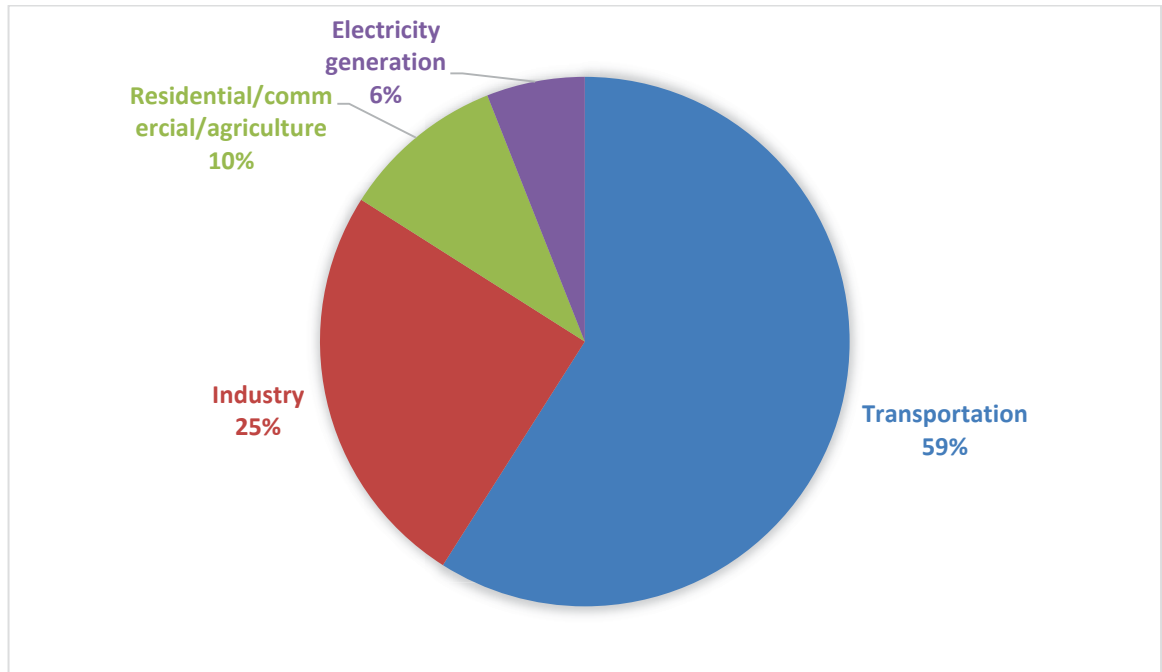
Figure 2-2: Percentage shares of world oil demand by sector in 2011[6]

Consequently, Electric Vehicles (EVs) have been widely accepted as a potential alternative for the current conventional combustion engine vehicle to expedite sustainable and green transportation. They are distinguished with superior features such as high-efficiency and a more flexible powertrain as well as reduced emissions. As the most promising transportation, EVs attract attention from all over the world. All the major automobile manufactures, e.g. General Motors, Renault–Nissan alliance, Mitsubishi, Audi, Ford, BMW, Volvo, Fiat, Mercedes-Benz, have already proposed their battery electric vehicle (BEV), hybrid electric vehicle (HEV), or fuel cell hydrogen electric vehicle. A great quantity of commercial BEVs and concept BEVs have been made and launched, as shown in Table 2-1
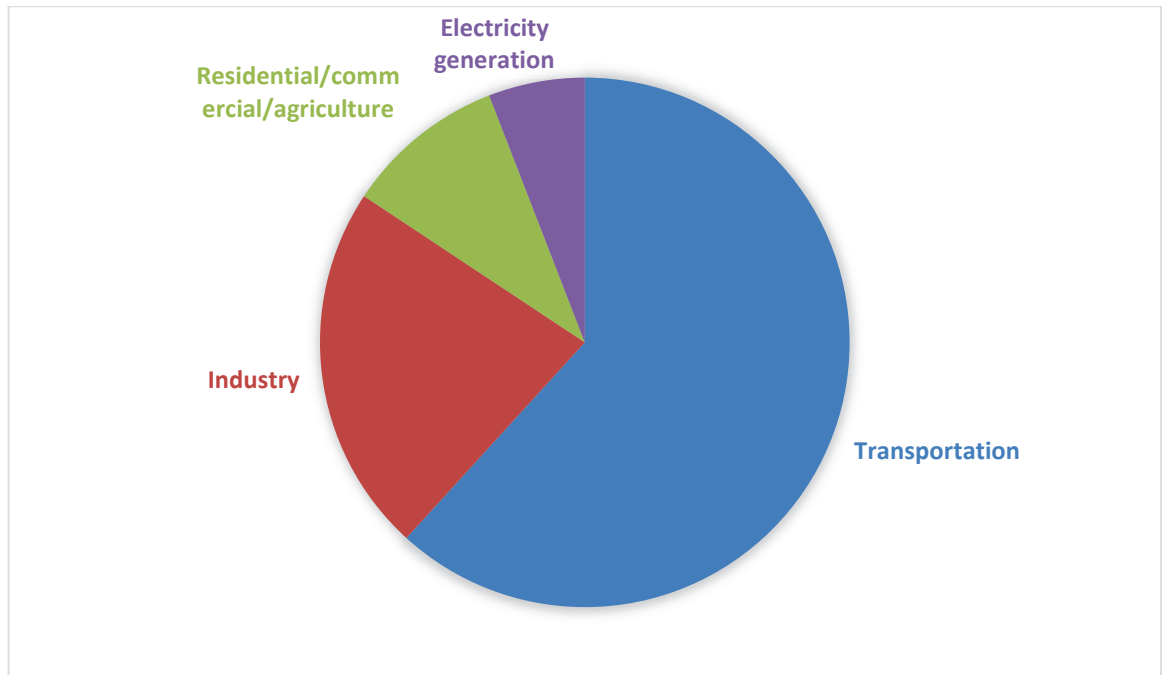
Figure 2-3: Percentage shares of world oil demand by sector in 2040 [6]

Table 2-1: Comparisons of Recently Launched BEVs

Specification	Tesla 90D	Renault Zoe	VW e-GOLF	Nissan Leaf	Mitsubishi MiEV	Ford Focus
Top Speed (Km/h)	248	135	140	130	130	135
Max Motor Power (kW)	311 (Battery Limit)	65	85	80	49	107
Max Motor Torque (Nm)	660	220	270	254	180	
Transmission type	Direct drive	Direct drive	Direct drive	Direct drive	Direct drive	Direct drive
Charging Time (h)	0.5 (80%) Supercharger	9 (16A)	4 (10A 220V)	6 (Home)	9 (Home)	4

Battery Capacity (kWh)	90 Li-ion	22 Li-ion	26.5 Li-ion	30 Li-ion	16 Li-ion	23 Li-ion
Max Range per charge (km)	470(NEDC)	130	115	180	150	123
Braking Energy Recovery	Y	Y	Y	Y	Y	Y

2.2 LITERATURE REVIEW

2.2.1 The propulsion motor for BEVs

Although it is already widely accepted that EVs will be the solution for urban mobility in the near future, a lot of problems need to be solved before large-scale application can occur. The choice of the electric motor suited to EVs should be the first issue to be discussed.

The motor for EVs is generally required to perform starting/stopping and accelerating/decelerating frequently, outputting high torque at low speed, outputting low torque at high driving speed and have a large speed range. There are a lot of options for EV's drive-train, e.g. permanent magnet motor (PM), induction motor (IM), switched reluctance motor (SRM) and brushed DC motor (DC). Briefly, PM motor has the highest efficiency for a fixed ratio electrified powertrain, SRM has the lowest weight, DC motor is the cheapest and IM has the optimal balance of several criteria. If we take into account other criteria, e.g. cooling, maximum speed, and fault-tolerance, safety, and

reliability, SRM is, theoretically, the most suitable motor for current EVs due to its outstanding performance in all-aforementioned aspects [7]. A similarly validated result can be found in West, J.G.W.'s study [8].

Up to now, the most used electric motors, considering the state-of-art development status and cost of motors, are IM and PM synchronous motors. The former is adopted for their durability and availability while the latter is usually chosen for their higher torque density and efficiency. A comparison between interior permanent magnet (IPM) and surface mounted permanent magnet (SPM) motors was carried out in [9].

The specifications of selected motor need to be carefully analyzed to meet a particular vehicle dynamic performance requirement. The method of calculating parameters of the motor, according to demand of vehicle's dynamic performance, is presented in [10]. The motor operating efficiency is improved by fitting an additional gearbox and the efficiency lost in the gearbox should be taken into consideration as well.

2.2.2 The multi-speed transmission systems on BEVs

2.2.2.1 Transmissions

Despite the long-term benefit of BEVs to customers and the environment, the initial cost and limited one-charge driving range present the major barrier for its wide spread commercialization. Therefore, it is necessary to pursue every possible avenue for minor efficiency gains. One of the possible methods is adding a multi-speed transmission system to BEVs, at least until a battery breakthrough and a reduction in the electronics VA rating and hence cost occurs. Up to now, fixed ratio single reduction (SR)

transmissions are applied on most first generation BEVs rather than multi-gear transmission, e.g. VW e-Golf, Nissan Leaf, BYD e6 and even Tesla Model S as shown in Table 2-1, because of the outstanding dynamic performance of electric motors and the cost containment required for BEVs. However, there is still great potential to improve a motor's efficiency. In fact, there is a 30% efficiency variation through the range of actual driving conditions for daily-use to peak efficiency regions, typically from 65% to 95% [11]. Unfortunately, the ratio of SR on BEVs must inevitably be designed as a trade-off between the longer driving range and satisfactory dynamic performance. Thus, the designed fixed ratio is selected at the expense of economy performance to achieve a satisfactory dynamic response.

Many people have worked on adding multi-speed transmissions to BEVs' powertrain to improve motor operating efficiency and enhance driving performance. It has been proved that multi-speed gearbox can not only improve the overall drivability and motor efficiency but also can downsize the battery and motor [12,13].

With the ability of 100% torque delivery from a standing start, wide speed range and excellent dynamic adjustable ability of motor, the requirements for transmission system design on EVs are much simpler than that for Internal Combustion Engine (ICE) vehicles. Aldo Sorniotti et al. demonstrated an EV simulation model based on a special commercial EV equipped with a two-speed automated transmission composed of a one-way clutch and a friction clutch to improve the overall powertrain efficiency [14]. An optimized two-speed transmission was integrated into an electric delivery van [15] to reduce acceleration time and energy consumption. The effects of adding a two-speed AMT to BEVs and a similar system were tested on a pure electric bus [16,17]. These

make up a handful of the available literature that has evaluated the improved economy of adding multi-speed transmissions to BEVs. Furthermore, clutchless four-speed EV transmission was promoted by Oerlikon Graziano to achieve a level of smoothness of operation to complement an EV's potentially linear performance [18].

The Dual Clutch Transmission (DCT) has the best compatibility for most market vehicles. The two clutches of DCT are linked to two input shafts (hollow and solid) respectively. One clutch is in charge of the odd number gears and the other is in charge of the even number gears and reverse. Pre-select gear is ready when the current gear is engaged. There is no clutch pedal for the driver. All procedures are done automatically. It works like a MT and feels like an AT. So, it can provide excellent fuel efficiency, responsiveness of the shift and launch comfort of a good planetary-AT. It is the first automatic with up to 10% better fuel economy and at the same time better performance than a manual [19]. Paul Walker firstly studied the performance for different transmission ratios using both single speed and two-speed gearbox configurations to provide a comparative assessment of the EVs [20,21].

With CVT it is possible to vary the transmission gear ratio without interruption of the torque flow. Therefore, an infinite number of ratios (between a minimum and maximum value) are possible. The key lies in its simple yet effective belt-and-pulley design. CVT works with an all-metal chain that runs between cone-shaped curved pulleys. The transmission ratio between the engine/motor and the wheels varies in a smooth manner in relation to the variable axial gap between the pulleys. The gap defines the possible chain radii on the pulleys. Due to their mechanical layout and the need for a torque converter to work with ICE vehicles, the efficiency of CVT is typically lower than that

of single-speed ones and they can suffer from a poor speed of response [22–24], particularly at launch [25].

However, with the help of outstanding motor dynamic performance, torque converter and relevant hydraulic system can be removed, which is the most inefficient and complicated component in CVT. Furthermore, the infinite number of transmission ratios allows the motor to always run at its optimum speed. It will be different in comparison to potential benefits from the viewpoint of overall powertrain efficiency. The variable ratios range will be narrower, which means a lighter and more compact CVT. A simple and simulation based conclusion was presented that 2, 3, 4-speed gearboxes and continuous variable transmission (CVT) improve the overall energy consumption 5%-12% depending on driving cycles [26]. An energy consumption comparison of BEV with 1-2 speed gearboxes, half/full toroid CVT and infinity variable transmission (IVT) showed [27] that different transmissions have a 2%-20% energy efficiency improvement depending on the selected driving cycles in simulation, which includes regenerative braking. As the gear ratio varying range in CVT is wide and continuous, the ratios control strategy needs to be compromised between fuel economy and drivability, which contributes to a poor speed response and unsatisfactory launching performance [14,28].

In addition, the new generation push-belt CVT has the ability to transfer more than 400 Nm torque, while the insufficient transmission torque capacity was usually regarded as the main drawback of CVT, covering the full range of most daily-used engines and motors [24].

Although a very large number of similar papers can be found, economy performance is just one of the key factors that need to be considered during vehicle design. Driving comfort and v deserve careful attention as well. Some limitations of the papers above are:

1. The lack of the analysis of whether the energy saved by adding multi-speed transmissions to BEVs will cover the additional manufacturing cost.

2. The lack of the analyses of each transmission's characteristics. Not all the existing transmissions are suitable for BEVs from the point of view of keeping the original advantages of BEV. For instance, Manual Transmission and Automated Manual Transmission may not be suitable for small passenger BEVs due to the inevitable torque interruption [29,30], although they are more efficient.

3. The lack of the shifting schedules optimization for transmission on BEVs. The characteristics of electric motor and ICE are totally different. It is necessary to design a special shifting map for transmission on BEVs to optimise motor performance.

4. The lack of the experimental validation of the hypotheses demonstrated in plenty of simulation results. The improvements in the simulation may be eliminated in bench testing as various losses that were not included in simulations compound. A convincing conclusion depends on the credibility of the experiments.

In this thesis, a two-speed DCT and simplified CVT (without torque converter) are applied in BEV models to boost motor efficiency and reduce energy consumption, while maintaining dynamic performance and shifting without torque interruption. Through

gear ratio design and shifting schedule optimization, higher motor efficiency and less energy consumption can be achieved.

Based on the achievements and limitations in previous work, a comprehensive analysis of multi-speed transmission selection process for BEVs is presented in this thesis in the following parts:

1. Comparison of the mechanical layouts of SR, two speeds DCT and CVT without torque converter.

2. Gear ratios design for SR, two-speed DCT and CVT based on the motor characteristics and vehicle performance requirements;

3. Shifting schedule optimization for two-speed DCT and CVT without torque converter;

4. Simulation results comparison of motor efficiency and energy consumption in urban and highway driving cycles;

5. Bench testing for SR and two-speed DCT in urban and highway driving cycles. Comparison of the motor efficiency and energy consumption of each scenario;

6. The relative selling prices of different transmissions based BEVs are calculated. The cost saved in manufacturing, particular driving range and lifetime mileage are presented based on experiment data;

2.2.2.2 Shifting schedules

Shift schedule determines the gear-shift timing of stepped automatic transmissions that directly affects the power performance, fuel economy, and emission of the vehicle. Under the circumstance with ever increasing concerns about the issues of energy saving

and environment protection, an optimized shift schedule that could make the powertrain system provide sufficient power with minimum fuel consumption is needed. Less emission has been becoming a very critical factor to improve the overall performance of vehicles equipped with a stepped automatic transmission. Generally, there are two kinds of control strategies for gear shifting; one is power performance dominated and the other is fuel economy dominated. Although the torque performance is important for shifting schedule design [31], especially in some extreme conditions such as overtaking during driving, the fuel saving oriented shifting algorithm attracts more concerns. An optimal gear-shifting schedule not only ensures a high utilization of the energy, but also that gear shifting is less likely to occur to attain a better driver feeling. A fuzzy-neural network control algorithm was proposed to optimal gear-shift controller to give more smooth driving, less fuel consumption, and less harmful exhaust gas emission than conventional approaches during shifting in the early 1990s [32]. A lot of shifting strategies were promoted to optimize the shifting quality of DCT in past decades. For example, Cheng Xiusheng, et al. described a pressure control method of dry dual clutch transmission shifting for BEV [33], in which the target torque of clutch and target pressure of cylinder in different stages of shift process was obtained based on shift jerk. Specific to the application of two-speed DCT on BEVs, some achievements were published in recent years. Hong, S, et al. proposed a shifting algorithm based on an EV equipped with a 2-speed DCT. It found that the overshoot torque of the drive shaft was reduced by the proposed control algorithm, which provided the improved shift quality. However the long-uphill slopes and overtaking situations, gearing down becomes inevitable since the maximum engine torque on the direct gear is not sufficient to propel

the vehicle within an acceptable speed range during long uphill slopes [34]. An enhanced precision of torque estimation and control in the electric machine was demonstrated in [35]. It showed that was possible to minimise powertrain response during and after gear shifting transients, thereby improving driver comfort. Unfortunately, all the results come from MATLAB/Simulation; they lack experimental verification. In this thesis, a specially optimized shifting schedule for two-speed DCT based BEV was promoted and experimentally validated to achieve an overall efficiency improvement of electrified powertrain.

2.2.3 The cooperation of regenerative braking and traditional friction braking

Energy recovery through regenerative braking is one of the most advantageous developments for EVs. It can contribute to prolonging the limited mileage, which is the biggest disadvantage comparing to its ICE counterpart, by recovering electric energy instead of dissipating heat during braking. The benefit of regenerative braking by blended braking systems, combining electric and friction brakes, has been theoretically and experimentally validated in many kinds of electric vehicle (EV), e.g. battery electric vehicle (BEV) [36,37], fuel cell electric vehicle (FEV) [38], and hybrid electric vehicle (HEV) [39].

In the designing of brakes, it is important to meet the essential demands which are operating environment, structural properties of a vehicle, basic dimensioning of the brake mechanisms, and the controllability of braking forces as well as regulations on brakes [40,41]. Theoretically, all the kinetic energy can be recovered by regenerative

braking in a BEV equipped with proper battery and motor [42]. However, regenerative braking actually cannot provide enough braking force all the time, because it is limited by various conditions (e.g. the battery state of charge (SOC), motor speed, and gear ratio). Thus, a friction brake system is needed to cooperate with the regenerative brake system. Also the braking force distribution ratio between front and rear axles needs to be restricted in a certain range to achieve a desirable braking performance according to several braking regulations and safety requirements, e.g. ECE, Ideal Braking Force Distribution Curve and Front/Rear Wheels Locked Curve [43]. Adding an electrical regenerative brake force to the original mechanical brake system will inevitably change the braking force distribution ratio and the structure to various degrees. Therefore, an optimal control algorithm for the cooperation of mechanical and electrical braking force has attracted many researchers' attention.

Antanaitis, D. has experimentally validated that different friction brake usage profiles that occur with regenerative braking systems can have significant effects on foundation brake performance [44] Walker, A, et al. discussed the demands on regenerative and friction braking based on an example of a hybrid heavy truck, which uses minimal friction braking over a particularly hilly driving route [45]. Gao, Y., Chen, L., and Ehsani, M. investigated three different braking patterns for evaluating the availability of braking energy recovery [46]. The results indicated that a significant amount of braking energy can be recovered even without active braking control, and the brake system does not need much changing from the brake systems of conventional passenger cars. Hartley, J., et al. developed an approach for Tata Motors Ltd. to optimise the design and operation of a regenerative braking system to maximise driving

range and energy efficiency [47]. An electrically controlled regenerative braking system designed by Zhang, J and his colleagues can reduce 25% energy consuming in a typical ECE driving cycle [48]. Results from the continental company, described by von Albrichsfeld, C. and Karner, J, showed that a series regenerative brake layout worked well in several pilot productions and achieved a competitive price at the same time [49].

Regenerative braking should cooperate with ABS and EBD, which are existing safety control systems in the vehicle. ABS is a popular driver assistance system that allows a short braking distance while simultaneously maintaining the stability and steering ability of the car and is installed in most modern vehicle. Regenerative brake system, as part of whole EVs' brake system, will be affected inevitably by ABS control strategy. Gao, Y. and Ehsani, M. proposed an electronically controlled braking system for EV and HEV, which integrates regenerative braking, automatic control of the braking forces of the front and rear wheels and wheels antilock function together [50]. In this control algorithm, the vehicle can keep direction stable and the steering ability during deceleration, even if a failure occurs in the electric system. Rosenberger, M., et al. outlined a possibility of including a generator as a second actuator in ABS [51]. Their regenerative braking system did not replace the hydraulic friction brake, but rather supports it to enhance the performance of the ABS. Selim A. Oleksowicz, et al. proposed several manoeuvres suitable to test regenerative braking strategy, which cooperate with active driving safety system (ADSS) and ABS, under ECE Regulations 13H and 13.11 [52].

Krueger, E, et al. presented a method to improve vehicle dynamics performance and reduce deceleration disturbance in EVs equipped with a regenerative brake system [53].

Several special conditions were discussed in this paper, for instance, a vehicle encounters a momentary road disturbance like a pothole on a high coefficient of friction surface. Optimal braking strategy can automatically distinguish this situation from a normal ABS event and keep regenerative brake force applying on the driveline to enhance the energy efficiency in every effort.

Most of above studies focused on optimizing braking energy recovery, but neglected the safety issues introduced by the addition of a brake-by-wire system. Although some papers discussed the control and stability of blended brake systems, they did not address the details of braking force distribution, the kinetic energy recovery ability, or the short and long term economic benefits. Many studies also neglect the fact that specially designed testing manoeuvres are required to validate the braking performance in all conditions. If a multi-speed gearbox such as an Automatic Transmission (AT), DCT or CVT is added to improve the dynamic performance and driving range, then additional problems of response delay and torque interruption are introduced [9-11]. These problems are of particular concern for the simplified two-speed Dual Clutch Transmission, which has been proven to be extremely suitable for EVs [20,54]. For any of these complicated powertrain architectures, specially designed algorithms are needed to ensure safe braking, while recapturing as much kinetic energy as possible. The safety-oriented control algorithms used in conventional vehicles, such as the ABS and EBD, should be integrated into blended braking strategies, after necessary modifications [55,56].

This thesis proposes a blended braking strategy with a manual selection function to achieve the balance between braking performance and energy recovery ability, but with

safety ensured by an automatic overriding control strategy. Firstly, the typical energy lost in conventional friction braking is reported, to indicate the maximum potential gains from regenerative braking. Then, strengths and weaknesses of blended braking in a two-speed DCT based front-drive BEV are discussed. One advantage examined is the transfer of the load to the motor-connected front axle during braking, while the torque interruption in gear shifting presents a disadvantage. Different strategies are designed to either recapture maximum braking energy, or achieve the best braking performance, or to compromise between energy recovery and braking performance. Next, a simulation model is established to analyse the details of braking force distribution, wheel slip, and kinetic energy recovery rates in various test conditions. One of the strategies is validated experimentally on an electric powertrain test bench for city and highway driving cycles. Finally, the economic performances of blended braking systems with different strategies are evaluated, regarding the fuel cost, initial manufacturing cost and maintenance cost.

In conclusion, this chapter has provided the framework for further investigation of the alternative multi-speed transmissions and blended braking systems for BEVs. The literature review shows the most cost-effective solution for energy saving and performance improvement are based on multi-speed gearboxes and regenerative braking with appropriate traction motor.

CHAPTER 3 :   MOTOR   SELECTIONS   FOR BATTERY ELECTRIC VEHICLES

3.1 INTRODUCTION

Before the electric machine was applied to drive a vehicle, there did already exist a variety of motor types, e.g. brushed DC motor, brushless DC motor, induction motor, permanent magnetic synchronous motor (PMSM) and switched reluctance motor (SRM), etc., which were widely used in industry. However, not all motors are suitable for EV propelling, regarding to the different purpose, using conditions and cost. The basic requirements for driving motors on EV are summarized as follows:

1) High instant power and power density;

2) Sufficient torque at the beginning for starting and grading;

3) Sufficient power during high speed range from cruising;

4) A reasonable ratio of constant torque and constant power range; a constant power operating range of around 3–4 times the base speed being a good compromise between the peak torque requirement of the machine and the volt-ampere rating of the inverter.

5) Rapid torque response. Intermittent overload capability, typically twice the rated torque for short durations;

6) High efficiency for driving and regenerative braking

7) Reliable and robust

8) Cost effective

9) Reasonable ratios of Capacity/Volume/Weight

10) High fault tolerance and strong anti-electromagnetic interference (EMI)

Up to now, only a few types of motor have been selected by manufacturers and applied to EV driving, e.g. brushed DC motor, SRM, IM, and PMSM. Each of them has its own strengthens and weakness:

3.2 BRUSHED DC MOTORS

The DC motor has been the dominant in electric powertrain because of its outstanding performance of outputting high torque from a standstill, and simple control method. The affordable inverter price in DC motors makes it a perfect choice for high power requirement. However, mechanical commutator depended structure results in a bloated volume, low operating efficiency, and poor robustness. Although some improvements were achieved in past decades, it still is losing the market share continuously. Especially in EVs market, compared to the closed and fixed working environment of conventional electric machines, the maintenance and repairing of motors on EV are much more time and money consuming. Therefore, commutator-less electric machines, such as PMSM and IM are more attractive for OEMs.

3.3 INDUCTION MOTORS

Thanks to the acknowledged excellent characteristics, e.g. affordable price, robustness, fewer maintenance times and reliability in a hostile environment, the induction motor is widely used in EVs and HEVs. IM has the ability to decouple its torque control from the field control. Extended speed range operation with a constant power beyond the base

speed is accomplished by flux weakening. For conventional IMs, the constant power range typically extends to 2–3 times the base speed. However, for traction machines, this can be extended to 4–5 times the base speed, which is desirable [57,58]. Conversely, weaknesses in IM include high power loss, low efficiency, low power factor, and low inverter-usage factor. The good news is some significant improvements were achieved during recent years [59–61], which make IM still a competitor in the electric powertrain market. There were plenty of HEVs powered by asynchronous IM, e.g. Chevrolet Silverado, Chrysler Durango and BMW X5 hybrid version. However, today all the hybrids are powered by DC brushless drives, with no exceptions. The notable uses of induction drives have been the General Motors EV-1and the luxury Tesla Model S.

3.3 SWITCHED RELUCTANCE MOTORS

The excellent ability of high speed operating, continuous outputting constant power and the minimal effects of temperature variations offset demonstrate the great potential of SRM to be widely used in an EV powertrain. The advantages and disadvantages of SRMs are well-documented [57,62,63], and are summarized as follows:

1) Simple and robust rotor structure, without magnets or windings, which is desirable for a high-temperature environment and high-speed operation. However, it can have a significant rotor iron loss;

2) Low-cost potential, although relatively high manufacturing tolerances are required due to the need for a small air gap;

3) Extended constant power operation, typically up to 3–7 times the base speed

4) Modest short-duration, peak torque capability as the magnetic circuit tends to be relatively highly saturated;

5) Smooth operation at low rotational speeds requires relatively complex profiling of phase current waveforms and accurate measurement of rotor position;

6) Unipolar operation requires nonstandard power electronic modules, but SR drives have an inherent degree of fault tolerance;

7) Since their operation is based on the sequential excitation of diametrically opposite stator coils in machines having the basic 6/4 and 8/4 stator/ rotor pole number combinations, the acoustic noise, vibration, and torque ripple tends to be relatively high.

Apart from an earlier application in Australia Holden E-Commodore, at the 2013 Geneva Motor Show, Land Rover unveiled a range of new electric Defender vehicles which are directly powered by a SRM electric motor and drive system.

3.3 PERMANENT MAGNET SYNCHRONOUS MOTORS (PMSM)

Not like other electric machines suffering low operating efficiency, the permanent magnet motor is inherently efficient [64–66]. Generally, PMSM can be classified into two types by the control methods, i.e. brushless DC (BLDC), or brushless AC (BLAC). For BLDC drives, in which the phase currents only have to be commutated on and off, low-cost Hall sensors are often employed, while for BLAC drives, in which the phase current waveforms have to be precisely controlled, a relatively high-cost resolver or encoder would generally be used. Also, however, numerous sensorless techniques have

recently been developed or are under development for both BLDC and BLAC drives. Essentially, all motors ultimately need an alternating current. Otherwise they wouldn't turn.

Although there are some drawbacks in PMSM that need to be considered e.g. degaussing and thermo-stability, more and more manufacturers take the PMSM as the primary option for their EVs and HEVs, such as Chevrolet Spark EV, BMW i3, VW e-Golf, Mercedes B250e, Nissan Leaf, Toyota Prius, Honda Insight and so on.

The following intuitional and interesting Fig.3-1 and Fig.3-2 illustrate the characteristics summarizing and comparing results of each motor types [7,67,68]. Each evaluation criteria in the Fig.3-1 has been rated up to five points. Widely used IM and PMSM are in the 1st and 2nd position.
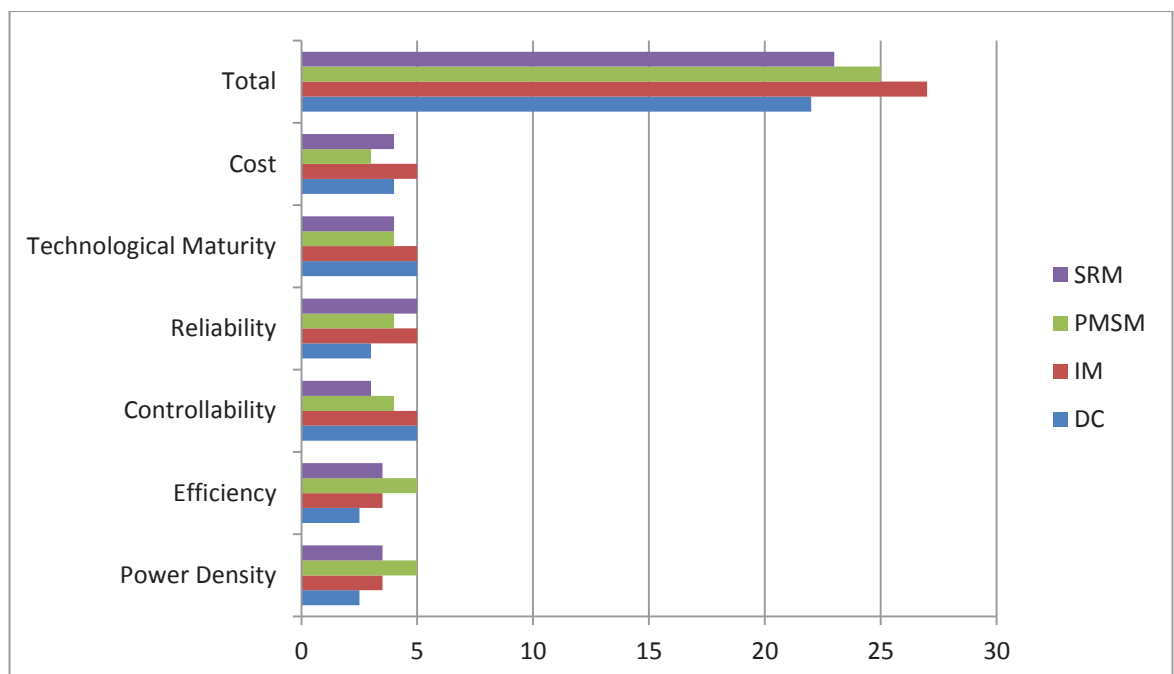
Figure 3-1: Evaluation and Comparison of Electric Propulsion System

BMW Group presented a more detailed report about the motor selection for EV. Five potential options were compared with each other, i.e. Permanent magnet motor with surface mounted magnets (PSM), Motor with buried magnets (IPM), Hybrid synchronous motor (HSM, special geometry of an IPM, designed for high reluctance torque capability), electrically excited synchronous machine (El.Ex.Sm) and Asynchronous machine (ASM).

Figure 3-2: Comparison of Different Machine Topologies Choice of Machine Type [68]
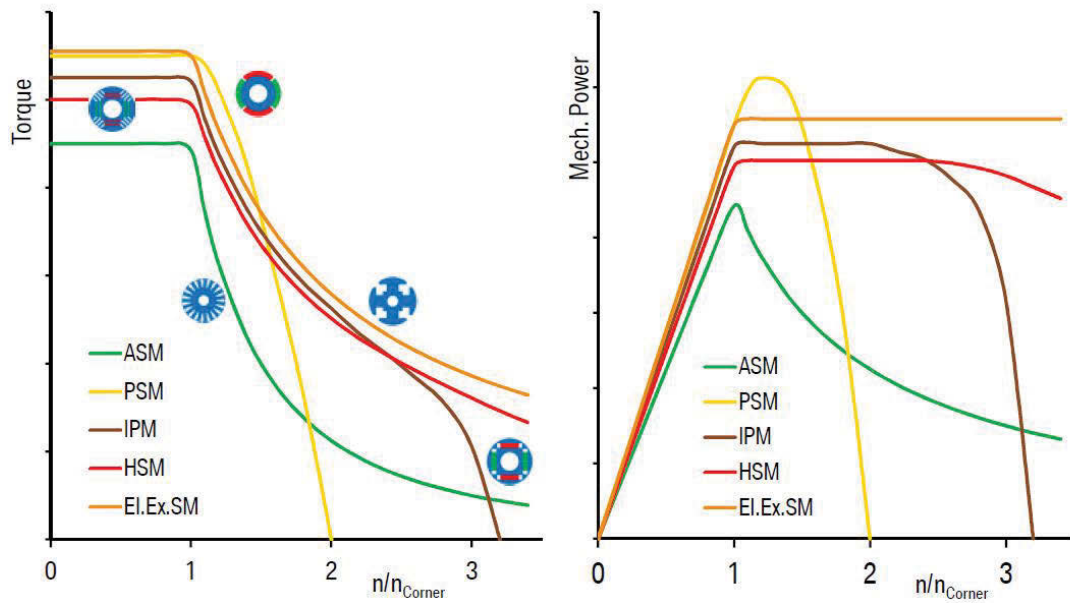
Figure 3-3: Comparison of Different Machine Topologies for Limited Stator Current

[68]

Considering the primary purpose of this thesis is to design a proper powertrain system for BEV, and controllability for transmission and regenerative braking cooperation, PMSM, as the mainstream product on the BEV market, is selected as a propulsion motor for further study.

Table.3-1 shows the specification of the selected motor for BEV powertrain testing.

Table 3-1: Selected UQM Powerphase 125 Specification

T_{peak}/T_{rate}	Motor Peak/Rated output torque	300/150	Nm
P_{peak}/P_{rate}	Motor Peak/Rated output power	125/45	Kw
N_{max}	Max Motor Speed	8000	rpm

e_{max}	Maximum efficiency	94	%
Power density (based on 125 kW)		3.05	kW/kg
Operating voltage input range		300 - 420	VDC
Input current limitation		500	A
Digital Signal Processor Nominal input voltage		12	VDC
Digital Signal Processor Input voltage range		8-15	VDC
Digital Signal Processor Input current range		0.3-0.5	A

According to the specifications in Table 3-1, this motor has only an approximate constant power range from 4000 to 8000 rpm (in fact, not even that, as the power dips at 4000 rpm), i.e. a 2:1 speed ratio. This range is lower than the 4:1 preferred for a fixed ratio transmission and is ideal for use with a 2 speed transmission, which can thus increase the system constant power speed range to 4:1. The characteristics of the selected motor in combination with the matching inverter UMQ Powerphase 125 are demonstrated in Fig.3-4, Fig.3-5 and Fig.3-6 [69]. This experimental data from UQM® is applied in the Simulink model to show the motor operating tracks in particular driving cycles.

The selected PM motor with aforementioned specifications not only has the ability to realize more precise control during high speed rotating, comparing to other motor types, but also has a highly competitive power density. The maximum available rotation speed and output torque are not outstanding due to the limited budget on motor, however, the saved money can be used for latter introduced multi-speed transmissions and give them

opportunities to boost the integrated powertrain performance with a similar, or even lower price, to the conventional motor & single reduction combination.

Figure 3-4: UQM Powerphase 125

a)

b)
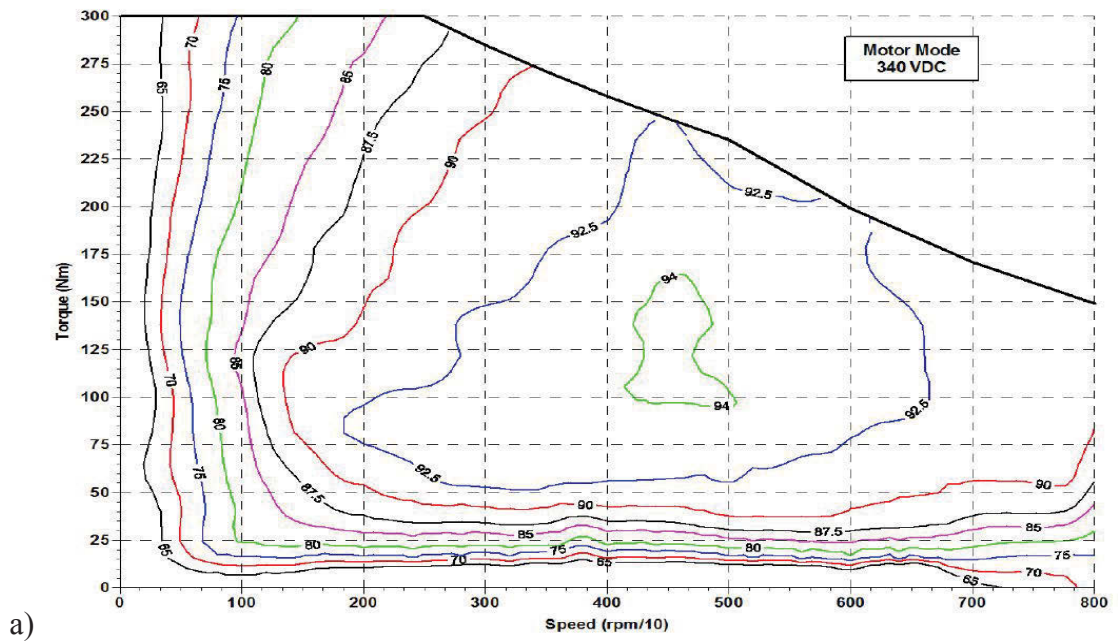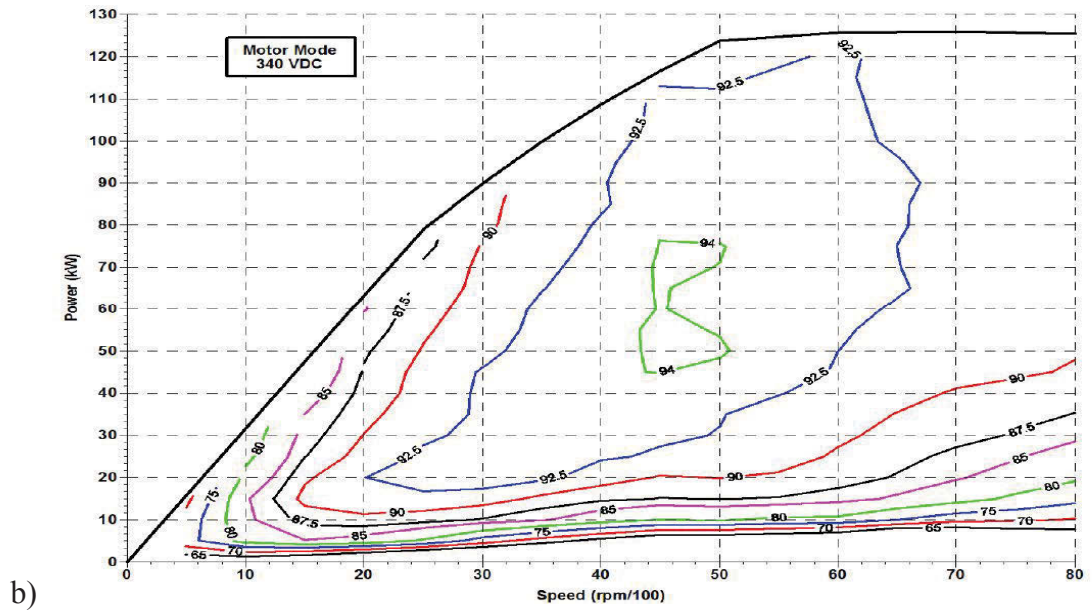
Figure 3-5: (a) UQM 125 Motor with Inverter Torque/Speed and Efficiency Map (b)

UQM 125 Motor with Inverter Power/Speed and Efficiency Map
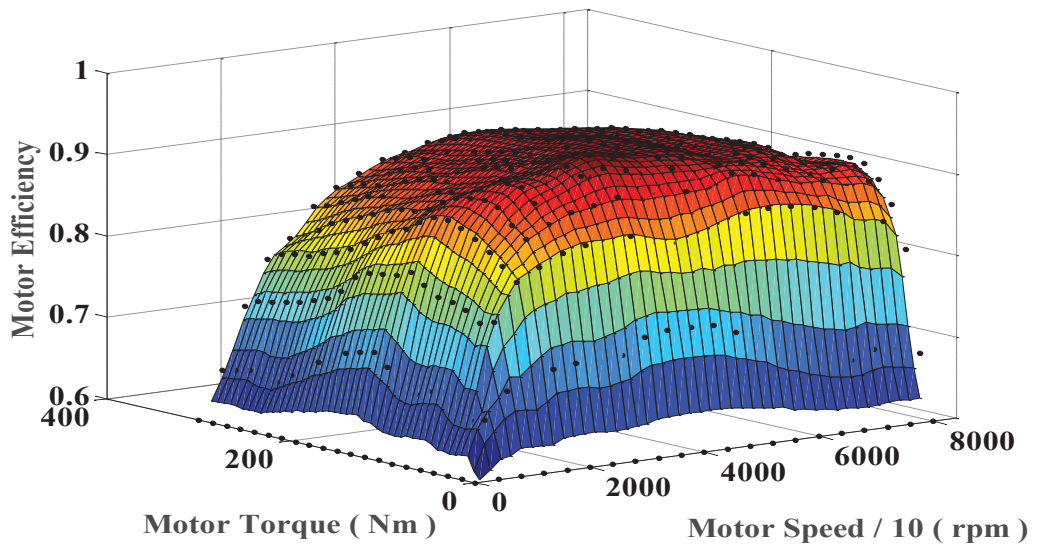
Figure 3-6: UQM Powerphase Motor with Inverter Efficiency data in Simulink model

CHAPTER 4 : ALTERNATIVE TRANSMISSION FOR BATTERY ELECTRIC VEHICLES

4.1 INTRODUCTION

Back to New Year's Eve in 1879, the first stationary gasoline engine developed by Carl Benz was a one-cylinder two-stroke unit which ran for the first time. Not like the modern vehicles with the help of multi-speed transmission, the world first vehicle was directly driven by an engine. The drawback was obvious, the engine output torque was too small and the speed was too fast to launch the vehicle smoothly. To solve this problem, French inventors Louis-Rene Panhard and Emile Levassor demonstrated their three-speed transmission in 1894, about two decades later than the first appearance of the modern vehicle. After that, various transmission types, such as MT, AT, AMT, DCT, CVT, were developed and applied on the vehicle. The reason why transmission is still an indispensable part in a vehicle today is the gasoline engine is not perfect. As shown in Fig. 4-1, it cannot output enough torque to launch the vehicle smoothly. Consequently, the purpose of transmission is to transfer certain power from the power source to the wheels at a proper torque and rotating speed.
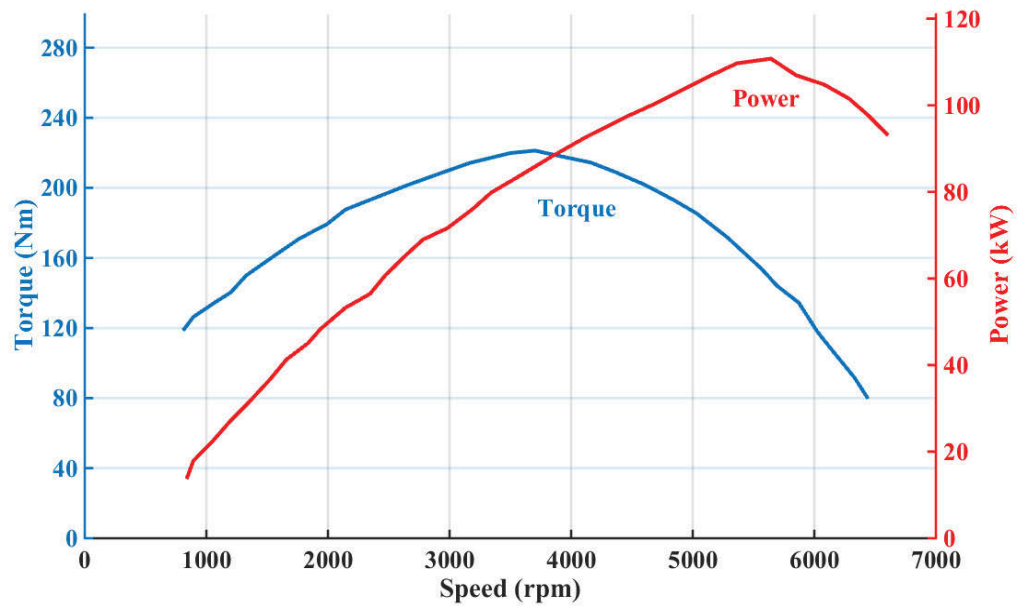
Figure 4-1: Typical gasoline engine power and torque curves [70]

With the emerging and booming of electric vehicles on the global market, especially in the US, Europe, Japan and China, the first generation modern BEVs are fitted with fixed ratio transmissions as a result of the enhanced capabilities of the electric machine over ICEs. Such vehicles were able to attain a satisfactory driving experience whilst offering an acceptable price.

It is very true that electric motors have a relatively higher wide operating range and higher average operating efficiency compared to the ICE, but it does not mean that electric motors are equally efficient at all driving speeds and torques. There are growing concerns from the manufacturers and researchers about whether the motor needs a transmission to adjust the output torque and speed. Additionally, considering the poor mileage per charge and the expensive battery pack, the application of multi-speed transmissions for BEVs has the potential to enhance the running range or even reduce

the required motor and battery size [71,72]. The integration of multi-speed transmissions to BEVs' powertrain systems in place of fixed ratio reduction transmissions is considered as a feasible method to improve powertrain efficiency and extend limited driving range for a fixed battery size. The aim of this chapter is to enable the researchers or BEV manufacturers, especially for transmission system OEMs, to estimate whether their products are worthwhile for the customer in terms of the price/performance relationship to others' design solutions. To do so a generic battery electric vehicle is modelled in Matlab/Simulink® to predict motor efficiency and energy consumption for single reduction, two-speed DCT and simplified Continuous Variable Transmission (CVT) equipped battery electric vehicles. A credible conclusion is made, through experimental validation of single speed and two-speed DCT scenarios and reasonable assumptions to support the CVT scenario, that both two-speed DCT and simplified CVT improve the overall powertrain efficiency, save battery energy and reduce customer costs. However, each of the configurations has unique cost and energy consumption related trade-offs.

This chapter is divided into four parts. Firstly, alternative electrified powertrains configurations such as fixed ratio single, two-speed DCT and simplified CVT are introduced and compared. Then, the energy loss in DCT and CVT, which is the weakness of multi-speed transmission comparing to single reduction, are elaborated. The gear ratios of individual transmission types are designed to meet the particular vehicle target performance. Finally, the economic and dynamic performance of BEV equipped with different transmissions are simulated in a backward-facing EV model.

The outcomes from typical and combined driving cycles show a significant benefit achieved in BEVs, which adopt multi-speed transmissions.

4.2 CONFIGURATIONS OF SINGLE REDUCTION AND MULTI-SPEED ELECTRIFIED POWERTRAINS

4.2.1 Fixed ratio single reduction BEV powertrain

Traction motor has the ability to supply maximum torque constantly from the very beginning until its rotation speed reaches a rated value. Then, the motor continues to output constant power with increasing speed. Thanks to this excellent dynamic performance, single reduction based BEV can meet the basic requirement of most users. Furthermore, even some extreme conditions can be covered as well when the motor operates in the over-load zone. Additionally, to increase the popularity and market share of this new energy vehicle, keep the price close to or at least not much higher than the same class traditional vehicle is very important. Therefore, most of the passenger electric vehicle on the market, such as VW e-Golf, Nissan Leaf, Tesla, BMW i3 and BYD E6, choose to use single reduction (SR) instead of multi-speed transmission. Fig.4-2 demonstrates a typical single speed powertrain including one fixed ratio and one final drive ratio. Additionally, as the motor has the capability to reverse rotation, the reverse shaft is eliminated in all BEVs.
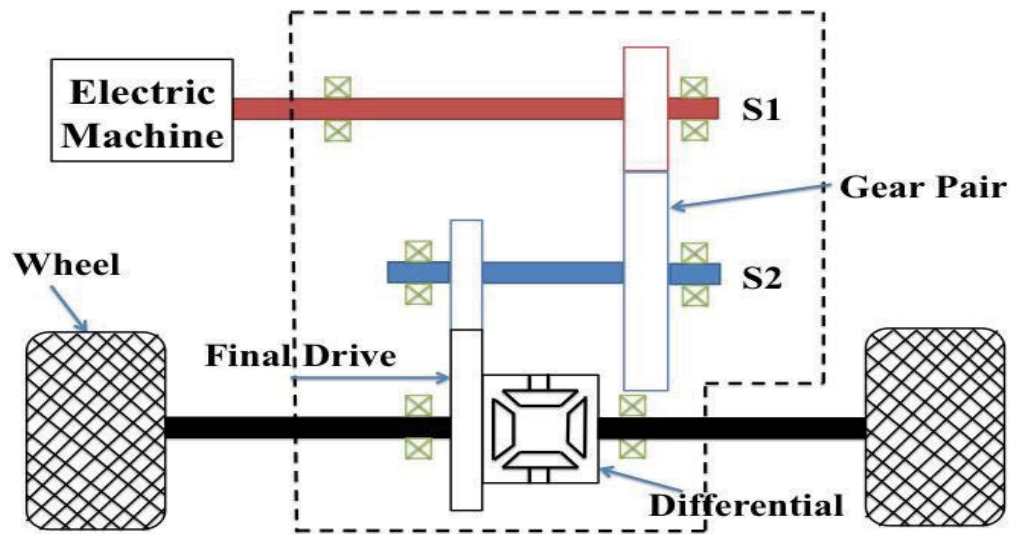
Figure 4-2: Single Speed Reduction in BEV Powertrain

4.2.2 Two-Speed DCT Electrified Powertrain

Although a more complicated transmission means additional cost, the potential of higher motor operating efficiency and reduced requirement for motor and battery capacity may pay back the extra cost eventually. At the same time, the user can enjoy a better driving experience.

DCT has the ability to transfer torque from one clutch to another with little interrupting of traction, thanks to controlling slippage of clutches. Two clutches engage alternatively and one of them will pre-engage before the other one disengages to eliminate torque interruption during shifting [73]. The heart of the two-speed DCT model design is the two clutches have a common drum attached to the input shaft from the motor, and the friction plates are independently connected to 1st and 2nd gear respectively. Thus, the

synchronizer will be removed from this DCT [74,75]. Analysis and modelling of transit shift situation in two-speed DCT equipped EV is proposed by [76]. Based on excellent output torque characteristics on starting period and an economy performance oriented shifting schedule, two-speed DCT will be validated against several alternative driving cycles in this chapter.

Fig.4-3 presents the structure of a front wheel drive two-speed DCT based powertrain of BEVs. With a common drum attached to the input shaft of the motor, the friction plates of two clutches are connected to the first and second gears directly. The uniqueness of this two-speed DCT powertrain is that it takes advantage of seamless clutch to clutch shifting, and with only two speeds added, the complexity for the synchroniser and its control is eliminated. Therefore, gear shifting is realized through dual clutch control only. The clutches are denoted with C1 and C2. S1 & S2 are the solid and hollow input shafts; S3 is the output shaft of DCT.
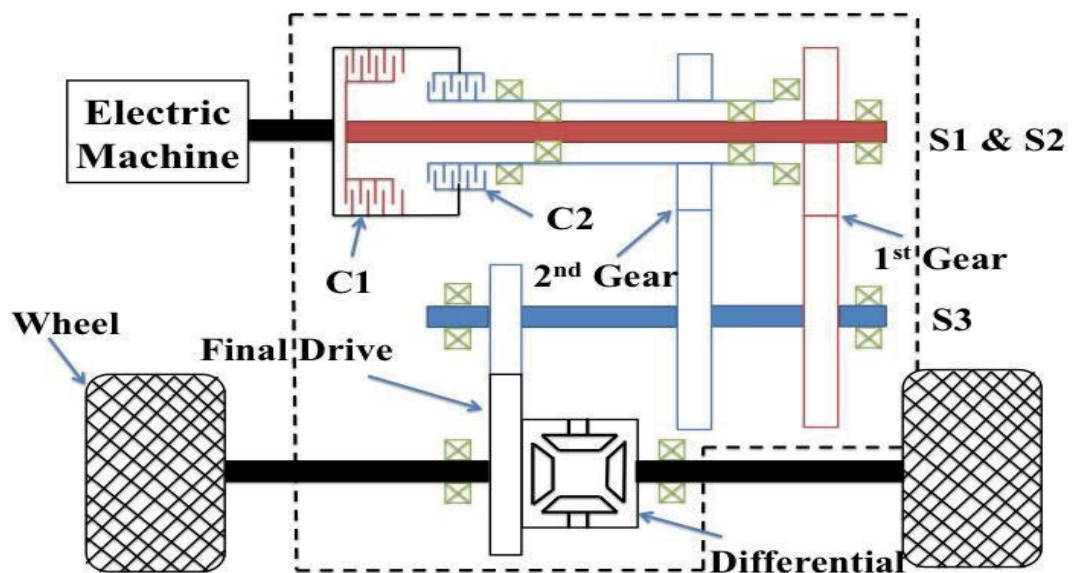
Figure 4-3: Two-speed Dual Clutch Transmission in BEV Powertrain

The major power losses in the transmission system comprise gear mashing, churning & windage, viscous shear, bearing and oil seal, power wasted by disengaged gear sets, which are shown in Eq. (1):

$$P_{loss} = \sum P_{gear\_mesh} + P_{churning} + P_{con} + \sum P_{Bearing} + P_{disengage\_gear} \tag{1}$$

P_{loss} represents the total power losses in gearbox; $\sum P_{gear\_mesh}$ is the sum of power losses in all gear meshing; P_{con} represents the power losses occurred in the concentric shaft; $P_{churning}$ is the power losses generated by churning and windage; $\sum P_{Bearing}$ is the sum of all bearings' drag torque; $P_{disengage\_gear}$ represents the power losses occurred in the disengaged gear set.

No matter which gear is selected to transfer the torque and rotation, all gear pairs in different gear numbers are always meshed. The gear selection process is controlled by shifting program and completed by fork and synchronizer. Therefore, although only one gear pair can be selected at one time, the other unselected and disengaged gear sets are still rotating with gearbox input shaft together in particular ratios. Driving these unutilized gear pairs introduces unnecessary power and torque loss. Specific to the two-speed DCT, if the vehicle runs in 1st gear, the power wasted by 2nd gear is expressed as:

$$\left(T_{in} - T_{con} - T_{bearing(1,2)}\right) \times r_1 = T_{1\_output\_outer} \tag{2}$$

$$\begin{aligned}
\Big[T_{1_{output_{outer}}} - T_{gearmesh_1} - T_{bearing(6,7)} \\
- \left(T_{gearmesh_2} + T_{disengage_{gear_2}} + T_{bearing(3,4,5)} \right) \times r_2 \Big] \\
= T_{2\_output} \times r_{main}
\end{aligned} \qquad (3)$$

$$T_{2\_output} - T_{gearmesh_{main}} - T_{ch} - T_{bearing(8,9)} = T_{final\_output} \qquad (4)$$

T_{in} is the gearbox input torque; T_{con} is the torque lost in concentric shaft viscous shear resistance; $T_{bearing}$ represents the drag torque generated by bearings; r is overall gear ratios of 1st or 2nd gear combined with final ratio; $T_{1\_output\_outer}$ is the output torque of the outer concentric shaft; $T_{gearmesh}$ represents the torque losses in gear pair meshing; $T_{disengage}$ is the torque consumed in unengaged wet clutch pairs. $T_{churning}$ is the drag torque generated by churning. In terms of power, the losses can be achieved by using Eq.5:

$$P_{losses}(kw) = \frac{T_{losses} \times n(rpm) \times 2 \times Pi \times r}{60 \times 1000} = \frac{T_{losses} \times n(rpm)}{9550} \qquad (5)$$

Consequently, the individual component power losses with engaged 1st gear are:

$$P_{con} = \frac{T_{con} \times n_{motor}}{9550} \qquad (6)$$

$$\sum P_{Bearing}$$
$$= \frac{\left(T_{bearing(1,2)} n_{motor} + T_{bearing(3,4,5)} n_{motor} \frac{r_2}{r_1} + T_{bearing(6,7)} \frac{n_{motor}}{r_1} + T_{bearing(8,9)} \frac{n_{motor}}{r_1 r_{main}} \right)}{9550} \qquad (7)$$

$$\sum P_{Gearmesh}$$
$$= \frac{T_{gearmesh\_1} \frac{n_{motor}}{r_1} + T_{gearmesh\_2} n_{motor} \frac{r_2}{r_1} + T_{gearmesh\_final} \frac{n_{motor}}{r_1 \times r_3}}{9550} \tag{8}$$

$$P_{churning} = \frac{T_{churning} \times n_{motor}}{r_1 \times r_{main} \times 9550} \tag{9}$$

$$P_{disengage\_gear} = \frac{T_{disengage\_gear\_2} \times n_{motor} \times r_2}{r_1 \times 9550} \tag{10}$$

In the same way, the individual power losses with engaged 2nd gear and disengaged 1st gear are:

$$P_{con} = \frac{T_{con} \times n_{motor}}{9550} \tag{11}$$

$$\sum P_{Bearing}$$
$$= \frac{\left(T_{bearing(1,2)} n_{motor} \frac{r_1}{r_2} + T_{bearing(3,4,5)} n_{motor} + T_{bearing(6,7)} \frac{n_{motor}}{r_2} + T_{bearing(8,9)} \frac{n_{motor}}{r_2 r_{main}}\right)}{9550} \tag{12}$$

$$\sum P_{Gearmesh}$$
$$= \frac{T_{gearmesh\_1} n_{motor} \frac{r_1}{r_2} + T_{gearmesh\_2} \frac{n_{motor}}{r_2} + T_{gearmesh\_main} \frac{n_{motor}}{r_2 r_{main}}}{9550} \tag{13}$$

$$P_{churning} = \frac{T_{churning} \times n_{motor}}{r_2 \times r_{main} \times 9550} \tag{14}$$

$$P_{disengage\_gear} = \frac{T_{disengage\_gear\_2} \times n_{motor} \times r_1}{r_2 \times 9550} \tag{15}$$

From the viewpoint of overall transmission, the efficiency is defined as:

$$E_{transmission} = \frac{n_{final} \times T_{final}}{n_{motor} \times T_{motor}} \qquad (16)$$

The above equations demonstrate the constituent parts of power losses in transmission. Specific to individuals, there are many factors which will determine their performance.

4.2.2.1 Energy losses in gears

The torques losses are generated in gears comprise meshing, windage and churning. Load depended meshing losses come from sliding and rolling in gears. Gear rotation in fluid causes the churning and windage power losses.

Gear mesh

The friction of rolling and sliding between gears pairs are the main power losses in meshing. In this study, the following shown equations, which were proposed by the British Standard Institution, are selected to calculate the power losses in gear meshing for their rigorous development and convincing experimental results [77].

$$P_m(kW) = \frac{f_m \times T_1 \times n_1 \times cos^2\beta_w}{9550M} \qquad (17)$$

where P_m represents the total power losses in gear meshing; the friction coefficient f_m can be obtained by using following Eq.18, if the gear meshing meets particular conditions, which is actually a normal meshing process.

$$\begin{cases} f_m = \dfrac{v^j K^g}{C_1 V^h} \\ 2\,m/s < V < 25 m/s \\ 1.4\,N/mm^2 < K < 14\,N/mm^2 \end{cases} \quad (18)$$

v^j is the temperature based kinematic viscosity of lubricant in transmission, mm²/s; j, g, h, C_1 are constant and equal to -0.223, -0.4, 0.7 and 3.239 respectively; V^h is the tangential velocity of pitch line in m/s; K-factor is represented by K^g and determined by the following equation:

$$K = \frac{100 T_1 (z_1 + z_2)}{2 \beta_w r_{w1}{}^2 z_2} \quad (19)$$

T_1 is pinion torque; n_1 stands for the pinion rotational speed in revolutions per minute; β_w is the operating helix angle, the unit is degree; M represents the meshing mechanical advantage, which can be obtained by sliding ratios based Eq. 32; r_{w1} is the pinion outside radius (mm). Additionally, Eq.21 and 22 are used to calculate the sliding ratios of external gears and recess action respectively:

$$M = \frac{2 \cos \alpha_\omega (H_s + H_t)}{H_s{}^2 + H_t{}^2} \quad (20)$$

$$H_s = (r + 1) \left[\left(\frac{r_{o2}{}^2}{r_{w2}{}^2} - cos^2 \alpha_w \right)^{0.5} - \sin \alpha_\omega \right] \quad (21)$$

$$H_t = \frac{(r + 1)}{r} \left[\left(\frac{r_{o1}{}^2}{r_{w1}{}^2} - cos^2 \alpha_w \right)^{0.5} - \sin \alpha_\omega \right] \quad (22)$$

$$r = \frac{z_2}{z_1} \qquad\qquad (\,23\,)$$

α_ω represents the angle of transverse operating pressure in degree; H_s and H_t are the sliding ratios at the beginning of approach action and at the end of recess action respectively; r is the ratio of currently meshed gear pair, which is achieved by Eq.24; r_{o1} and r_{w1} are the pinion outside radius and pinion operating pitch radius in mm; r_{o2} and r_{w2} stands for the outside radius and operating pitch radius of meshed gear; z_1 and z_2 are the numbers of gear teeth and pinion teeth.

Gear windage and churning

Gear windage losses at different rotation speeds, e.g. roughly high, mid and low, were demonstrated by Dawson [78], Diab et al. [29], Eastwick and Johnson [79] respectively, where it became gradually more prominent in high speed. For the churning loss, both Changenet and Velex [80] and British Standards [77] presented a study for a general gear box. However, the formulas presented in [80] assumed that all the gears are submerged in the fluids, and too many parameters are required to be validated to get a reasonable practical dimensionless drag torque coefficient Cm. Considering the rigors and universality of standard models, British Standards formulas are adopted here. As shown in [77], a gear dip factor, fg, must be considered before obtaining gear windage and friction loss. This factor is based on the amount of dip that the element has in the oil. When the gear or pinion does not dip in the oil, $f_g = 0$. When the gear dips fully into the oil, $f_g = 1$. When the element is partly submerged in the oil, linearly interpolation between 1 and 0 is used to acquire the transient gear dip factor. The primary dip factor of the final gear is 0.21. The higher the speed, the smaller the dip factor becomes. When

the speed increases, it will range from 0.21 to 0.1 according to the speed. The primary depth value with 0.21 is calculated via opening the transmission, and measuring the height of the shaft, gear size and the oil tube. The final 0.1 is an estimated value after debugging the model [81]. The power loss equation for the tooth surface is named as a roughness factor R$_f$. Eq.24 is a reasonable approximation of the values from Dudley's model.

$$R_f = 7.93 - \frac{4.648}{M_t}$$ (24)

where R_f is the roughness factor, M_t is transverse tooth module (mm).

Power losses generated by gear windage and churning comprise three primary parts: power losses in smooth outside diameter, smooth side of disc and teeth surface. The amount of power losses in smooth outside diameter, e.g. outside diameter of shaft, is:

$$P_{gearmesh} = \frac{7.37 \times f_g \gamma n^3 D^{4.7} L}{A_g \times 10^{26}} \ (kw)$$ (25)

The power losses in smooth side of disc such as gear face are:

$$P_{gearmesh} = \frac{1.474 \times f_g \gamma n^3 D^{5.7} L}{A_g \times 10^{26}} \ (kw)$$ (26)

The power losses in teeth surface are:

$$P_{gearmesh\_i} = \frac{7.37 \times f_g \gamma n^3 D^{4.7} F \left(\frac{R_f}{\tan \beta}\right)}{A_g \times 10^{26}} \ (kw)$$ (27)

where $P_{gearmesh\_i}$ is the power loss of each individual gear, kW; f_g is the gear dip factor; D represents the outside diameter of gear in mm; A is constant and equals to 0.2; F is the face width in mm; L represents the length of the gear in mm; β is the generated helix angle in degrees.

4.2.2.2 Bearing and oil seal model

The bearing loss in varieties of bearing designs have been analyzed [82], considering both viscous friction caused torque and applied load generated torque. This work is widely accepted as the forefront on the topic, with similar results being applied in works [83,84]. Eq.28-31 are selected in this study to simulate the power losses in the bearing model, which are widely used in the German gear industry [77].

Load based bearing power losses:

$$P_{bearingloss\_load} = f_L F_b D_m \qquad (28)$$

Speed based bearing power losses:

$$P_{bearingloss\_speed} = \begin{cases} 1.6 \times 10^{-8} f_0 D_m{}^3 & n < 20000 \\ 10^{-10} f_0 n^{2/3} D_m{}^3 & n \geq 20000 \end{cases} \qquad (29)$$

The adjustable factor f_0 represents the bearing dip condition. It varies from $f_{0(min)}$ to $f_{0(max)}$ depending on if the rolling elements dip into the lubricant oil [15].

The oil seal power loss is expressed in the following equation [77]:

$$P_{oil} = 7.69 \times 10^{-6} \times v_{oil} \times d_m{}^2 \qquad (30)$$

The total power losses in bearing and oil seal are the sum of the above three equations:

$$P_{b\_o} = P_{bearingloss\_load} + P_{bearingloss\_speed} + P_{oil} \qquad (31)$$

4.2.2.3 Concentric shaft drag torque

The 'Couette flow' proposed by Schlichting in [85] defined the critical Taylor's number—1708—is bigger than 779, which is the corresponding value of maximum test input speed, 4000 rpm. Therefore, the drag torques generated in concentric shafts is:

$$T_{con} = 4\pi\mu h_{con} \frac{R_{con\_o}{}^2 \times R_{con\_i}{}^2}{R_{con\_o}{}^2 - R_{con\_i}{}^2} \Delta\omega \qquad (32)$$

R_{con_o} and R_{con_i} are the inner radius of the outer shaft and outer radius of the inner shaft respectively; $\Delta\omega$ is the relative speed between two concentric shafts; h represents the concentric length; continuous flow lubricated annular area is a precondition in this equation.

4.2.2.4 Drag torque within multi-plates wet clutches

The theories for the clutches drag torque within wet multi-plate-transmission have been discussed by many researchers in the past decades. The governing equations presented by Hashimoto et al. [86] described the flow between adjacent flat rotating plates which has laid down a framework for subsequent clutch studies. Then Kato et al. [87] explained oil film shrinking between two adjacent clutch plates due to centrifugal force which is widely accepted and referred to. Kitabayashi et al. [88] demonstrated the drag

torque which is accurate in low-speed ranges, but it is not accurate for predicting drag torque at high-speed region as it can only show the rising portion of a typical drag torque curve at the low-speed region when the clearance is full of the oil film. A new shrinking model was promoted with a reasonable accuracy at both low and high speeds, which was conducted by Li et al. [89] based on analytical and experimental investigation.

Before starting the analyzing of power losses in a disengaged wet clutch, there are some preconditions:

1. Lubricant fluid is incompressible and in steady state;

2. Fluid flow in the wet clutch clearance is laminar and symmetrical;

3. Gravity is neglected;

4. Wet clutch plate is un-grooved;

5. Friction plate and counter plate do not glide with their surfaces' oil layer;

Not like the traditional AT, DCT has two concentric shafts connecting clutches to odd and even gear pairs alternatively in sequence. These two shafts are always rotating together, but at different speeds, through the constant mesh gear pairs as shown in Fig.4-4 and Fig.4-5. Consequently, the relative speed between each shaft will generate viscous shear resistance.

When vehicle runs in 1st gear, C1 is engaged and C2 is open, as shown in Fig.4-4. Then,

$$\begin{cases} \omega_1 = \omega_0 \\ \omega_2 = \omega_1 \times \dfrac{r_2}{r_1} \end{cases} \qquad (33)$$

Then, the relative speed between the input clutch plates and the 2nd output clutch plates is:

$$\Delta\omega = \omega_1 - \omega_2 = \omega_1 - \omega_1 \times \frac{r_2}{r_1} = \omega_0 \left(\frac{r_1 - r_2}{r_1}\right) \qquad (34)$$

Similarly, when C2 is engaged and C1 is open, as shown in Fig.4-5, the relative speed is:

$$\Delta\omega = \omega_2 - \omega_1 = \omega_2 - \omega_2 \times \frac{r_1}{r_2} = \omega_0 \left(\frac{r_2 - r_1}{r_2}\right) \qquad (35)$$
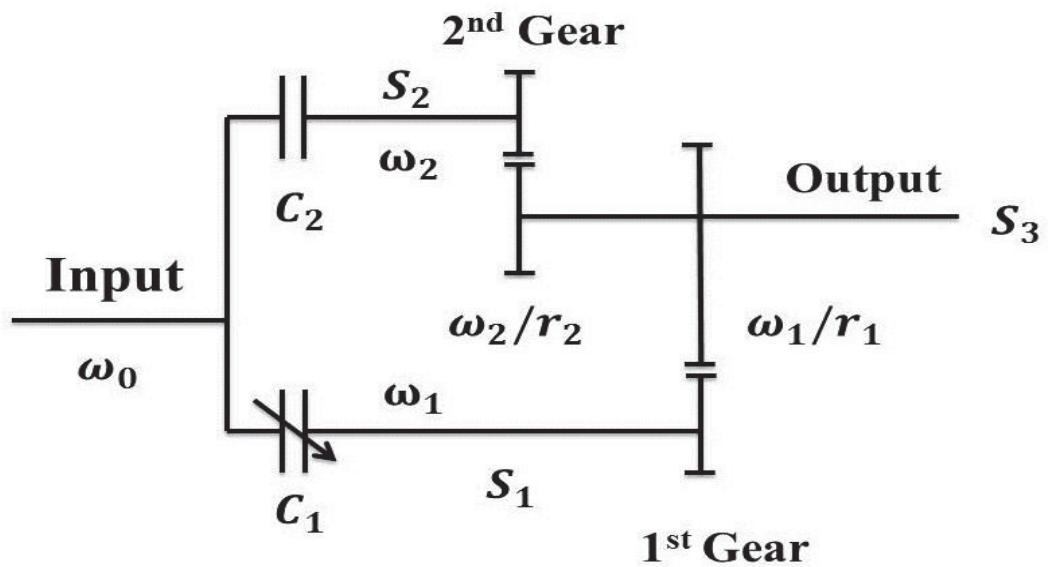
Figure 4-4: Schematics of two-speed DCT, clutch 1 closed, clutch 2 open
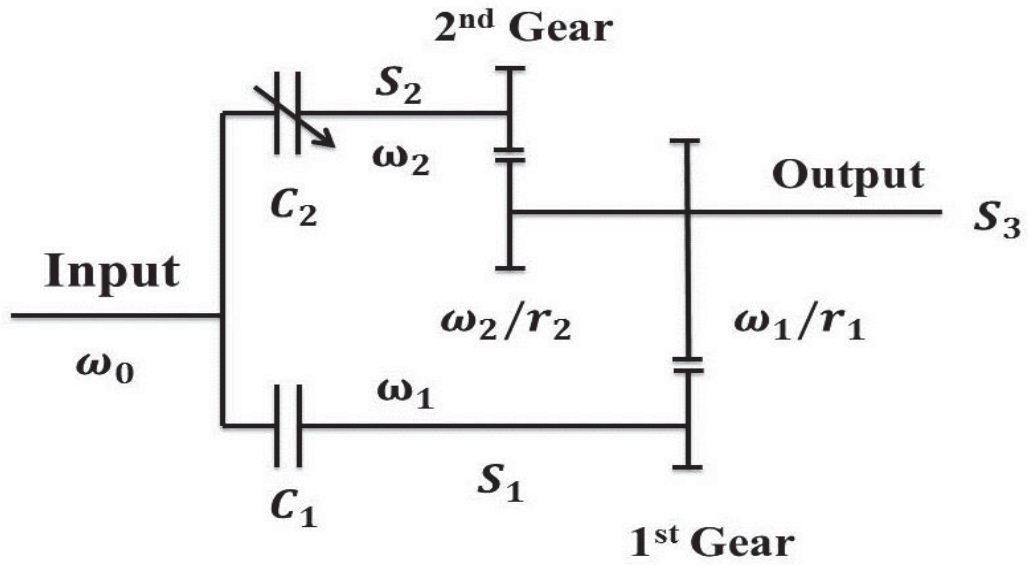
Figure 4-5: Schematics of two-speed DCT, clutch 2 closed, clutch 1 open.

The following equations, which are based on the [89,90], are used to obtain the drag torque in terms of multi-plate:

$$\tau_{\theta z} = \mu \frac{\partial V_\theta}{\partial Z} |z = h_c = \frac{\mu \Delta \omega r}{h_c} \qquad (36)$$

$$T_{disengage\_gear} = 2\pi N \int_{R_1}^{R_0} r^2 \tau_{\theta z} dr = \frac{\pi \mu \Delta \omega N}{2h_c} \left(R_o{}^4 - R_i{}^4 \right) \qquad (37)$$

N is the number of plates, which is equal to 2 in this study; R_i and R_o are the inner and outer oil film radius; μ is the viscosity of the lubricant oil; h_c represents the clearance of clutch plate.

Substitute Eq.34 and Eq.35 into Eq.37, the wet clutch torque losses with engaged 1st and 2nd gear are expressed as:

$$T_{disengage\_gear2} = \frac{\pi\mu\Delta\omega N}{2h_c}\left(R_o{}^4 - R_i{}^4\right)$$

$$= \omega_0\left(\frac{r_1 - r_2}{r_1}\right) \times \frac{\pi\mu N}{2h_c}\left(R_o{}^4 - R_i{}^4\right)$$

(38)

$$T_{disengage\_gear1} = \frac{\pi\mu\Delta\omega N}{2h_c}\left(R_o{}^4 - R_i{}^4\right)$$

$$= \omega_0\left(\frac{r_2 - r_1}{r_2}\right) \times \frac{\pi\mu N}{2h_c}\left(R_o{}^4 - R_i{}^4\right)$$

(39)

When the clearance is full of oil film, i.e. $r = R_i$, the required input lubricant fluid flow

rate is [89,90]:

$$Q = \frac{\frac{6\mu}{\pi h_c{}^3}\ln\frac{R_i}{R_o} + \sqrt{\left(\frac{6\mu}{\pi h_c{}^3}\ln\frac{R_i}{R_o}\right)^2 - \frac{81\rho\Delta\omega\left(R_0{}^{-2} - R_i{}^{-2}\right) - 540\left(R_0{}^{-2} - R_i{}^{-2}\right)\nabla p}{700\pi^2 h_c{}^2}}}{\frac{27\rho}{70\pi^2 h_c{}^2}\left(R_0{}^{-2} - R_i{}^{-2}\right)}$$

(40)

Apparently, except for some constant characteristics of lubricant fluid and shaft, the

required fluid flow rate is determined by the varying clutch angular velocity, $\Delta\omega$. The

relationship of $\Delta\omega$ and required flow rate is presented in Fig.4-6. [89,90]
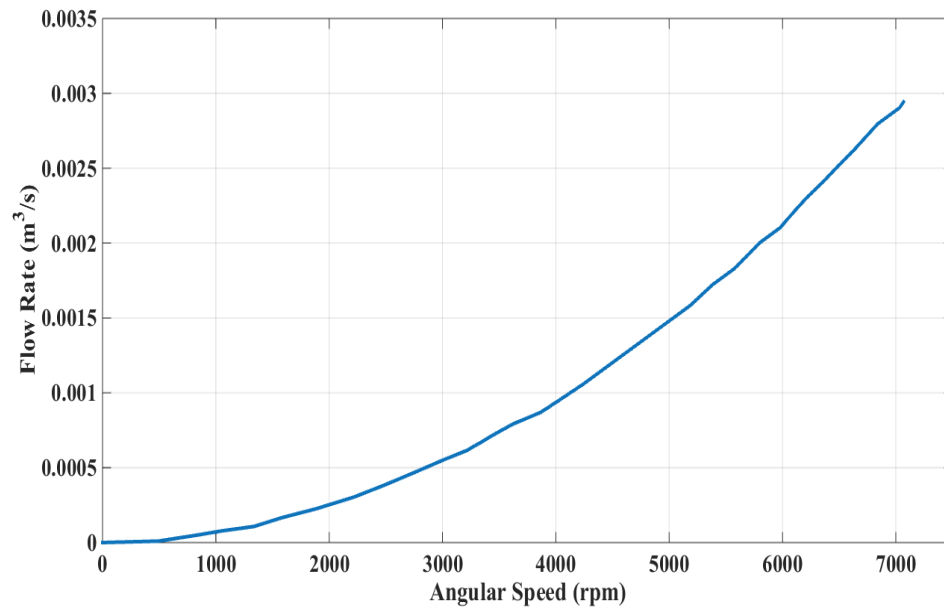
Figure 4-6: Required flow rate VS clutch angular speed

The required input flow rate of full oil film between plates increases in proportion to the growing rotation speed. The oil firm will shrink when the actual flow rate cannot meet the requirement. However, the fluid flow rate is deliberately kept constant in practice. When the vehicle accelerates, clutch angular velocity goes higher and higher. The oil film will shrink because the actual flow rate cannot catch up to the theoretical required flow rate. If the required value is Q, the actual value is Q_i, the outer oil film radius is R_0:

If $Q_i > Q$,

$$R_0 = R_2 \qquad\qquad (41)$$

If $Q_i < Q$, a special equation is used to express the relationship of oil flow rate and equivalent oil radius:

$$\frac{Q_i}{Q} = \frac{R_0{}^2 - R_1{}^2}{R_2{}^2 - R_1{}^2} \qquad (42)$$

Rearrange the Eq.42:

$$R_0 = \sqrt{\frac{Q_i}{Q}R_2{}^2 + R_1{}^2\left(1 - \frac{Q_i}{Q}\right)} \qquad (43)$$

In transmissions, if the input speed from the motor is same, as r_1 is larger than r_2, it comes out that $\Delta\omega_{c2} > \Delta\omega_{c1}$. Thus the relative rotational speed for clutch 2 (run with 2nd gear) is always larger than that of C1 (1st gear). If the effective radius of clutch 1 and clutch 2 are the same, the drag torque in the 2nd gear should be larger than that of 1st gear. However, the effective radius of plates in clutch 2 of this particular DCT is larger than that of C1. Therefore, the final drag torque will be determined by both of the differences in effective radius and gear ratios.

The above work about DCT energy losses was conducted by Jiageng Ruan and Dr.Xingxing ZHOU jointly.

4.2.3 Simplified CVT Electrified powertrain

CVT has the ability to adjust gear ratios without interruption of the power flow and an infinite number of ratios are possible. The basic configuration of CVT comprises two variable diameter pulleys kept at a fixed distance apart and connected by a power-transmitting device, e.g. belt or chain. One of the sheaves on each pulley is movable. The belt/chain can undergo both radial and tangential motions depending on the torque

loading conditions and the axial forces on the pulleys. This consequently causes continuous variations in the transmission ratio to keep ICE or motor running around most efficient area [91]. Due to the mechanical layout and the need of torque converter to work with ICE vehicles, the efficiency of CVT is typically lower than that of SR system, and inevitability suffers from poor speed response [22–24], particularly at launch [25]. The torque and rotation transferred from driving pulley to driven pulley depends on the clamping force between melt belt and conical surface of pulley. For a given coefficient of friction, the required minimum clamping force increases in a linear fashion as torque amplifying ratio increases. Therefore, adjustable clamping force and movable pulleys need an additional hydraulic system, which reduces the efficiency of the integrated transmission system.

The key to CVT lies in its simple yet effective belt-pulley design. The transmission ratio between the motor and driven wheels varies in a smooth manner in relation to the variable axial gap between the pulleys. Considering the advantage of excellent motor dynamic performance, e.g. 100% torque output ability from stall, accurate and fast adjusting ability and no limitation of minimum speed for steady running, the torque converter is not an essential component for EVs, while it is vital to CVT in ICE vehicles aiming at smooth launching and isolating vibration from the engine. However, CVT does not exhibit a higher overall efficiency than other automatic transmissions, because the driving torque is transferred through contact and friction. The primary efficiency losses in a traditional integrated CVT system comprises of hydraulic pump power loss, variator torque loss and torque converter power loss. Nevertheless, from the beginning of the 21st century to 2010s, lots of manoeuvres have been taken to improve the

efficiency. The overall efficiency was improved from less than 70% to more than 85% during the past decade [92–94]. Firstly, the axial displacement of moveable pulleys is implemented by two independent servo-electromechanical actuation systems, instead of the hydraulic-mechanical pump, which significantly reduces the power loss. The promoted structure, in this thesis, is an optimized version based on the principles and experimental results from published literature [92]. Then, restructured variator control circuit and optimized belt pressure control strategy help further increase the overall efficiency [93]. Another even more important improvement is that a torque converter is not a necessary part of BEVs' powertrain anymore and the ratio range could be narrow, thanks to the outstanding motor characteristics. Therefore, a lighter and more compact CVT is possible for BEVs. Moreover, an infinite number of transmission ratios help the motor to keep running at its optimum speed all the time. Thus, any increase in losses through the CVT, i.e. drag or control system, can be compensated through improved use of the motor, which leads to an improvement in overall powertrain efficiency.

In this study, efficiency improved and structure simplified CVT schematic is used and presented in Fig.4-7:
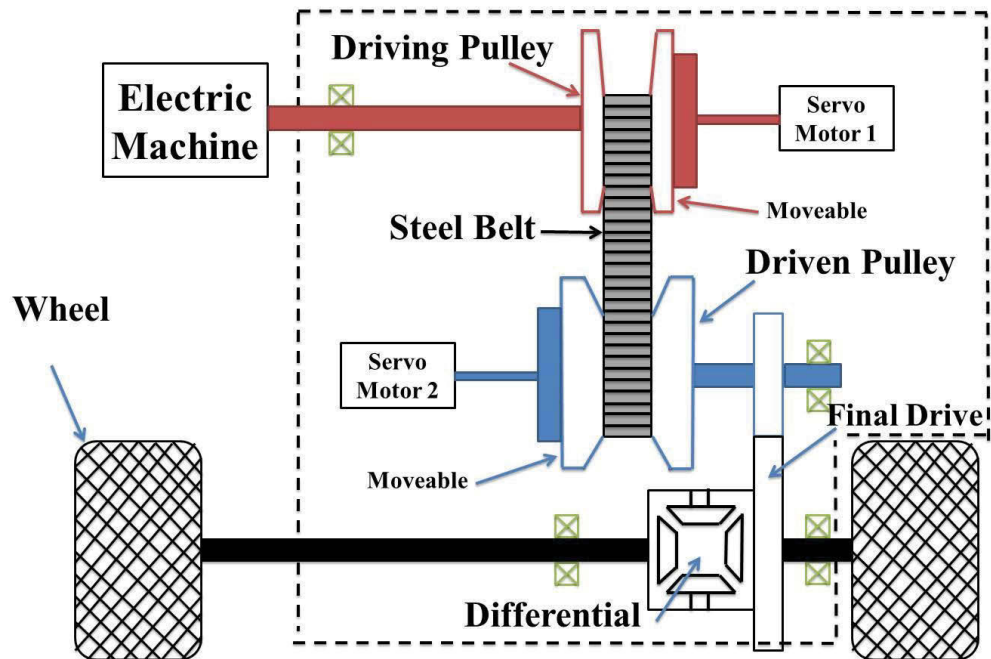
Figure 4-7: Continuously variable transmission with servo-electromechanical actuator

The main benefits of using two-speed DCT or CVT without torque converter powertrain in BEVs are:

1. Improved motor efficiency over the vehicle driving range;

2. Decoupled top speed and acceleration capabilities.

The disadvantages include:

1. Increased weight from additional components;

2. Poorer transmission efficiency;

3. Additional manufacturing costs.

Both the advantages and disadvantages need to be considered to evaluate the selected multi-speed transmissions for BEVs.

4.3 GEAR RATIOS DESIGN AND OPTIMIZATION

The basic vehicle information for BEV powertrain design is summarized as follows:

Table 4-1: Basic Vehicle Specification

Parameter	Description	Value	Units
m	Vehicle mass	1760	kg
r	Wheel radius	0.3125	m
i_g	Gear ratio		-
CR	Coefficient of rolling resistance	0.016	-
g	Gravity	9.81	m/s^2
φ	Road incline	-	°
Cd	Drag coefficient	0.28	-
A	Vehicle frontal area	2.2	m^2
u	Vehicle speed	-	m/s
V_{bat}	Battery voltage	380	V
C_{bat}	Battery capacity	72	Ah
E_{bat}	Battery energy content	27.4	kW·h

Table 4-2: BEV Performance Targets

Performance specification	Target performance
Acceleration 0-100km/h	12 s
Top speed	150 km/h

Range @ 60kph	150 km
Range NEDC	100 km
Maximum Grade	30% (@ 15km/h)

4.3.1 Ratio design for top speed

The maximum speed achieved in the vehicle of specifications Table.4-1 & 4-2 can be used to determine the upper limit of gear ratios:

$$V_{max} \gg \frac{N_{max} \times 2\pi r}{60 \times 3.6 \times i_g} = \frac{0.377 N_{max}(rpm)r}{i_g} \qquad (44)$$

$V_{max} = 150\ km/h,\ \ n_{max} = 8000\ rpm, r = 0.3125$ m are substituted in Eq.44:

$$i_g \leq 6.3 \qquad (45)$$

Additionally, from the viewpoint of motor efficiency, a lower speed, e.g. 5000-6000 rpm, should be utilized for a vehicle continuously running at 150 km/h. The required gear ratio should be lower further than 6.3.

4.3.2 Ratio design for maximum grade

The lower gear ratio limit is set based on the rolling resistance for a specified grade (Table 4-2) over the maximum motor torque multiplied by the overall powertrain efficiency. The relationship of minimum required gear ratio and driving grade is given in Eq.46. For low vehicle speeds, the aerodynamic drag is assumed to be zero. Considering the different efficiency of transmissions, $\eta = 0.8$ is selected in this

calculation for design redundancy. The required gear ratio to propel vehicle on 30% grade road at 15 km/h is expressed in Eq.47:

$$\frac{T_{motor}\eta i_g}{r} = \left(mgC_R \cos\varphi + mg\sin\varphi + \frac{C_D A}{21.15}u^2 + \delta m\frac{d_u}{d_t} \right) \tag{46}$$

$$i_{gmin} \geq \frac{rmg(C_R \cos\varphi + \sin\varphi)}{T_{motor-max}\eta} = 6.8 \tag{47}$$

Using the data provided in Tables 4-1 and Table 4-2, the minimum usable gear ratio for different grades are presented below.

Table 4-3: Road grade based gear ratio

Grade	Design ratio
30%	6.5
40%	8.7

However, as we can see from Fig.4-8, a typical motor characteristics map, motor available torque varies with speed. Motor can provide constant maximum torque from standstill to rated rotation speed. Then, the available torque decreases with motor speed rising.
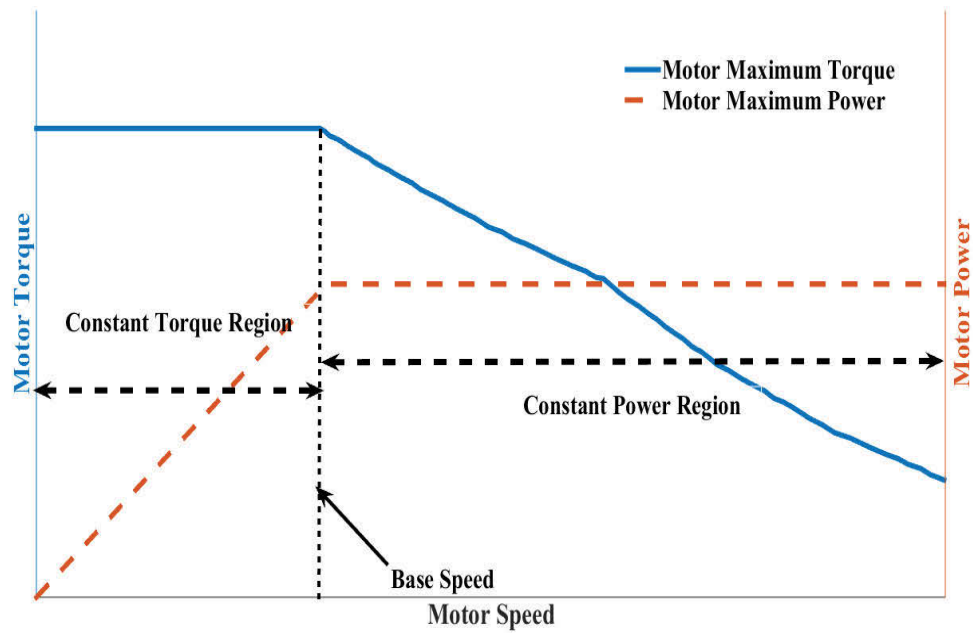
Figure 4-8: Typical Electric Motor Characteristic Map

Therefore, this ratio needs to make motor's operating speed lower than the rated speed to provide maximum torque during climbing. Substitute $u = 15$ km/h , $i_g = 6.8$, $\eta = 0.8$

$$n = \frac{15}{3.6} * \frac{60 \times 6.5}{2pi \times 0.3125} = 828 \quad (rpm) \tag{48}$$

As shown in Eq.48, the climbing motor speed is lower than the rated speed. Thus, Eq.47 can be used to determine the minimum gear ratio.

4.3.3 Ratio design for acceleration time

The acceleration time from 0 to 100 km/h is expressed in Eq.49 and Eq.50

$$\frac{d_u}{d_t} = \frac{f}{m} = \left[\frac{T_{m-max}\eta i_g}{r} - \left(mgC_R \cos\varphi + mg\sin\varphi + \frac{C_D Au^2}{21.15} + \frac{\delta m d_u}{d_t} \right) \right] \quad (49)$$

$$/m$$

$$t_{0-100} = \int_0^{100} \frac{21.15mr(1+\delta)}{21.15T_{m-\max}(v)i_g\eta - 21.15mrgC_R - C_D Arv^2} dv \quad (50)$$

The maximum variable motor torque T_{motor} through the speed range falls with speed more closely matches a straight line, which is shown in Fig.3-4 is expressed as following equation:

$$T_{m-max}(v) = \begin{cases} 300 & (n < 2500\ rpm) \\ 370 - 0.028n & (n \gg 2500\ rpm) \end{cases} \quad (51)$$

Thus, substitute Eq.51 and Eq.49 into Eq.50:

$$t_{0-100}$$

$$= \begin{cases} \displaystyle\int_0^{\frac{0.1178 \times 2500}{i_g}} \frac{21.15mr(1+\delta)}{21.15 \times 300 \times i_g\eta - 21.15mrgC_R - C_D Arv^2} dv \ (n < 2500) \\ \displaystyle\int_{\frac{0.1178 \times 2500}{i_g}}^{100} \frac{21.15mr(1+\delta)}{21.15\left(370 - \frac{0.028vi_g}{0.377r}\right)i_g\eta - 21.15mrgC_R - C_D Arv^2} dv \ (n \gg 2500) \end{cases} \quad (52)$$
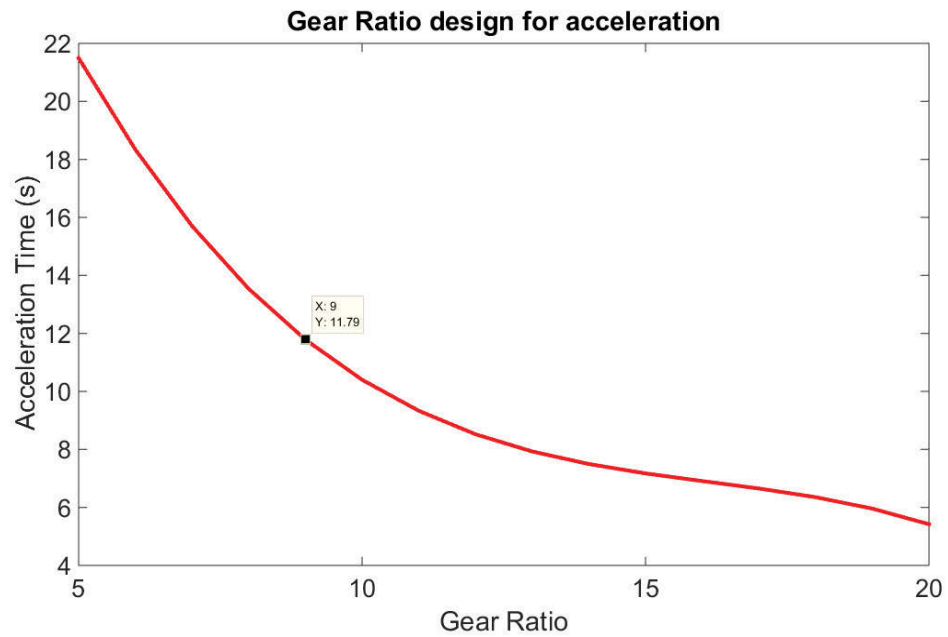
Figure 4-9: The relationship of 0-100 km/h acceleration time and gear ratio based on

motor specifications of Table.4-1

As shown in Fig.4-9, the gear ratio should be no less than 9 for a 12s or shorter 0-100

km/h acceleration time.

$$i \geq 9 \qquad\qquad (53)$$

4.3.4 Gear Ratio design for single reduction, two-speed DCT and CVT

Based on the above results, the gear ratio requirements for specifications of Table 4-1

are summarized:

$$\begin{cases} 150 \ km/h \ Top \ Speed: \ i_g \leq 6.3 \\ 30\% \ Climbing \ Grade: \ i_g \geq 6.8 \\ 12s \ 0-100 \ Acceleration: \ i_g \geq \ 9 \end{cases} \qquad (\ 54 \ )$$

The ratio requirement for top speed is in conflict with that for grade climbing and acceleration time in SR ratio design. It cannot be attained in one single ratio. It means an inevitable dynamic performance trade-off for SR transmission. For the two-speed DCT, 1st gear is selected for accelerating and climbing, thus meeting the last two requirements in Eq.54; 2nd gear is used to cruise at high speed, thus meeting the first requirement in Eq.54. The designed ratio coverage for CVT scenario is 5 (0.5-2.5) with a final ratio 4. Such value for mainstream and leading products are much higher than 5 [95], which means the special designed CVT in this study is lighter, cheaper and more compact.

In this study, the ratios of two-speed DCT are taken from 2nd and 3rd gear in DQ250, which is a six speeds wet clutch DCT used in VW Golf range. As the selected ratio for this study is limited to the designed system of the powertrain testing rig, to achieve a creditable result with minimum cost, the ratio of SR is selected as the same as the 1st gear ratio in two-speed DCT. This ratio supplies a fast acceleration time, better grade ability, but, a reduced top speed.

The following table lists all the ratios for SR, two-speed DCT and CVT (Incl. final drive):

Table 4-4: Gear ratios in different transmission systems

SR		Two speed DCT		CVT	
2.15	Final:3.93	1st : 2.15; 2nd : 1.46	Final:3.93	Pulley: 0.5~2.5	Final : 4
Total: 8.45		Total: 1st 8.45 2nd 5.36		Total: 2-10	

4.4 CVT OPTIMIZATION FOR BEV POWERTRAIN

Replacing fixed ratio single reduction with CVT will provide a feasible way to reduce the requirement of battery capacity and optimize motor operation efficiency area by a wide and continuously variable gear ratio. Table 4-5 shows a typical CVT specification on the market:

Table 4-5: Typical CVT specifications (A simplified model from Ref. [96])

Parameter	Description	Value
i_m	Main reduction ratio	4
i_{cvt}	CVT ratio varying range	0.5~2.5
$i_{converter}$	Torque converter ratio	1~2.2
η_{cvt}	CVT pulley-belt efficiency	0.9~0.95
$\eta_{converter}$	Torque converter efficiency	0~1

The economic performance of traditional CVT heavily relies on torque converter characteristics. The working stages of a torque converter can be roughly divided into three:

Stall: The prime mover is applying power to the impeller, but the turbine cannot rotate. At stall, the torque converter can produce maximum torque multiplication which lasts for a brief period. The efficiency is zero.

Acceleration: The load is accelerating but there still is a relatively large difference between impeller and turbine speed and it will decline accounting for the difference. The efficiency increases quickly from zero and the torque multiplication ratio drops from maximum value, e.g. 2.5 in this model.

Coupling (Lock-up): The speed of impeller and turbine are almost equivalent. The efficiency is almost 100% due to the mechanical lock between input and output shafts. There is no torque multiplication function in this period.

Fig.4-10 and Fig.4-11 demonstrate the hydrodynamic and torque amplifying performance attributes of a typical torque converter.
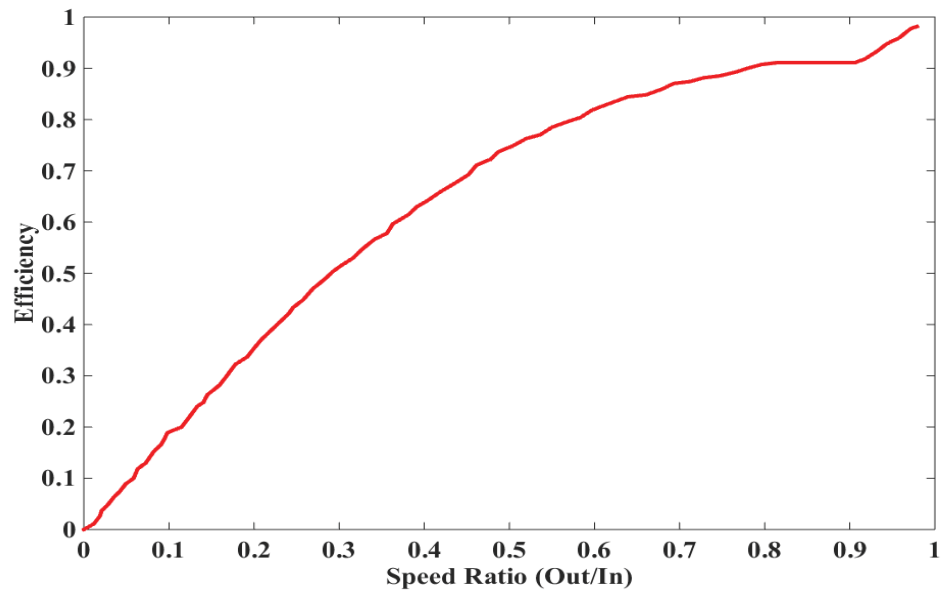
Figure 4-10: Speed ratio based torque converter efficiency [97,98]
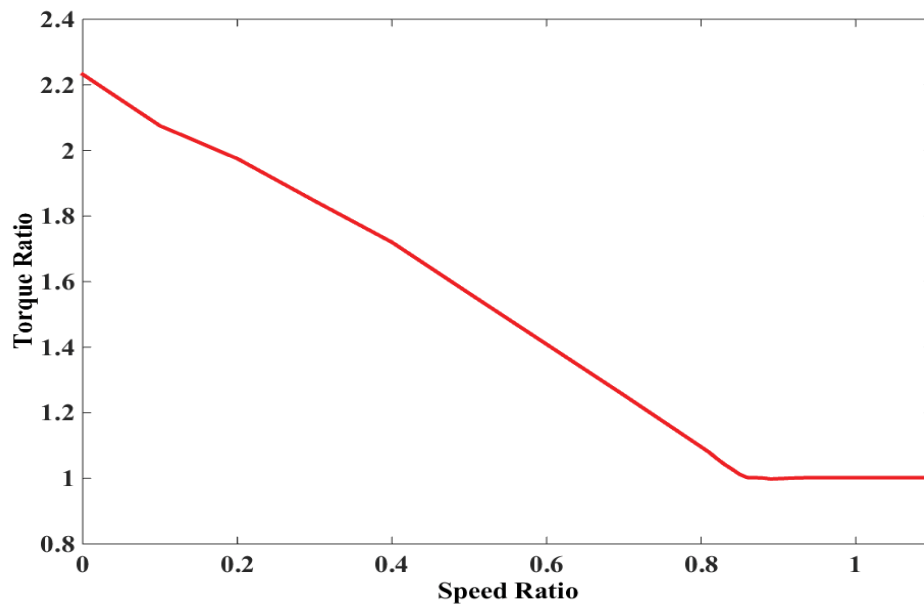
Figure 4-11: The relationship of torque ratio and speed ratio in torque converter [97]

The relative higher manufacturing cost and lower efficiency, comparing to an automatic transmission, constitute the primary barrier for the commercial popularization of CVT in the early days. For a traditional early version CVT powertrain, more than 30% of input power is wasted by internal hydraulic and mechanical components, i.e. hydraulic pump, torque converter, direction gear sets, friction between belt and variator which accounts for about 14%, 6%, 3% and 10% respectively [93], which is shown in Fig.4-12. The efficiency of the torque converter increases proportionally to output/input speed ratios from zero at stall to 100% when the turbine and impeller are locked together [99].
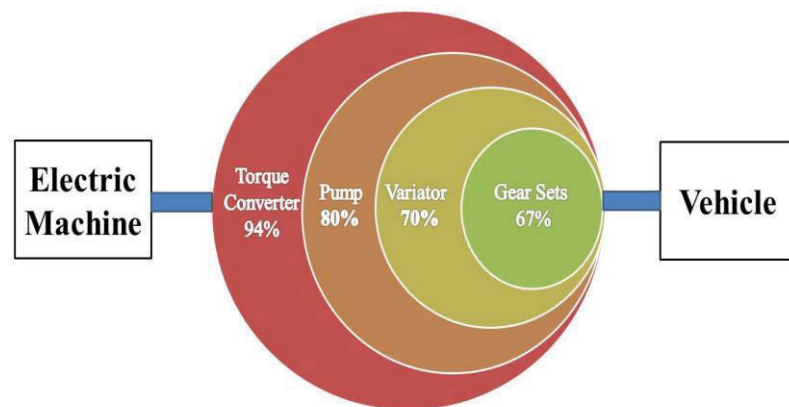
Figure 4-12: Remaining power after power loss in each component for a conventional CVT

However, CVT offers a great potential for efficiency improvement by introducing the electrified variator control system and optimized belt pressure control strategy, which were validated by both simulation and experiment. A load-dependent efficiency improvement for actuators from 25% to 50% can be achieved by using a servo-electromechanical mechanism, inside of the inefficient hydraulic ones, and optimizing melt belt push force control strategy [92,93]; additionally, a 2.7% efficiency benefit can be expected by restructuring the direction gear sets [93]. Furthermore, the eliminated power loss by removing the torque converter in this electrified drivetrain will make CVT more competitive. At last, the overall CVT efficiency, according to different load conditions, can be boosted to 83%-89% from less than 70% in early models.

An input torque and speed ratio-joint dependent Matlab/Simulink® model is established to precisely predict CVT efficiency in [100]. The bottom four dotted curves, in Fig.4-13, stand for the power loss in each CVT component at 1500 rpm input speed. The wasted power has already been reduced by above mentioned methods, i.e. electrified actuator, optimized belt pressure, restructured pressure control circuit and gear set. The reason why the last bottom dotted curve shows the variator power loss almost keeping constant is that the efficiency of variator is mostly determined by the speed ratio of driven/driving pulleys, rather than the input torque. The varying efficiency range of actuators (Pulleys), according to speed ratio, is represented by the top red solid curve. A conspicuous monotonic increase could be found in the influence of input torque to the first three components loss.
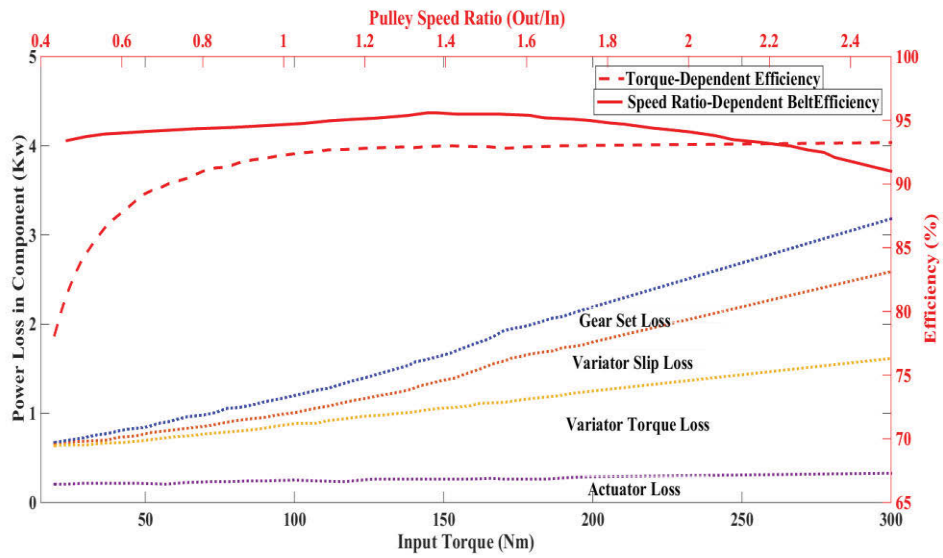
Figure 4-13: Component efficiency and power loss in CVT

Then, the torque and speed ratio dependent CVT efficiency are expressed by Eq.55, Eq.56 and Eq.57, which are used in simulation of Fig.4-14 model.

$$e_{torque} = \left(1 - \frac{\sum P_{loss}}{\frac{Tn}{9550}}\right) \tag{55}$$

$$e_{speedratio} = f(ratio) \tag{56}$$

$$e_{cvt} = e_{torque} \times e_{speedratio} \tag{57}$$
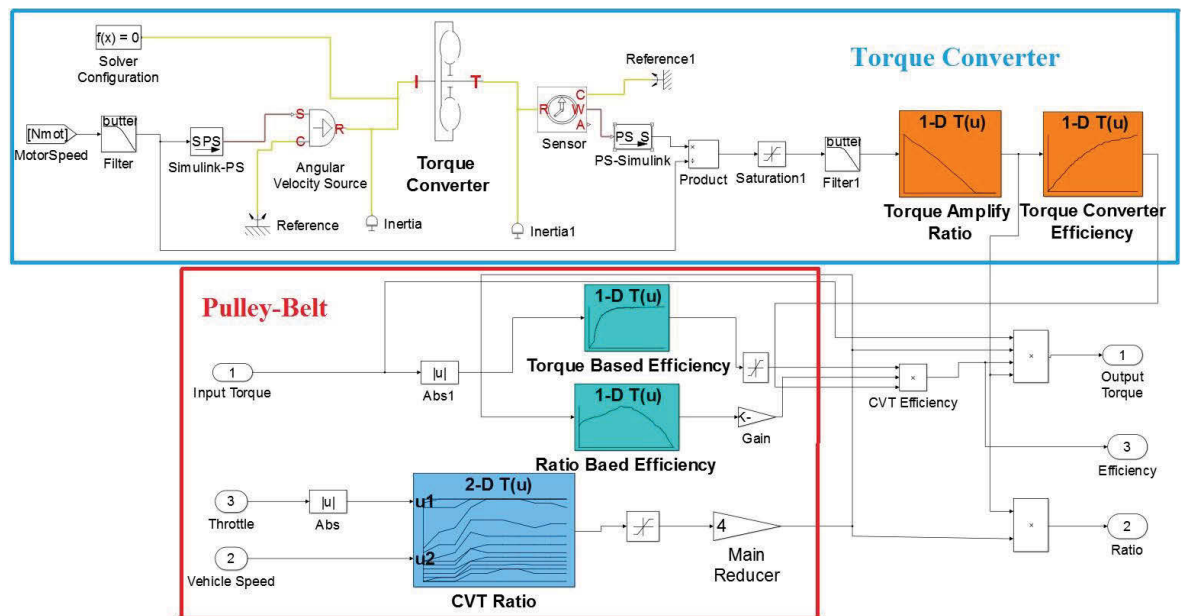
Figure 4-14: CVT simulation model in Matlab®

4.5 SHIFTING SCHEDULES DESIGN FOR MOTOR BASED MULTI-SPEED TRANSMISSIONS

4.5.1 Two Speed DCT shifting schedule

Economy shift schedule design for a two-speed DCT drivetrain is based on the motor efficiency map Fig.3-4 and Fig.3-5 through calculating motor operating efficiency curves of two gears with speed varying at constant throttle [101]. The intersection point of these two curves is the shifting point for this given vehicle speed and input throttle. Fig.4-15 shows the intersection points of efficiency curve for 1st and 2nd gear at particular throttle and speed. On the right side of intersection points, the efficiency of motor operating in 2nd gear is higher than that in 1st gear. To achieve a more accurate and smoother shifting curve, it is necessary to provide more efficiency crossing points at

different throttle opening positions, as shown in Fig.4-16. With the speed of gear shifting and corresponding throttle opening, economy oriented shifting schedule for two-speed DCT is achieved in Fig.4-17. To avoid gear hunting, i.e. unnecessary and repeated gear shifting, a buffer zone is introduced to the gap between up and down shifting curve.

$$A_n = \frac{v_n \uparrow - v_{n+1} \downarrow}{v_n \uparrow} \qquad (58)$$

where, $v_n \uparrow$ is the upshift speed threshold from gear (n) to gear (n+1), $v_{n+1} \downarrow$ is the downshift speed threshold. A_n is usually selected between 0.4~0.45 [102]. The optimized downshift schedule can be modified based on obtained upshift schedule as Fig.4-18:

$$v_{n+1} \downarrow = (1 - 0.4)v_n \uparrow \qquad (59)$$
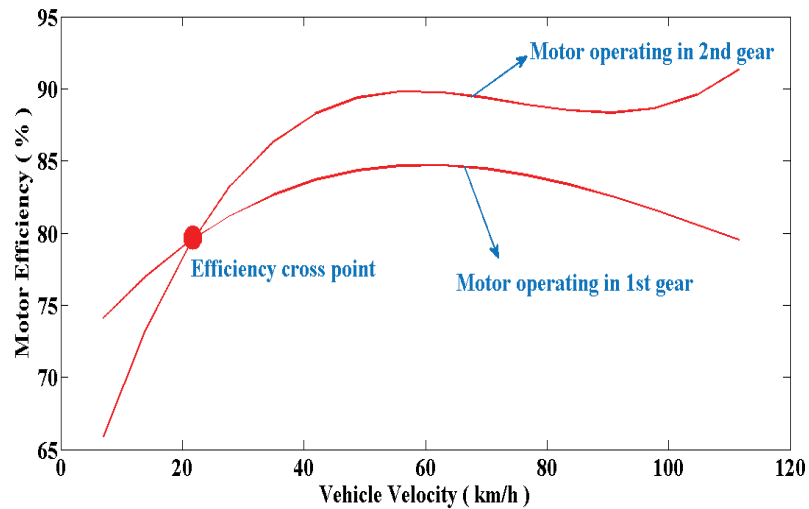
Figure 4-15: Two-speed DCT economy shifting point selection sample
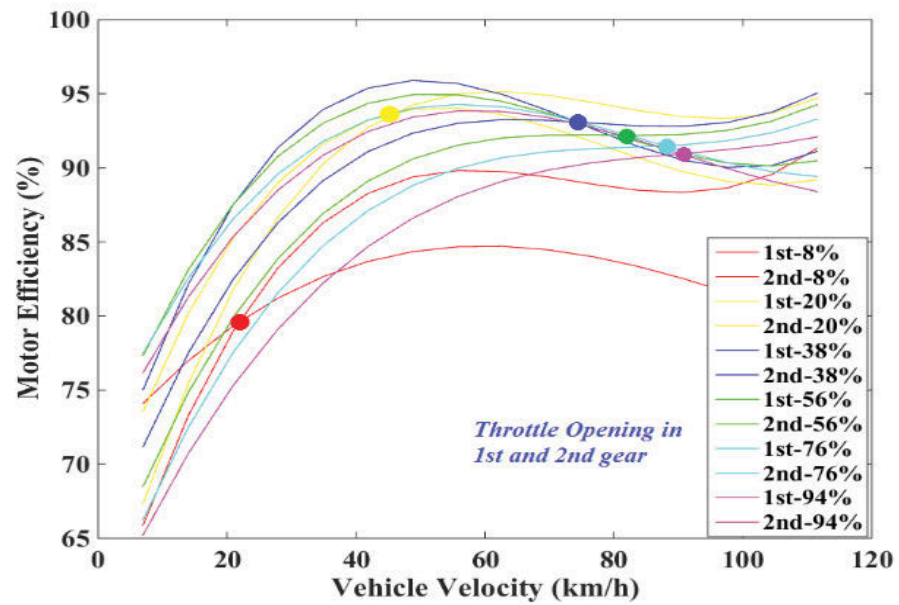
Figure 4-16: Two-speed DCT all shifting points at different throttle opening
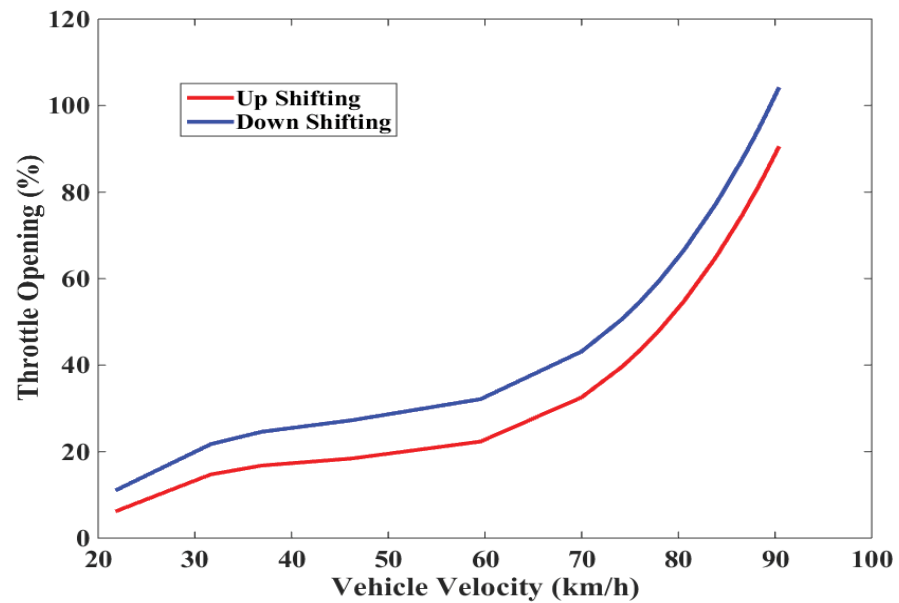
Figure 4-17: Original two-speed DCT shifting schedule
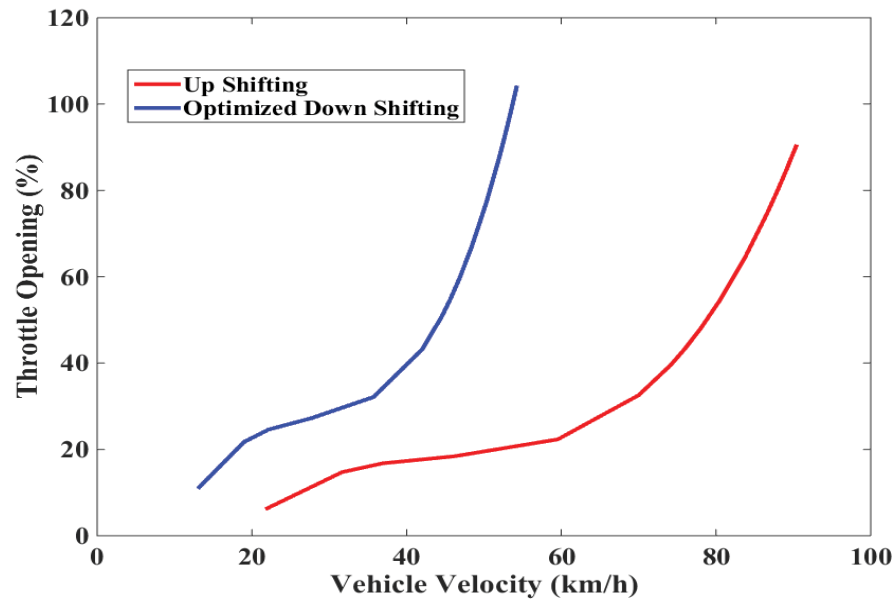
Figure 4-18: Optimized two-speed DCT shifting schedule

4.5.2 CVT shifting schedule

The ratios of CVT can vary continuously; thus, an infinite number of gear ratios are available between the limitations. For certain vehicle speed and throttle pedal position, the motor speed can continuously vary, according to the selected gear ratio in the shifting schedule. Therefore, the most economic gear ratio at a particular vehicle speed and throttle position can be determined, by comparing the motor efficiency at such speed with different gear ratio. By this analogy, all the economy performance oriented shifting points at particular speed and throttle position can be achieved. The step length of selecting points in available gear ratio coverage is 0.1. For instance, with 70 km/h vehicle speed and 40% of pedal travel, 1.3 is the gear ratio that can help the motor work in the most efficient area. Part of speed and pedal position based CVT ratios are presented in Table 4-6.

Table 4-6: CVT ratio calculation data

Throttle Pedal Position Gear Ratio Speed (km/h)	0.1	0.2	0.3	0.4	0.5	0.6	0.7	0.7	0.9	1
10	2.5	2.5	2.5	2.5	2.5	2.5	2.5	2.5	2.5	2.5
30	2.3	2.3	2.3	2.5	2.5	2.5	2.5	2.5	2.5	2.5
50	1.2	1.4	1.4	2	2	2	1.9	1.8	1.9	1.9
70	1	1	1	1.3	1.4	1.4	1.4	1.4	1.4	1.4
90	0.8	0.8	0.8	1	1.1	1.1	1.1	1.1	1.1	1.1
110	0.6	0.6	0.6	0.9	0.9	0.9	0.92	0.9	0.9	0.9
130	0.5	0.5	0.5	0.7	0.7	0.8	0.8	0.7	0.7	0.7

Fig.4-19 demonstrates the continuous varying gear ratios in CVT depending on the throttle and vehicle speed.
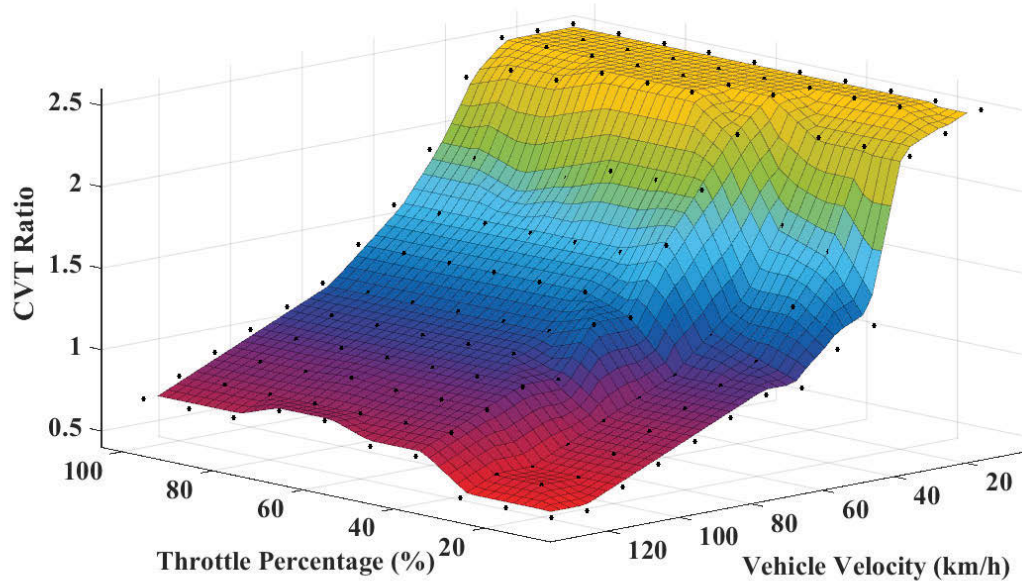
Figure 4-19: CVT shifting strategy for BEV

4.6: ECONOMIC AND DYNAMIC PERFORMANCE SIMULATION OF MULTI-SPEED BATTERY ELECTRIC VEHICLE

This study introduces a complete EV model in Matlab/Simulink, which consists of driver unit, vehicle control unit (VCU), motor unit, transmission unit, battery unit and vehicle unit.

In order to make the simulation results more convincing, all the parameters in the model are from real devices used in this experiment. (E.g. Permanent Magnet Motor from UQM Technologies, modified two-speed DCT from NTC and UTS and an example EV characteristic from Beijing Electric Vehicle Co., Ltd.)

In "Driver" unit, a lot of typical city driving cycles can be chosen. (E.g. New Europe Driving Cycle (NEDC), Urban Dynamometer Driving Schedule (UDDS), New York City Cycle (NYCC) and Japan 10-15 Cycle)

Motor unit is the prototype of a permanent- magnet motor equipped on the testing rig, which can provide 300 Nm peak torques in a short time and 45 kW power continuously.

The transmission systems in the model are quite different from other multi-geared transmissions in EVs. They are an optimized two-speed DCT and a simplified CVT, which are introduced previously.

The simulation model used in this study, which is designed for the evaluation of the performance of multi-speed transmission, is a backward-facing model shown in Fig.4-20. Vehicle Control Unit (VCU) calculates the required driving and braking torque from speed profile and power from the battery, starting from the assigned driving schedule. From the viewpoint of braking, total required brake torque is divided into three parts, i.e. front friction brake, front motor brake and rear friction brake in 'Brake Torque Distribution' block, according to selected strategy. Not like the mechanical friction brake can be directly applied on wheels by a hydraulic system, required regenerative brake, firstly, is limited by speed based motor torque ability, then, the charging current ability of the battery, goes through multi-speed transmission, finally, applies on the driven axle.
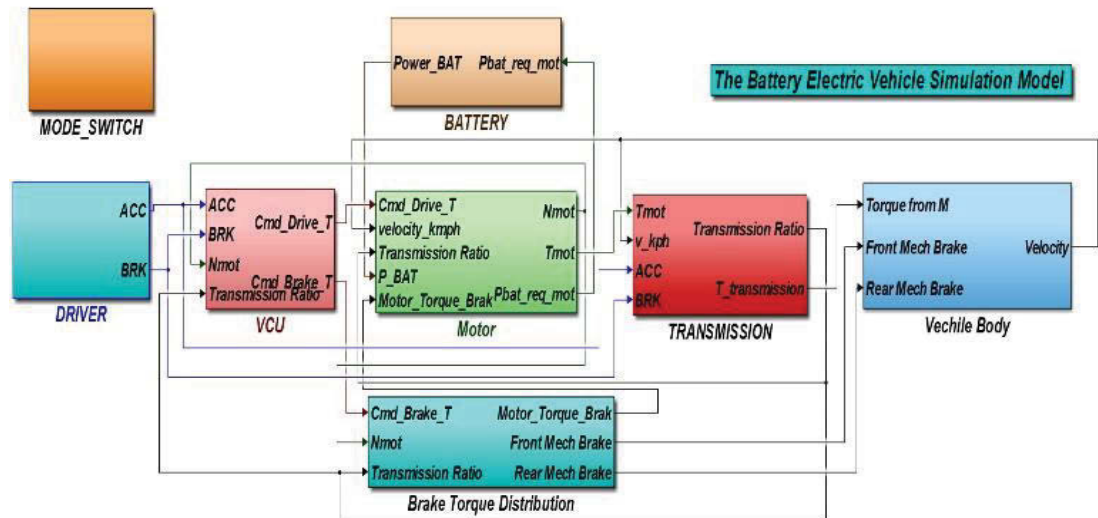
Figure 4-20: Battery electric vehicle Simulink® Model

4.6.1 Economy benefit of different transmissions based BEVs

The absence of torque converter eliminates power loss and improves dynamic performance in the transmission system. However, without the help of the torque amplification function of the converter, the demanded motor torque will be higher at the same torque requirement at the wheel, which usually leads to an inefficient motor working area, especially for the low speed. As we can see from the first column in the Table 4-7, the motor works a little bit more efficiently, no matter in city or highway driving cycles, with the help of the torque converter. However, this advantage of traditional CVT system is offset by the improved efficiency in CVT by taking out the torque converter, comparing column 2 & 3. Thus, from the viewpoint of overall efficiency of integrated powertrain system, the simplified CVT has a better economy

performance in all driving conditions.

Table 4-7: Simulation results for CVT on BEVs with / without Torque Converter

	Motor Efficiency	Simplified CVT Efficiency	CVT (Incl. Converter) Efficiency	Total Efficiency
ECE				
Simplified CVT	83.57%	74.18%	N/A	61.99%
CVT (Incl. Converter)	82.06%	N/A	70.55%	57.89%
LA-92				
Simplified CVT	82.70%	78.86%	N/A	65.22%
CVT (Incl. Converter)	82.93%	N/A	74.69%	62.69%
HWFET				
Simplified CVT	88.88%	83.57%	N/A	74.28%
CVT (Incl. Converter)	89.10%	N/A	80.89%	72.07%

Fig.4-21 (b), (d), (f) show the motor operating regions using each of the three transmissions, namely SR, two-speed DCT and simplified CVT, separately in different driving cycles. Due to the gear ratio selected in the SR being a trade-off between economy and dynamic performance, the motor inevitably runs at high speed-low torque

and low speed-high torque areas, which usually leads to lower efficiency. Two-speed DCT is more flexible than SR when selecting a proper ratio to meet the driving requirement. With the help of continuous variable gear ratios and economy shifting schedule, the motor saves more energy and has the best economy performance in comparison with the previous two, as shown in following figures.

HWFET, speed profiles showed in Fig.4-21 (a), is a high speed cruising testing cycle; thus, required torque is usually small except in some accelerating sections. With the smallest available gear ratio and continuously varying ability, simplified CVT helps the motor run at relative higher torque and lower speed region, presented in Fig.4-21 (b), compared with SR based motor. The performance of two-speed based motor in HWFET is better than SR based motor as well, thanks to a smaller fixed ratio in 2nd gear.

LA-92, speed profiles presented in Fig.4-21 (c), is a very aggressive driving cycle with higher speed, higher acceleration, less stops per km and less idle time. Two-speed DCT and simplified CVT based motor can achieve a higher efficiency, shown in Fig.4-21 (d), by reducing speed and increase output torque using a relatively smaller gear ratio.

In contrast to the previous two cycles, ECE is a low speed, low load and frequent start-stop city testing cycle, which is presented in Fig.4-21 (e). The multi-speed transmissions do not show a significant advantage compared to SR based motor as minimal gear changes are performed.
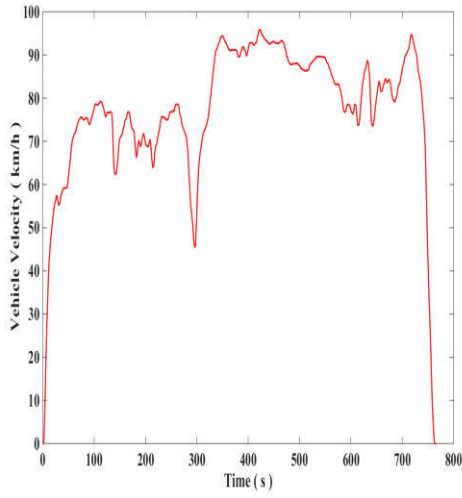
(a) HWFET profile
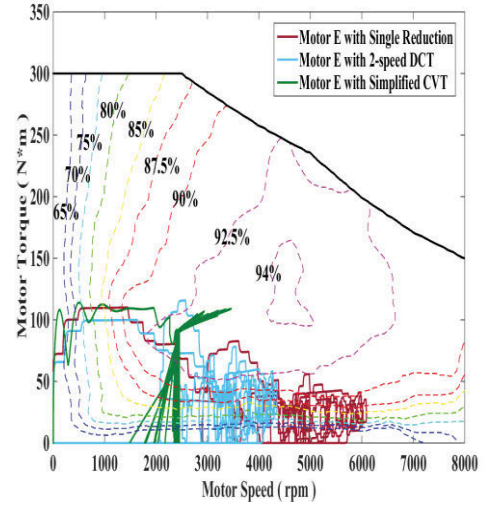
(b) Motor operating points in HWFET
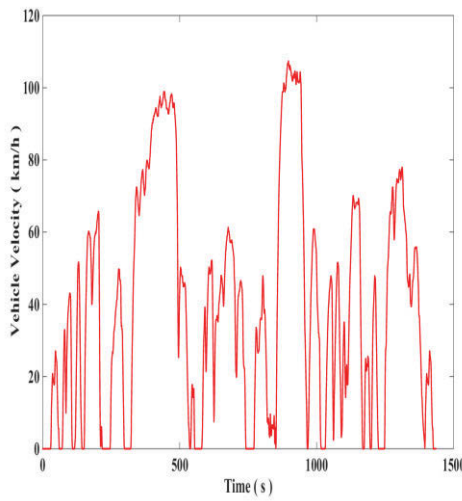
(c) LA-92 profile

(d) Motor operating points in LA-92

(e) 4 x ECE profile   (f) Motor operating points in ECE
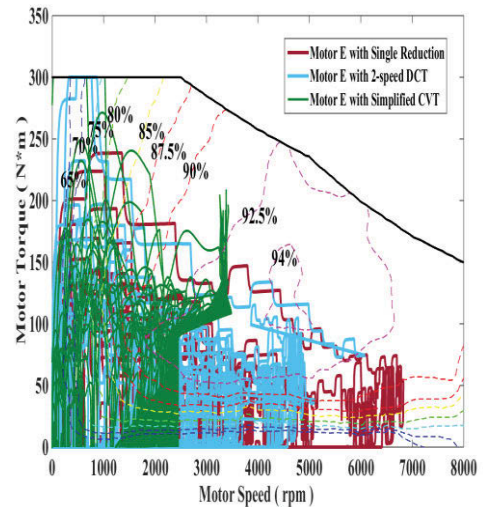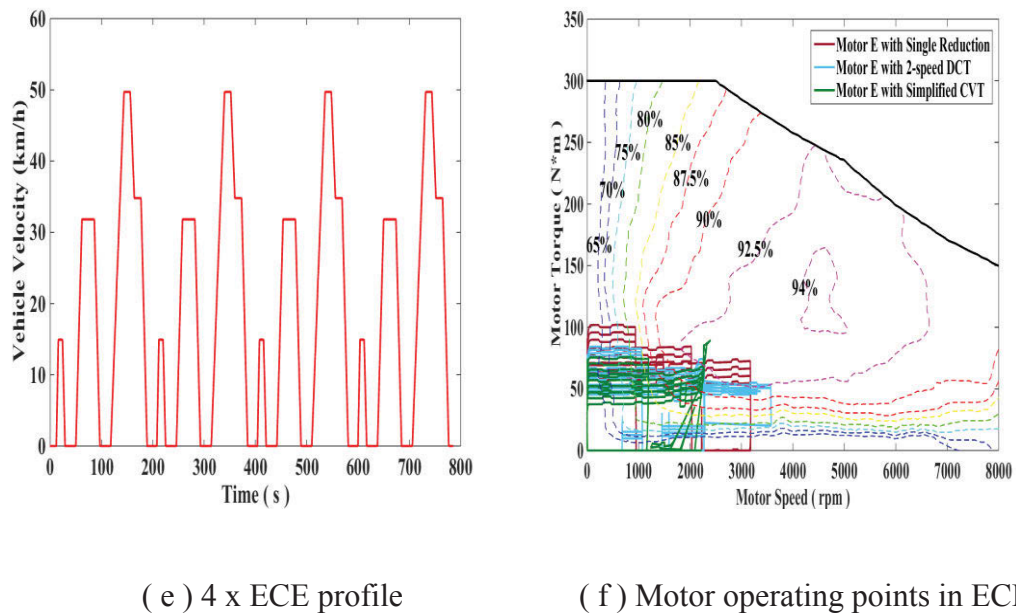
Figure 4-21: Motor operating tracks in efficiency map of BEVs with three different

transmission scenarios

The details of average motor efficiency and energy consumed, in term of the state of charge (SOC), in each testing cycle are demonstrated in Fig.4-22 & 4-23. According to the simulation results, CVT improves motor efficiency by 5%-16% and reduce power consumption 6%-10%, compared to the BEVs equipped with SR transmission system. Less improvement is achieved in two-speed DCT scenario with raising of motor efficiency 2%-10%.

With a continuously variable transmission ratio, CVT based motor has the highest operation efficiency, which is followed by 2-speed DCT based motor, then, single reduction based motor. However, this advantage is offset and transcended by 2-speed DCT based powertrain, in terms of overall energy consuming, because more energy is wasted in CVT itself.
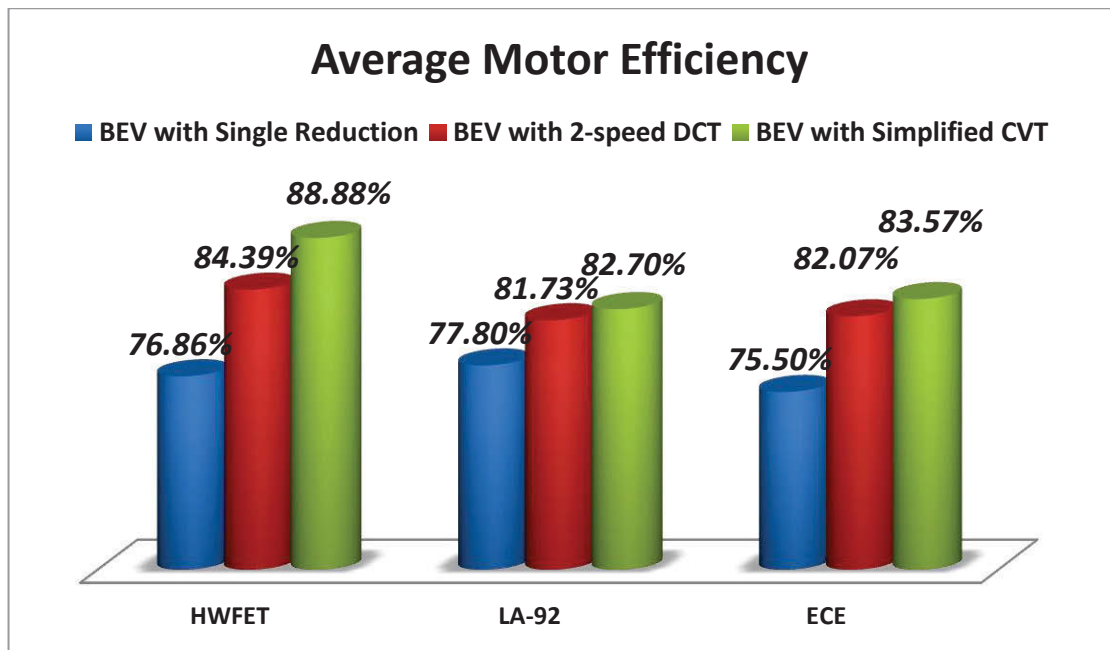
Figure 4-22: Average motor efficiencies for different driving cycles
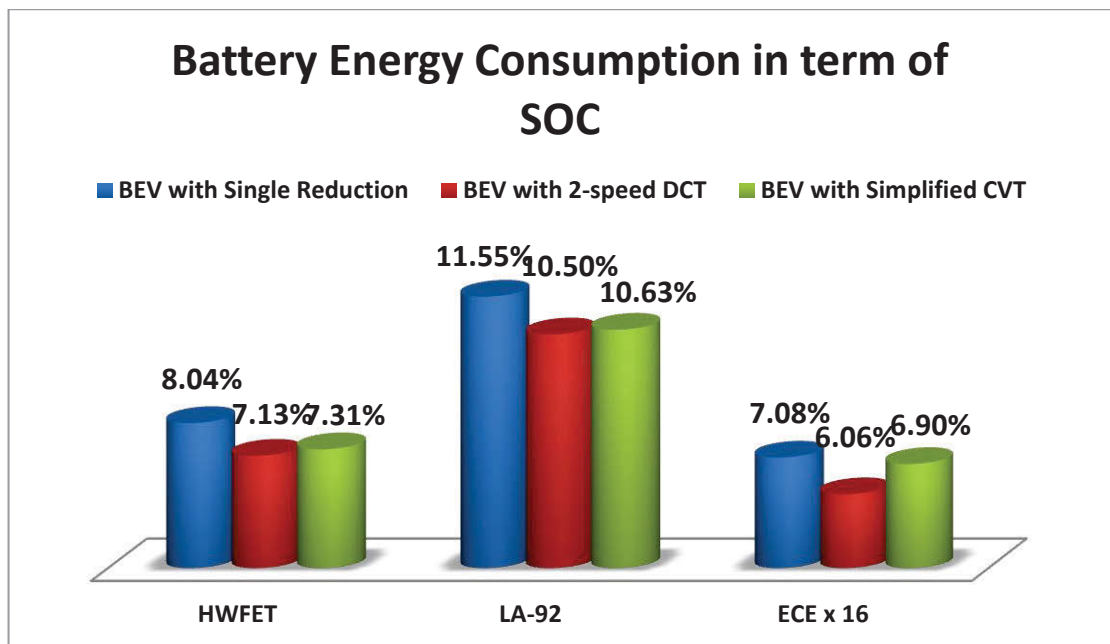
Figure 4-23: Energy consumed in battery for different driving cycles

4.6.2 Dynamic performance of different transmission based BEV

The dynamic performance of different transmission systems based BEVs is shown in Table 4-8. The same acceleration time is achieved in SR and two-speed DCT based BEVs with the same highest gear ratio. A higher upper ratio limit helps the CVT based BEV improve the acceleration time by one second. For the same reason, the maximum driving grade is improved by 25% in CVT based BEV. The 2nd gear of two-speed DCT helps boost top speed 57% from 112 km/h to 176 km/h comparing with SR BEV. Although the lowest ratio in CVT is less than half of that in DCT, the top speed is limited to 181 km/h as a consequence of limited motor power. Therefore, the CVT ratios could be further optimised and may improve results.

Table 4-8: Dynamic performance of different transmission system based BEVs

Transmission Type	Top Speed	0-100 km/h Acc	0-60 km/h Acc	Max Grade
SR	112 km/h	14.4 s	7.3 s	48 %
Two Speeds DCT	176 km/h	14.4 s	7.3 s	48 %
Simplified CVT	181 km/h	13.4 s	6.3 s	60 %

CHAPTER 5 : DEVELOPMENT AND CALIBRATION OF TESTING RIG

5.1 INTRODUCTION

The powertrain-testing bench consists of high voltage power, BLDC motor, and controller, differential integrated two-speed DCT, wheels, flywheels and dynamometer. According to the requirement of the whole system, the four flywheels are designed to simulate the inertia of a vehicle with a mass of 1500 kg. The dynamometer is used to supply battery load, aerodynamic drag and rolling resistances. Fig.5-1 & Fig.5-2 demonstrate the structure and components of the powertrain-testing rig. The performance of CVT on BEVs has not been experimentally verified due to the limited experimental resources. Nevertheless, the consistency of simulation and experimental results of the SR and two-speed DCT testing is excellent. However, the analysis of the CVT results needs further experimental verification.
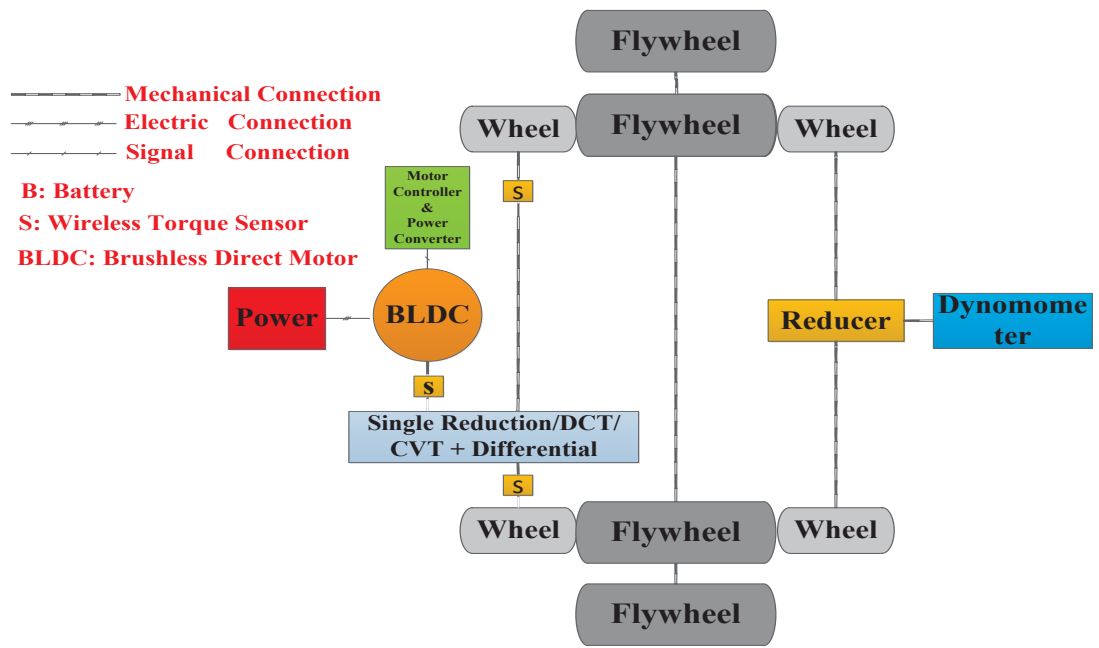
Figure 5-1: Experimental equipment structure schematic
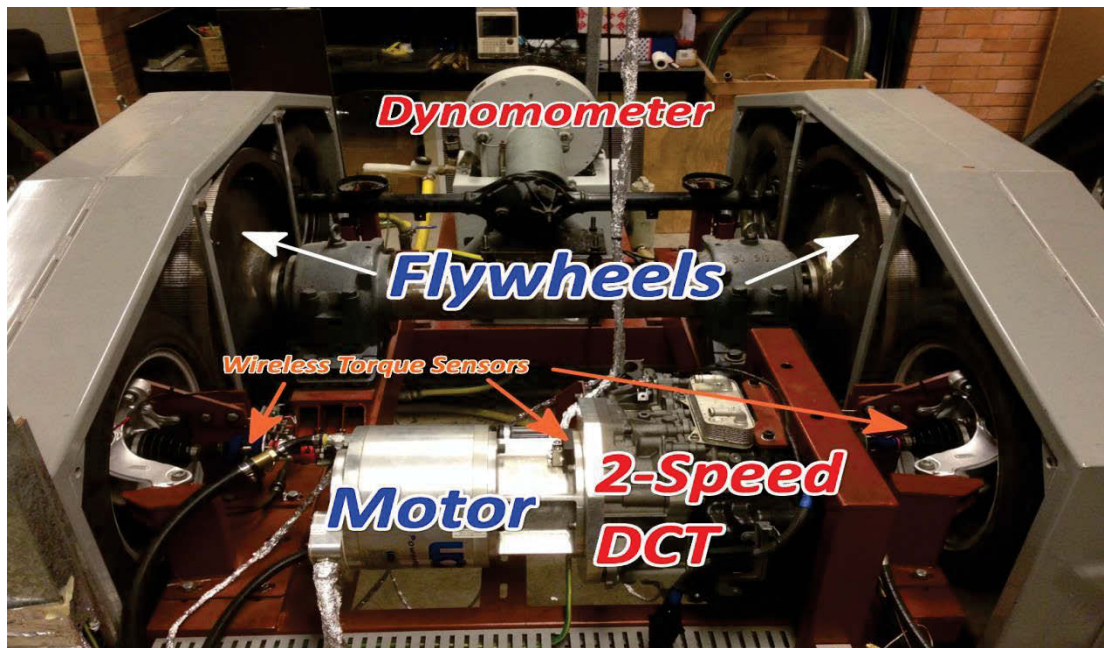
Figure 5-2: Plan view of testing bench

5.2 TORQUE SENSORS CALIBRATION FOR TRANSMISSION EFFICIENCY TESTING

To investigate the transmission efficiency, three wireless torque sensors are installed on the left and right output shafts and input shaft of the transmission respectively.

ATi 2000 series is selected in this study to transmit data from rotating shafts to a stationary receiver by using telemetry transmitters. As shown in Fig.5-3, a miniature strain gage is adhered to the shaft in order to transmit shaft torque and thrust, while the system is running. Power is supplied to the transmitter inductively for continuous, non-interrupted measurements. No batteries are required because the IPS delivers power through a stationary loop antenna, as shown in Fig.5-4, to a rotating antenna. The rotating loop antenna and induction power converter are embedded into the collar assembly. The receiver features a built-in induction power supply. A digital backlit LCD display and analogue outputs are included as well, as shown in Fig.5-4.

The specifications of selected torque sensor are shown in the Appendix Table A1.
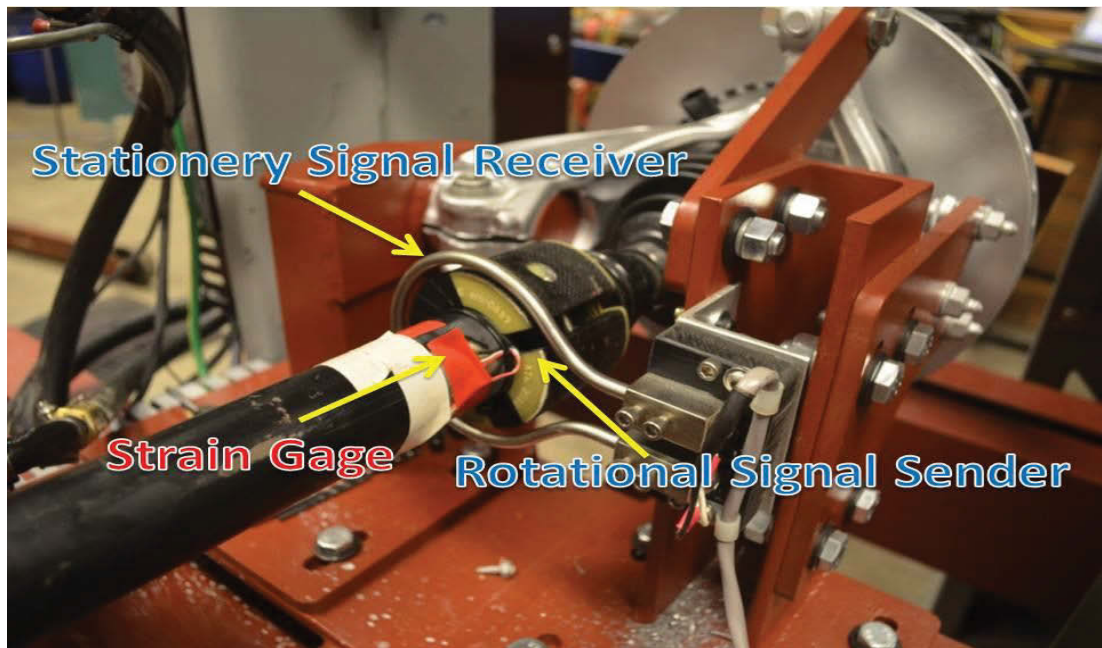
Figure 5-3: ATi 2000 series wireless torque sensor

Figure 5-4: ATi 2000 series display

Because the torque related-elastic deformation of strain gage in sensors is displayed in terms of digital voltage, the relationship of torque applied to the shaft and the voltage from the sensor display should be calibrated before implementation.

As shown in the Fig.5-5 to Fig.5-8, torque is applied to the shaft through a two-meter bar, which is connected to the wheel rotor, from a weight hanging on the end of the bar. The turning angle generated by applied torque is measured by a digital inclinometer. The actual torque on the measured shaft can be expressed as:

$$T_{measure} = (Weight \times \cos\theta) \times Length_{Bar} \qquad (60)$$
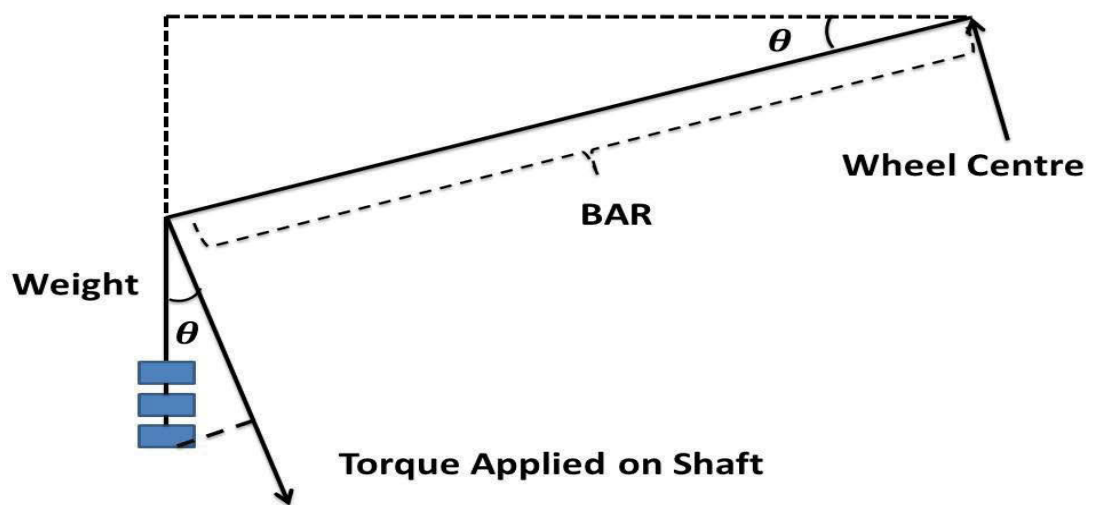
Figure 5-5: Schematic of torque sensor calibration

Figure 5-6: Torque sensor calibration (a)

Figure 5-7: Torque sensor calibration (b)
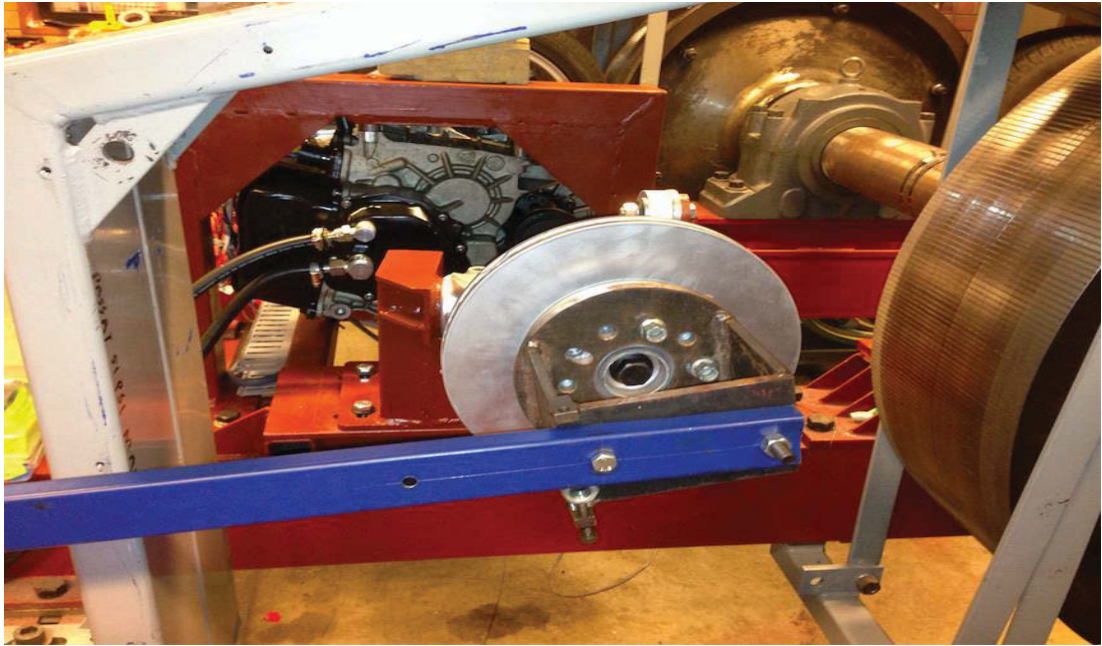
Figure 5-8: Torque sensor calibration (c)

The raw calibration data of transmission output shafts torque sensors are presented in Appendix Table A2.

Thus, torques applied on the transmission output shaft by particular weight and bar are:

$$
Long\ Shaft \begin{cases} 10\ kg: 2 * cos\left(5 * \dfrac{3.14}{180}\right) * 10 * 9.8 = 195.3\ (Nm) \\[2mm] 20\ kg: 2 * cos\left(2 * \dfrac{3.14}{180}\right) * 20 * 9.8 = 391.8\ (Nm) \\[2mm] 30\ kg: 2 * cos\left(-1 * \dfrac{3.14}{180}\right) * 30 * 9.8 = 588.0\ (Nm) \\[2mm] 40\ kg: 2 * cos\left(-5.5 * \dfrac{3.14}{180}\right) * 40 * 9.8 = 780.4\ (Nm) \\[2mm] 50\ kg: 2 * cos\left(-10.5 * \dfrac{3.14}{180}\right) * 50 * 9.8 = 963.6\ (Nm) \end{cases} \quad (\ 61\ )
$$

$$Short\ Shaft \begin{cases} 10\ kg: 2 * cos\left(0.3 * \dfrac{3.14}{180}\right) * 10 * 9.8 = 196.0\ (Nm) \\[2mm] 20\ kg: 2 * cos\left(-2 * \dfrac{3.14}{180}\right) * 20 * 9.8 = 391.8\ (Nm) \\[2mm] 30\ kg: 2 * cos\left(-4.5 * \dfrac{3.14}{180}\right) * 30 * 9.8 = 586.2\ (Nm) \\[2mm] 40\ kg: 2 * cos\left(-7 * \dfrac{3.14}{180}\right) * 40 * 9.8 = 778.2\ (Nm) \\[2mm] 50\ kg: 2 * cos\left(-9.5 * \dfrac{3.14}{180}\right) * 50 * 9.8 = 966.6\ (Nm) \end{cases} \quad (62)$$

The relationship of display voltage and actual torque can be obtained by subtracting the voltage of hook and bar from each weight's voltage. Considering the gearbox amplification ratio, the required measuring range of sensor on transmission input shaft is much smaller than that of output shafts. The calculation procedures can be reproduced to the input shaft sensor, except changing the step and range. Appendix Table A3 presents the breakdown calibration result for torque sensors in Lab. The relationships of display voltage and torque measured by sensors are shown in Fig.5-9.
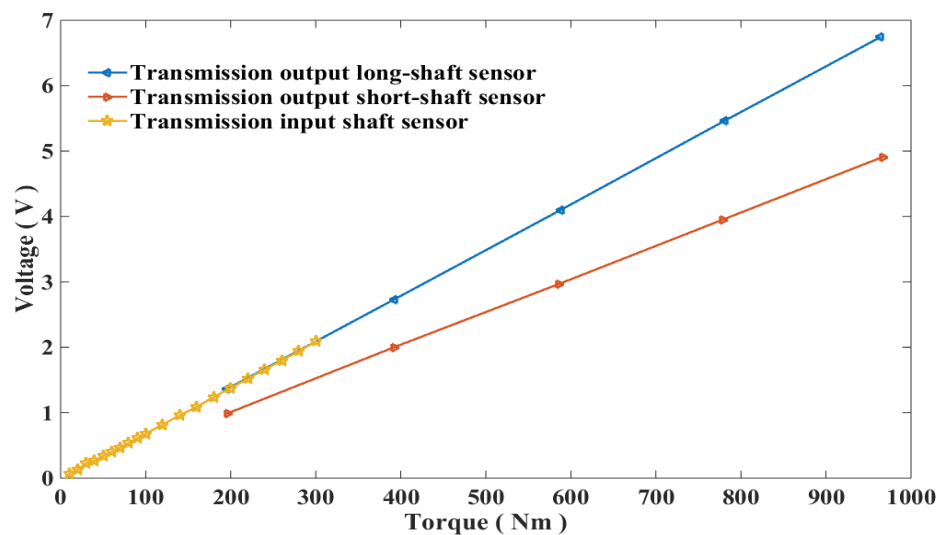
Figure 5-9: Real torque on the shaft VS sensor display voltage

5.3 dSPACE CONTROL SYSTEM AND ELECTRIC CONTROL PANEL

The whole control system of BEV powertrain comprises dSPACE MicroAutobox, dSPACE RapidPro and self-designed electric control panel.

dSPACE MicroAutoBox, as shown in the left picture of Fig.5-10, is a prototyping solution for numerous gateway and bypassing applications in the field of Electronic Control Unit (ECU) development/rapid prototyping, and is also able to provide CAN channels required to prototype advanced controls systems for electric/hybrid drives.

Rapid Prototyping (RP) technology makes it possible to design products in a virtual environment, shorten the product development cycles, and reduce development costs. Application of RP technology significantly reduces the time to market for new products, and this saves the cost of new product development and model manufacturing. After the introduction of real-time testing of RP technology, electronic control system design and control algorithms were renamed rapid control prototyping (RCP) technology. In the early stages of system development, to quickly build a controller model, and the entire system offline, and online, several tests were employed to verify the feasibility of the control scheme. This process became known as rapid control prototyping. The RCP and Hardware in Loop (referred to as HIL) simulation system for the design of the electronic control system provides the advantages of development speed and acceleration of the design and development process. The RCP system, shown as the right of Fig.5-10, has

therefore been adopted by this study to reduce expensive, disruptive test drive requirements.
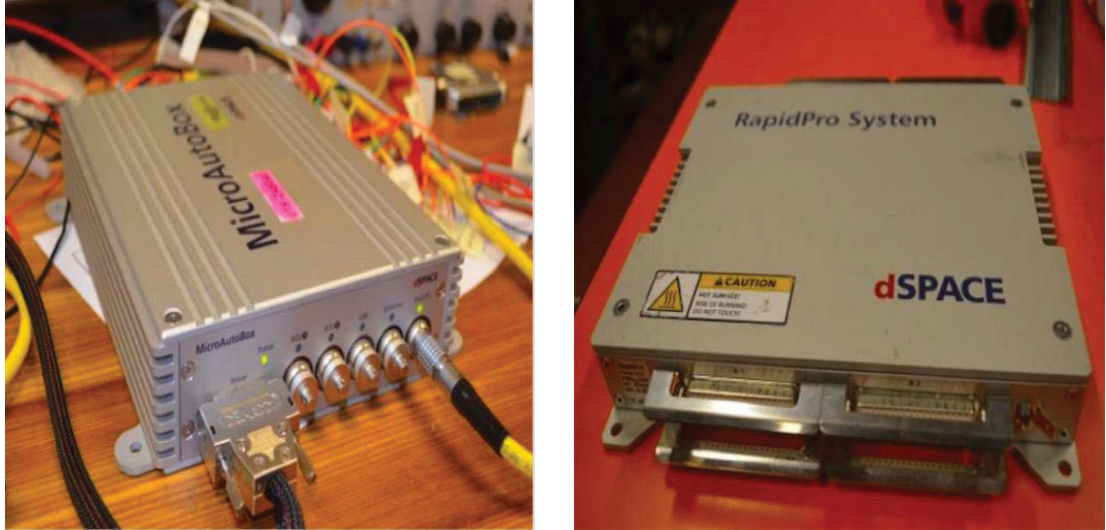
Figure 5-10: dSPACE control system （MicroAutoBox（Left）/ RapidPro（Right））

Additionally, an electric control panel was designed, for example, for power supplying, voltage transformation, application switching, overcurrent protection, cooling. The details are shown in the Fig.5-11 and Fig.5-12:
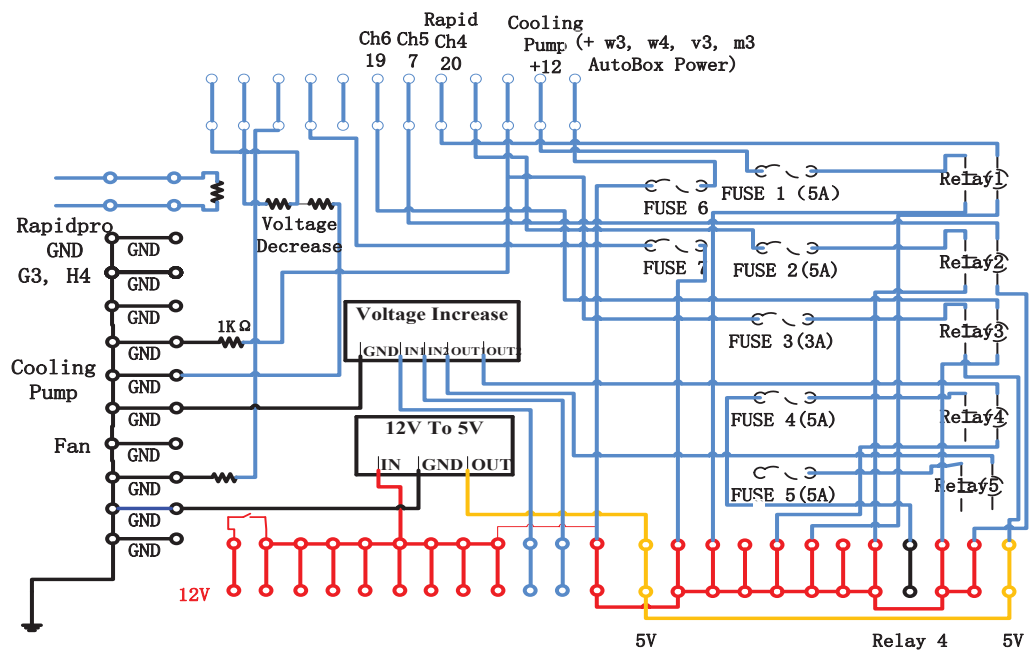
Figure 5-11: Schematic of control panel
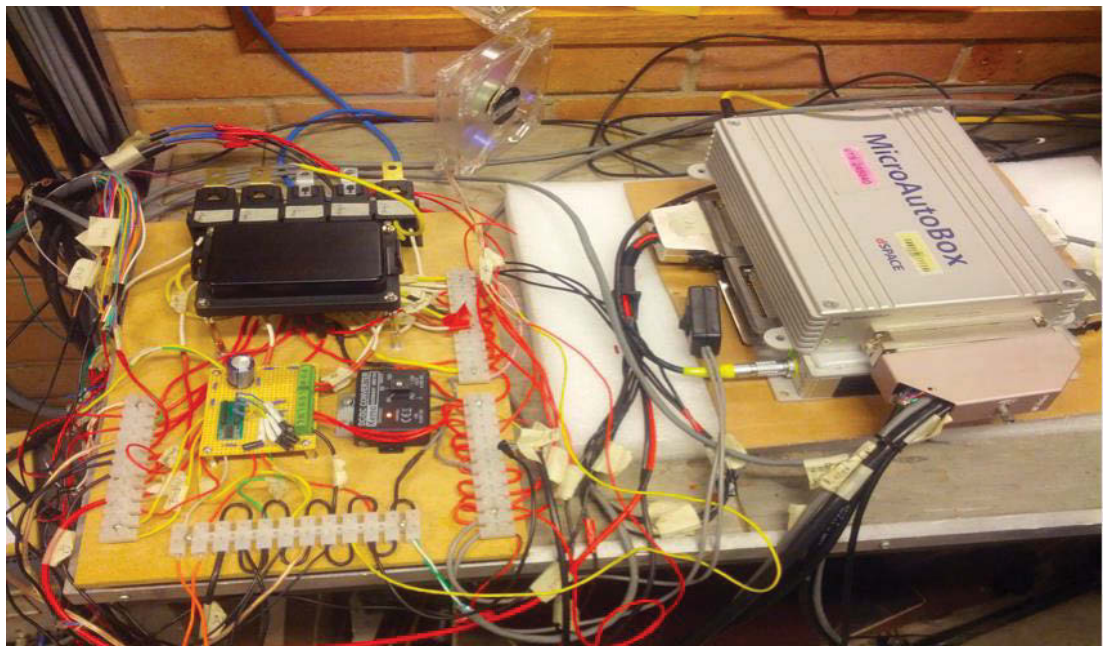
Figure 5-12: Electric control panel in the powertrain testing (left)

Basically, an offline tested powertrain control model can be loaded into MicroAutobox to acquire data, watch and change variables, through setting up an interactive window in PC, as shown in Fig.5-13. RapidPro is controlled by the signal from MicroAutobox to drive the actuators, such as transmission pump and hydraulic brake. Simply, MicoAutobox works like an ECU to send, receive and process signal; RapidPro works like a power amplifier to drive the mechanical actuators; the electric control panel is more like an auxiliary equipment to switch power and provide overcurrent protection. The workflow of powertrain testing control process is demonstrated in Fig.5-14.

Figure 5-13: PC display panel for data acquiring, variables changing in ControDesk®
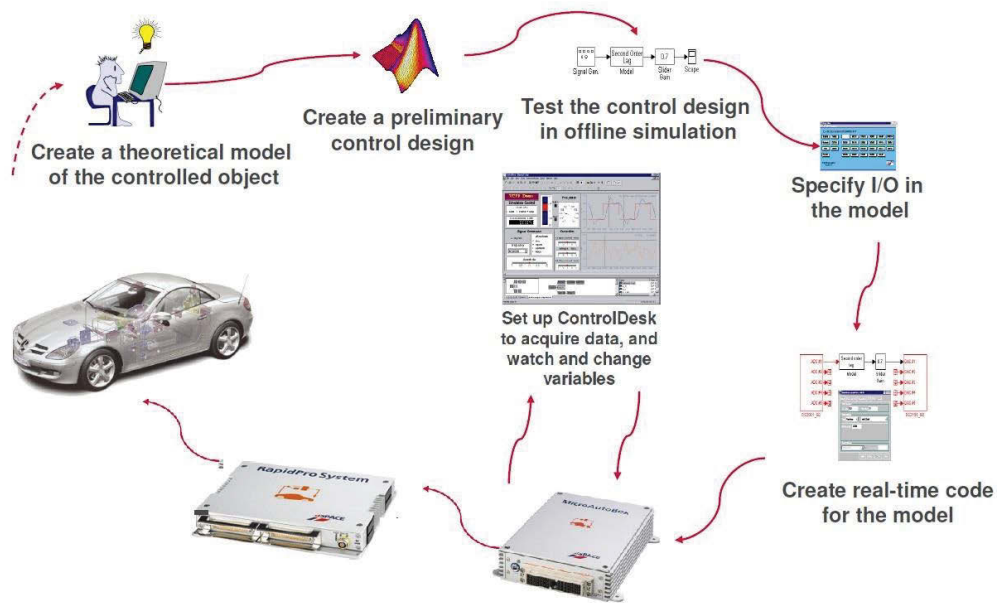
Figure 5-14: A typical development process

5.4 DYNAMOMETER

An eddy current dynamometer is used in the powertrain testing to supply additional 250 kg battery load and driving dynamic resistances. A special formula Eq.63 is provided in the dynamometer setting to simulate vehicle rolling resistance, aerodynamic resistance, and acceleration resistance:

$$M(n) = M_0 + a_0 + a_1 \times (n/n_0) + a_2 \times (n/n_0)^2 + I \times \frac{dn}{dt} \qquad (63)$$

Referring to vehicle dynamic equation Eq.64, a_0, a_1, a_2 are variables corresponding to rolling plus grading, acceleration and aerodynamic respectively; n is the dynamometer input speed (rpm); I is the coefficient of translational equivalent inertia for rotation parts.

$$\frac{Ti_0 i_g \eta_T}{r} = Gf + G\sin\theta + \frac{C_D A}{21.15}u^2 + \delta m\frac{du}{dt} \tag{64}$$

where n/n_0 is regarded as the vehicle speed (km/h). Due to a reducer being installed between the input shaft of dynamometer and vehicle wheels to adjust the input speed, which has a 5.1 gear ratio, the variable n_0 is expressed as:

$$u = 0.377 * \frac{n \times r}{i_{gear}} = \frac{n}{i_{gear}/0.377/r} = \frac{n}{n_0} \tag{65}$$

$$n_0 = \frac{1}{5.1/0.377/0.3125} = 43.3 \tag{66}$$

For half loaded no climbing testing:

$$a_0 = G_f + G_i = (1780 + 375/2) \times (0.016 + \sin 0) = 31.5 \tag{67}$$

For full loaded 30% grade testing:

$$a_0 = G_f + G_i = (1780 + 375) \times (0.016 + \sin(\tan^{-1} 0.3)) = 653.6 \tag{68}$$

Comparing the aerodynamic part of Eq.63 and Eq.64, then, a_2 is expressed as:

$$a_2 = C_D * A/21.15 = 0.28 * 2.2/21.15 = 0.029125 \tag{69}$$

Figure 5-15: Parameters setting in dynamometer

CHAPTER 6 : EXPERIMENTAL RESULTS ANALYSIS OF MULTI-SPEED ELECTRIFIED POWERTRAIN IN DRIVING CYCLES

6.1 TWO-SPEED DCT TEMPERATURE TESTING

It is very important to keep the motor-based modified two-speed DCT operating in a proper temperature range. According to the experimental results shown in the Fig.6-1 and Fig.6-2, 2nd gear has a higher overall and average operating temperature than 1st gear, due to the relative higher rotation speed. According to the characteristics of transmission fluid [103,104], a higher efficiency can be expected for 2nd gear.
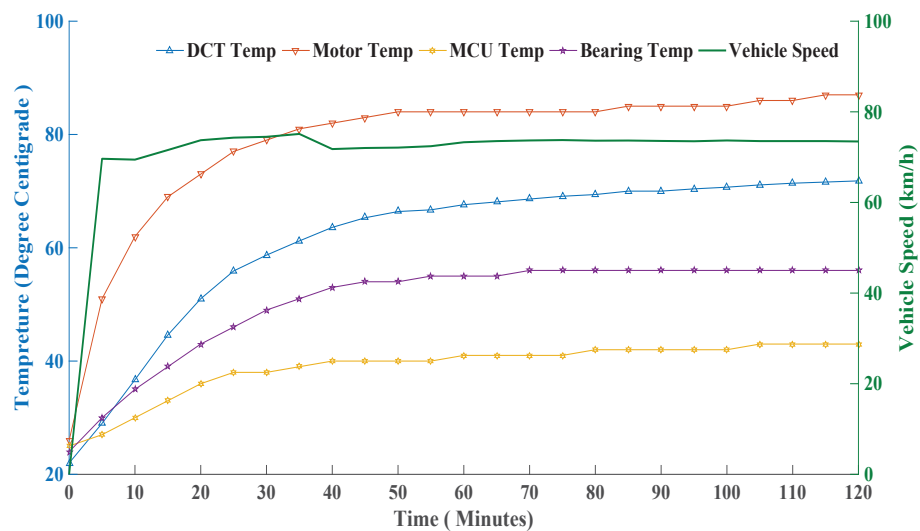
Figure 6-1: Temperature variation of 1st gear in two-speed DCT
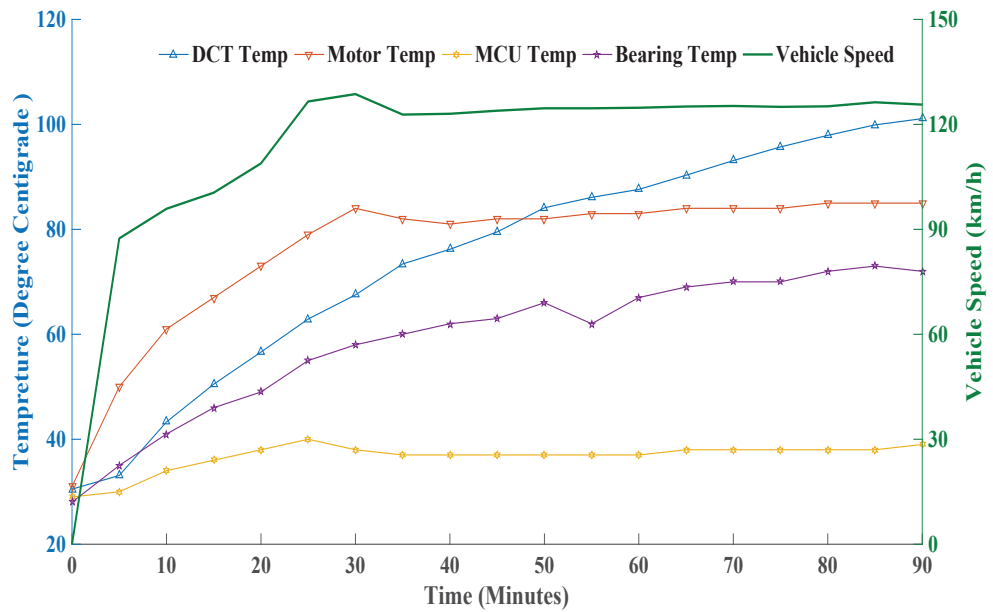
Figure 6-2: Temperature variation of 2nd gear in two-speed DCT

The breakdowns of temperature testing results are shown in Appendix Table B1 and B2.

6.2 DCT EFFICIENCY TESTING

Based on the data obtained from transmission output and input sensors and Eq.70, the efficiencies of two-speed DCT at particular torque and rotation speed are shown in Fig.6-3-Fig.6-6.

$$Efficiency_{DCT} = \frac{Torque_{output\_left} + Torque_{output\_right}}{Torque_{input} \times i_g} \times 100\% \qquad (\,70\,)$$
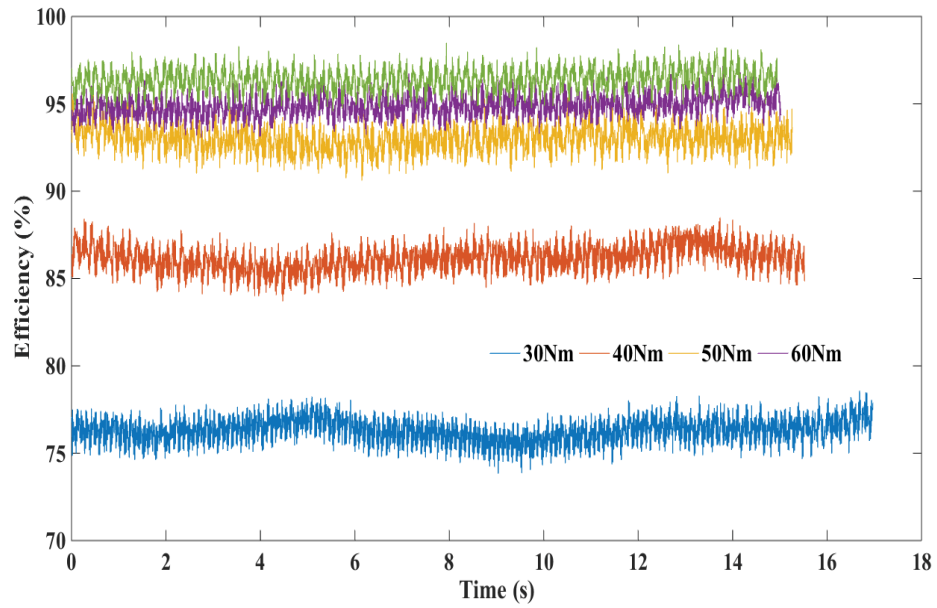
Figure 6-3: 1st gear efficiency at 3000 rpm input speed with different input torque
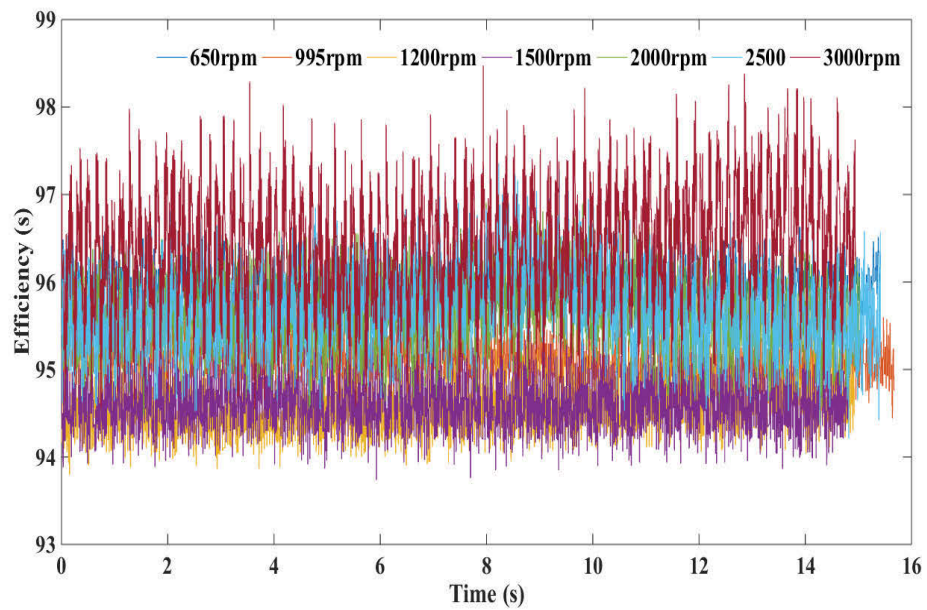
Figure 6-4: 1st gear efficiency at 60Nm input torque with different input speed
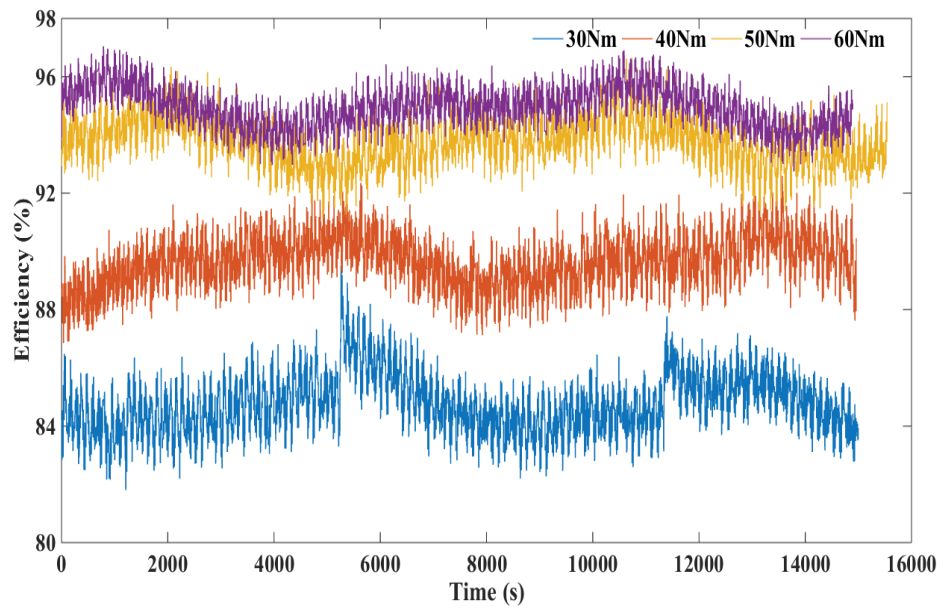
Figure 6-5: 2nd gear efficiency at 3000 rpm input speed with different input torque
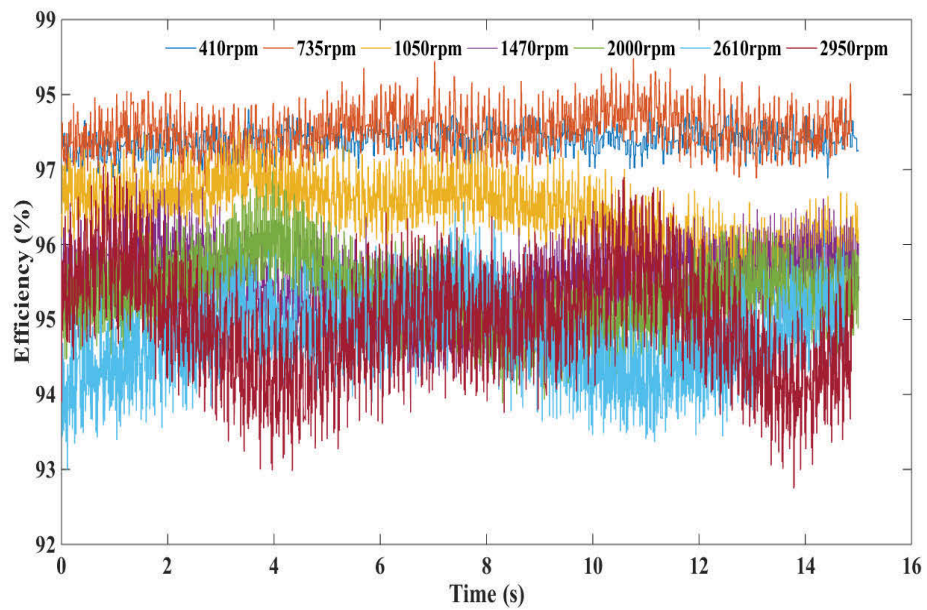
Figure 6-6: 2nd Gear Efficiency at 60Nm Input Torque with Different Input Speed

As shown in the above four pictures, the efficiencies of different input torque at particular input speed (3000 rpm) are in a wide range of 78% to 95% in 1st gear, 84% to 96% in 2nd gear. On the contrary, the efficiencies of different input speed with fixed torque (60 Nm) are all around 95%-97%, no matter in 1st or 2nd gear. Therefore, a conclusion that input torque has a greater effect on transmission efficiency than input speed can be made. Additionally, the transmission efficiency goes up vary fast with increasing input torque. It quickly goes over 90% when input torque is higher than 40 Nm. After iterative testing, 85% and 90% overall operation efficiencies of 1st and 2nd gear in two-speed transmission can be expected.

6.3 HWFET TESTING

In this experiment, HWFET and ECE cycles are selected to make up a combined driving cycle to simulate consumers' daily driving conditions.

Eq.71 is used to calculate motor efficiency when propeling:

$$Motor\_E_{experiment} \qquad (71)$$

$$= \frac{Torque_{out} \times Speed_{motor}(rpm)/9550}{Voltage_{in} \times Current_{in}/1000} \times 100\%$$

During regenerative braking, however, the equation is inverted as power is now fed from the powertrain to the motor and mechanical energy is converted to electric. As predicted in simulations, a relatively small ratio in a higher gear will reduce motor speed and increase motor output torque at particular speed and torque demand on wheels. In other words, it leads to the motor running in a higher efficiency area after the

shifting from 1st to 2nd gear, shown in Fig.6-7 (a). A significant motor efficiency difference between the two models is demonstrated by Fig.50 (b-c). With 77.3% and 83.0% efficiency in SR and two-speed DCT based motor respectively, 7.4% average motor efficiency improvement is achieved. During this transition period as current approaches zero and moves to the negative current quadrant a lag between torque sensor and voltage/current sensors results in erronious efficiency calculations efficiencies. These results must be ignored.
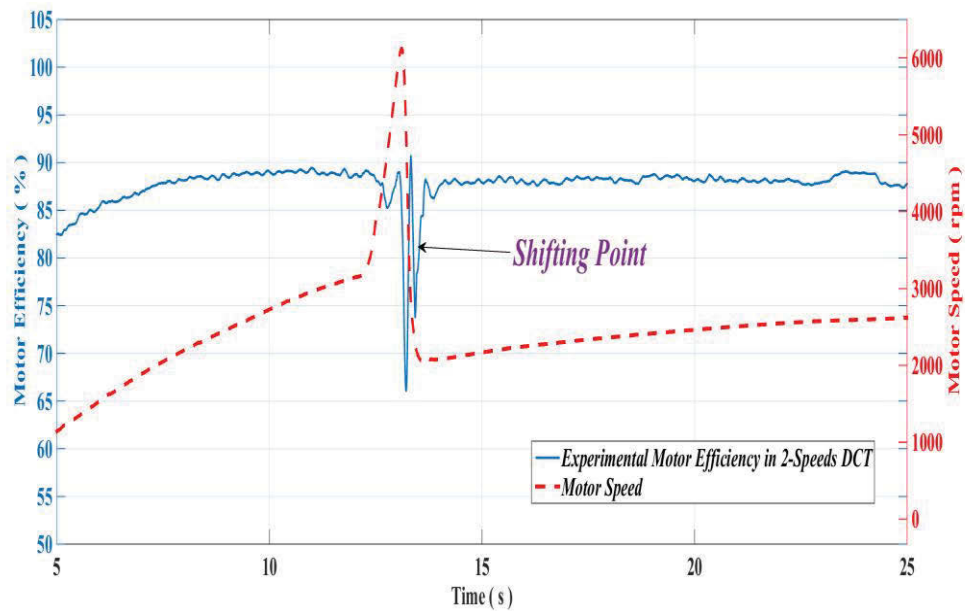
(a) Motor efficiency varying around shifting point in two speeds DCT
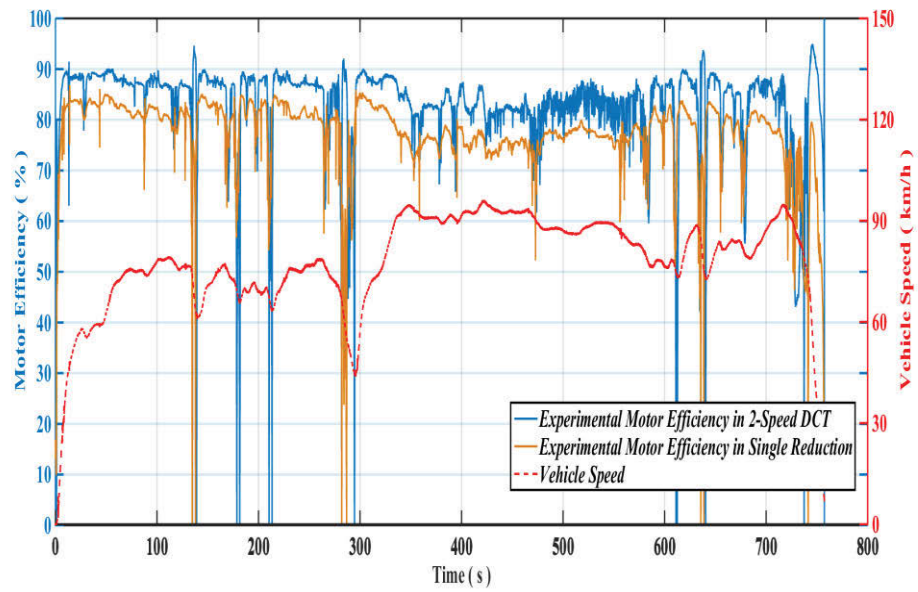
(b) Efficiency comparison of SR and two-speed DCT based motor in HWFET
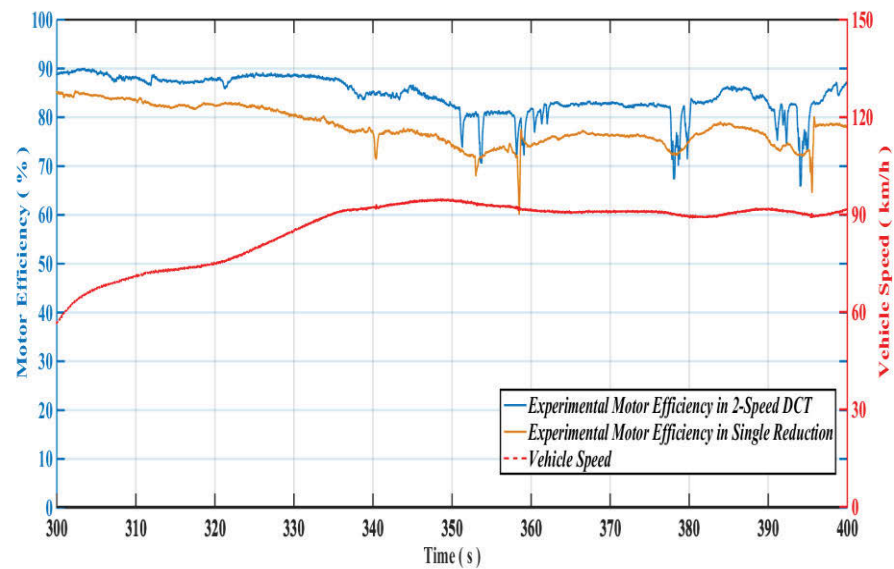
(c) Detailed view of motor efficiency gap between SR and DCT based motors

Figure 6-7: Experimental results of SR and two speeds DCT scenarios in HWFET

Eq.72 is used to calculate SOC in simulation and experimental results analysing:

$$SOC = \frac{\int_0^{time(s)} current(A)}{3600 \times Capacity_{motor}(Ah)} \times 100\%$$

(72)
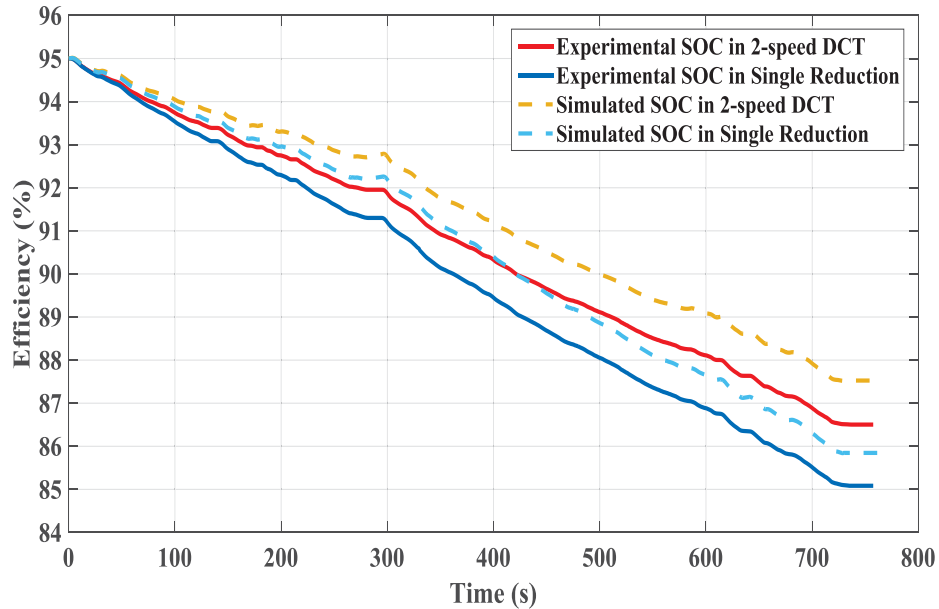
Figure 6-8: SOC consumption in HWFET

Comparing to the 9.9% SOC consumption in SR based BEV testing bench, two-speed DCT help save more than 14.14% battery energy by only consuming 8.5% SOC in one HWFET cycle. Differences between simulation and experimental results can be put down to (1) using a linear loss model for the transmissions, (2) variations in motor and inverter drive temperatures as well as transmission temperatures resulting in variance of simulated and actual losses, and (3) variation in PID vehicle control strategies resulting in different demand requirements for simulations and experimental results. The simulation and experiment results of consumed energy in HWFET, in term of SOC, are shown in Fig.6-8.

6.4 ECE TESTING

Comparing to the HWFET, ECE is an urban traffic oriented testing cycle. There are many acceleration and braking events at a low speed. Therefore, the 2nd gear of the two-speed DCT has far less use in the ECE cycle as compared to other cycles. It has a role to play in influencing the overall motor efficiency. The average motor efficiency is 82%, 5.6% higher than that of SR scenario. The improvement is slightly lower than that in HWFET. Fig. 6-9 (a-c) present motor efficiency varying around shifting point, whole range and partial motor efficiencies of SR and two speeds DCT based motor in ECE testing cycles respectively.
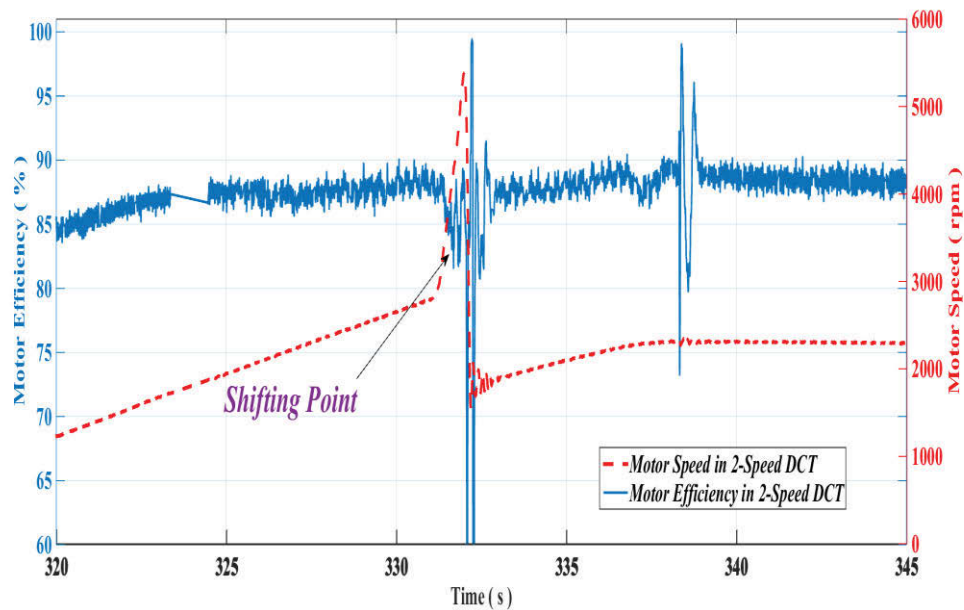
(a) Motor efficiency varying around shifting point in two speeds DCT
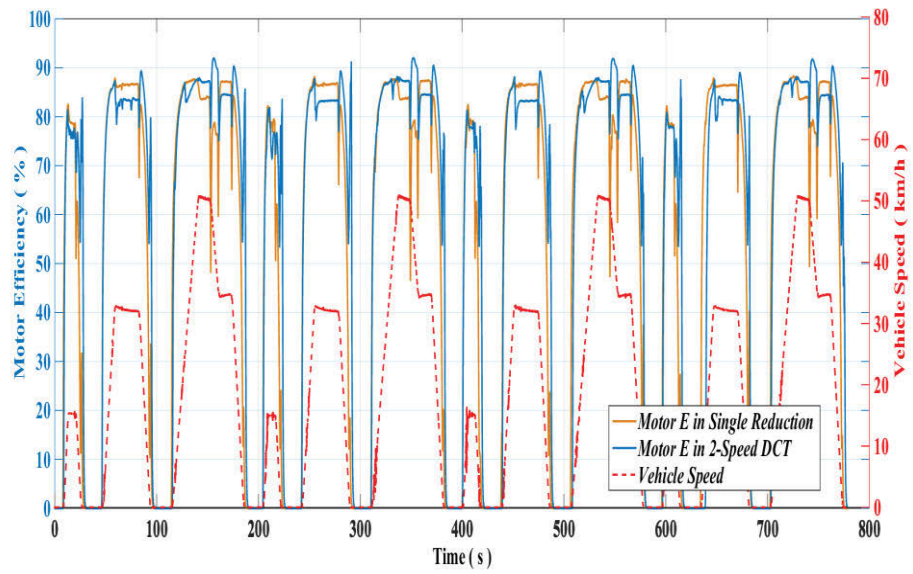
(b) Efficiency comparison of SR and two-speed DCT based motor in 4 ECE cycles
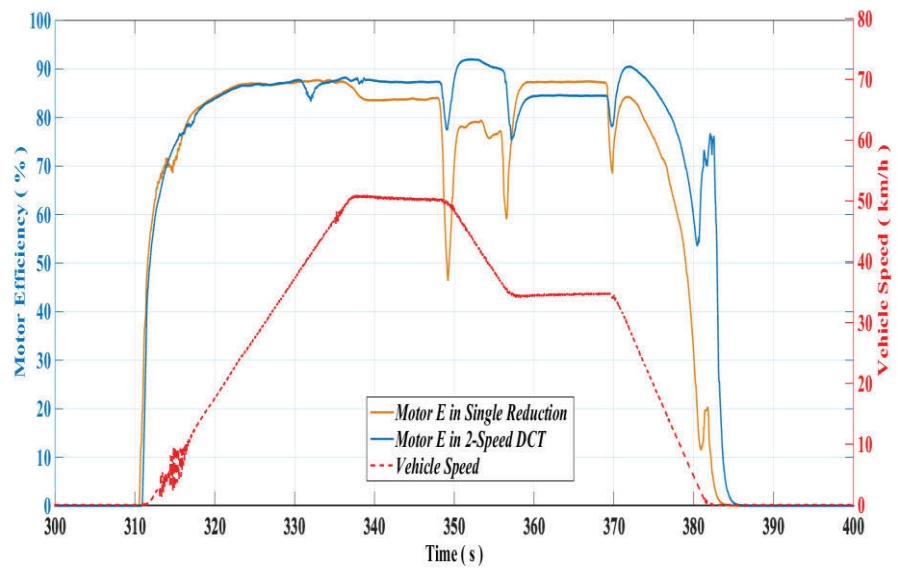
(c) Detailed view of motor efficiency gap between SR and DCT based motors

Figure 6-9: Experimental results of SR and two speeds DCT model in ECE

Additional 2.6% SOC is saved in the experiment by two-speed DCT in four ECE cycles compared to SR based BEV. The experimental results are consistent with the predictions in the previous simulation in battery energy consuming tendency, although a reasonable difference exists due to the mechanical loss, which is demonstrated in the HWFET testing section. The simulation and experiment results of consumed energy in ECE, in term of SOC, are shown in Fig.6-10.
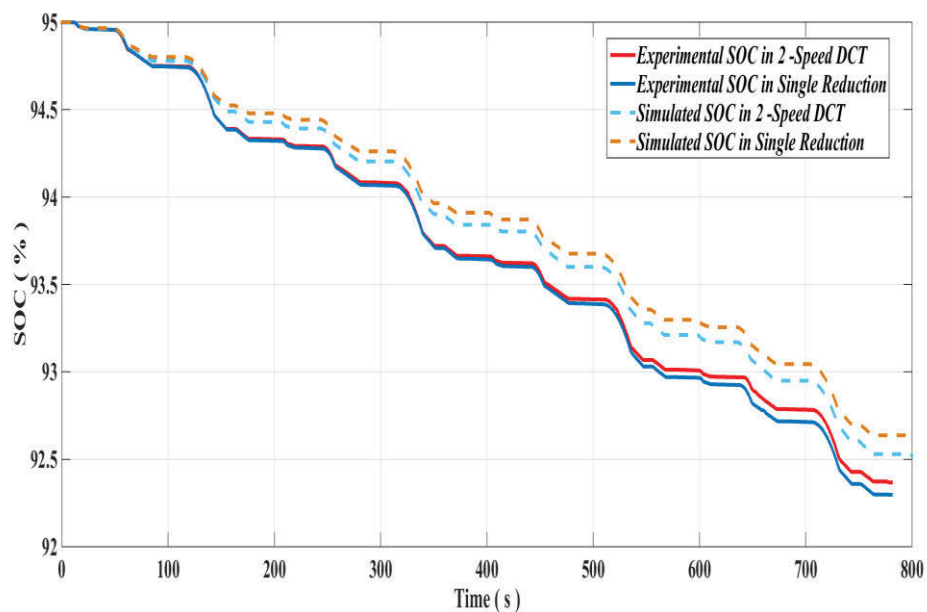
Figure 6-10: SOC consumption in four ECE cycles

Fig. 6-11 and Fig.6-12 clearly show the significant improvement achieved in motor efficiency and battery energy saving by multi-speed transmission systems. As shown, two-speed DCT is more efficient for highway cruising due to an alternative smaller ratio. The experimental results match the prediction in modelling simulation very well. Therefore, the ratio of experimental and simulation results, in 2-speed DCT studying, is applied to CVT scenario to attain a reasonable assumed experimental result. The

outcomes therefore suggest that use of a two-speed transmission or CVT can result in a significant improvement in the overall driving range of BEVs.
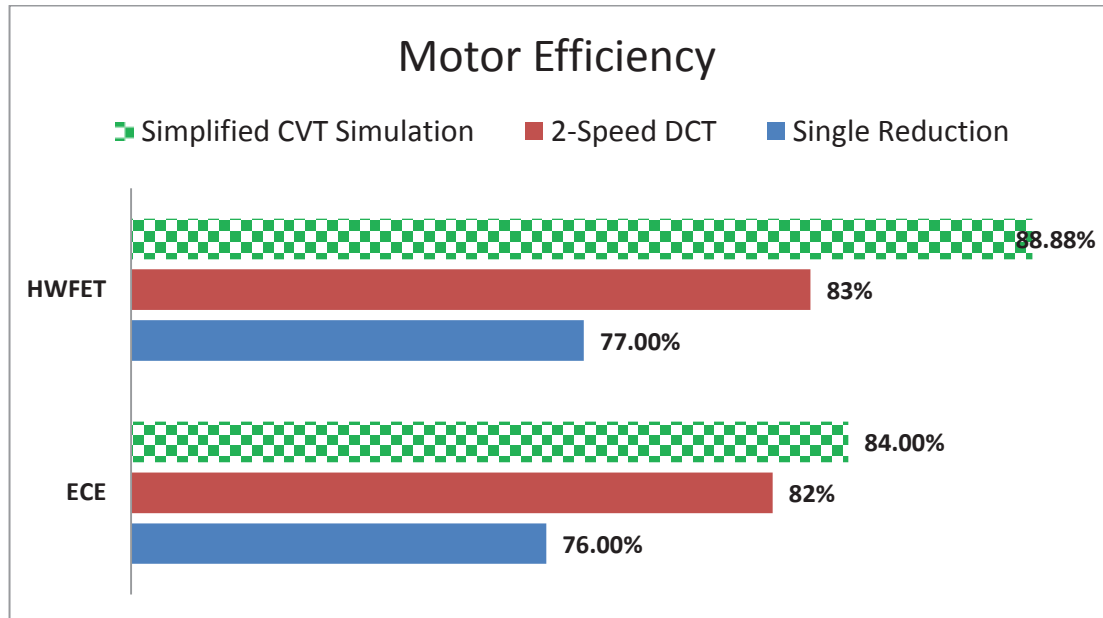
Figure 6-11: Motor efficiency comparison of BEVs equipped with different powertrains
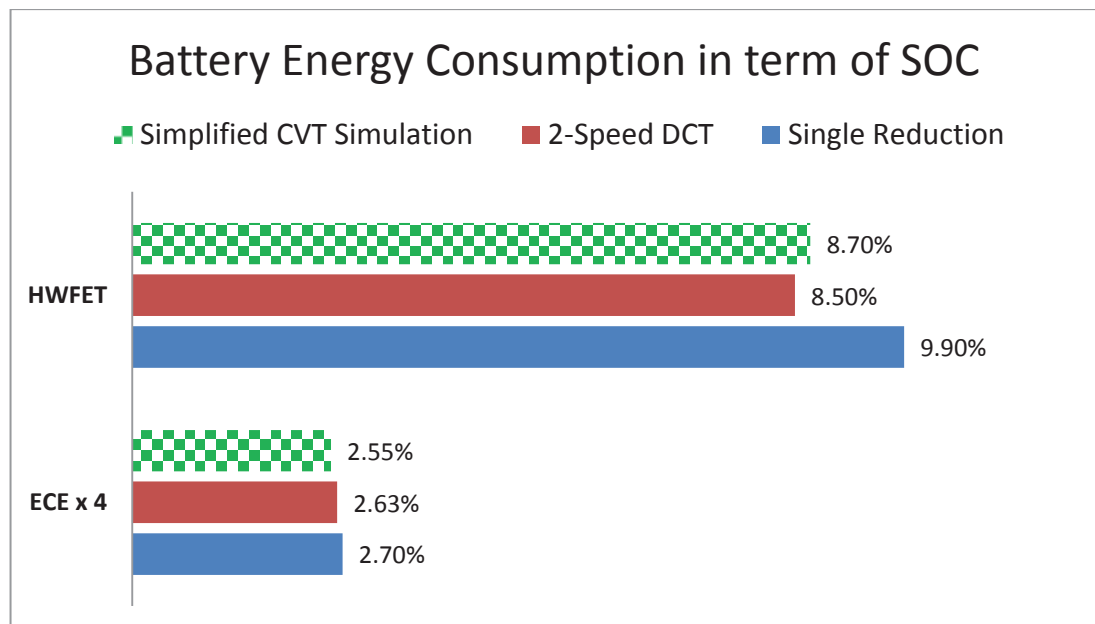
Figure 6-12: Comparison of power consumption in term of SOC

The total distance of one ECE and HWFET cycle are around 1 km and 16.5 km respectively. Based on the motor capacity of Table 3-1, Table 6-3 presents the energy economy performance of different transmissions based BEVs in an easier understand way, which is similar to the evaluation of gasoline vehicles:

Table 6-1: Economic performance of BEVs (driving kilometres per kW·h, KPK)

Energy Consumption (KPK)	SR based BEV	Two-Speed DCT based BEV	Simplified CVT based BEV
HWFET	6.09	7.09	6.93
ECE	5.41	5.56	5.73

6.5 ECONOMIC BENEFIT OF MUTI-SPEED TRANSMISSION FOR BATTERY ELECTRIC VEHICLE

Despite the potential of long-term savings to consumers, the initial cost of BEVs presents a major market barrier to their widespread commercialization. To identify and evaluate the value of adding multi-speed transmission to BEVs, the increased manufacturing cost and reduced daily-use cost for three transmissions based BEVs are analysed and presented below.

According to the method of "design using characteristic values [105], the transmission relative selling price (RSP) can be related to the input torque T_1, the maximum ratio $i_{G,max}$, and the number of gears z, shown in Eq.73.

$$RSP = 0.0183 \times (i_{G,max} \times T_1)^{0.512} z^{0.256}$$

<div align="right">(73)</div>

In this study, the input torque T_1 equals motor maximum output torque---300 Nm. $i_{G,max}$ could be found in table 3-4. Thus, the estimated gearbox RSP are presented in Table 6-2:

<div align="center">Table 6-2: Estimated gearboxes relative selling price</div>

Type	$T_1 = 350$ Nm, $z = 6, i_{G,max} = 5.5$	SR	Twos-speed DCT	Simplified CVT*
RSP	1	0.5	0.6	0.86

*The selling price of belt CVT is estimated to be similar with a 6-speed Automatic Transmission [106]

Combined fuel economy performance testing cycle, which is calculated by harmonically averaging the city and highway fuel economies with weightings of 43 percent and 57 percent respectively [107], is used to determine vehicle average fuel economy in this study. After transformation of the original formula in the reference, the economy performance in combined range is:

$$COMBINE_{KPK} = \frac{1}{0.57/HWFET_{KPK} + 0.43/ECE_{KPK}}$$

<div align="right">(74)</div>

Based on the experiment results in Table 6-1 and Eq.74, SR, two-speed DCT and simplified CVT based BEVs can run 5.78 km, 6.34 km and 6.36 km in combined cycles

by consuming 1 kW·h electricity respectively. Then, the one-charge driving range of BEV equipped with SR and 72 Ah battery is calculated:

$$Range_{SR} = Battery_{capacity}Combine_{SR\_KPK} = 380 \times \frac{72}{1000} \times 5.78 \qquad (75)$$

$$= 158km$$

Similarly, the one-charge driving ranges for the other two multi-speed transmissions equipped BEVs are shown in Table 6-3. Based on the same target performance in Table 4-1, 158 km driving range per charge, the required battery capacity is presented in Table 6-3 as well, comparing to the 72 Ah (380 V) battery in SR BEV.

$$C_{capacity\_SR} = 72 \times 380/1000 = 27.36\ kWh \qquad (76)$$

$$C_{capacity\_DCT} = 158/6.34 = 24.92\ kWh \qquad (77)$$

$$C_{capacity\_CVT} = 158/6.36 = 24.84\ kWh \qquad (78)$$

Table 6-3: Required Motor Capacity of different powertrains based BEVs

	SR based BEV	Two-Speed DCT based BEV	Simplified CVT based BEV
Driving Range for 27.36 kW·h Battery	158 km	173 km	174 km
Required Motor Capacity for 158 km Driving Range	$27.36\ kWh$	$24.92\ kWh$	$24.84\ kWh$

The estimated vehicle lifetime mileage is 300000 km [31] and the efficiency of charger is 81% at Level 2 standard charging voltage [109], as a result of same 90% efficiency for both plug-in charger and lithium-ion battery charge/discharge [110]. The total electricity consumed in 300000 km is presented as:

$$E_{SR\_lifetime} = 27.36 * 300000/158/0.81 = 64135 (kWh) \qquad (79)$$

$$E_{DCT\_lifetime} = 24.92 * 300000/158/0.81 = 58415 (kWh) \qquad (80)$$

$$E_{CVT\_lifetime} = 24.84 * 300000/158/0.81 = 58228 (kWh) \qquad (81)$$

According to OAK Ridge National Laboratory [111] and some commercial technical reports [112–114], the basis for battery electric vehicle cost calculations are shown in Table 6-4:

Table 6-4: Basic parts manufacturing cost of BEV

Vehicle Component	Cost (US $)
Battery Manufacturing	$ 400/kW·h
BMS, Power Electronic, etc.*	$ 238/kW·h
Battery Pack Final Cost (Incl. Margin and Warranty)	$ 800/KW·h
Motor	$ 40/kw
Transmission	$ 12.5/kw (Motor Power)
Average Electricity Fee (In Australia) [115]	$ 0.3/kW·h

*This part includes battery management system (BMS), power electronics, connections, cell support, housing and temperature control.

Considering the SR and two-speed DCT are not available on the market, simplified CVT is more specifically suited to setting the benchmark price by using the method in Table 6-2. Then, the price of two-speed DCT can be achieved by RSP in Table 6-7. However, SR is more like the primary reducer in multi-speed transmissions than a real transmission. The estimated price for SR by using RSP may be too high. Therefore, SR's price is reduced to zero in this study to testify if the two-speed DCT, or simplified CVT, has the ability to make up the cost disadvantage through saving battery energy.

Comparing to ICEs, electrical components such as traction motors and controllers require little maintenance. For instance, motor brake (regenerative brake) largely reduces the frequency of brake pedal replacement. The estimated maintenance costs for BEVs are around 70% [116] of an equivalent ICE vehicle, with a cost of $ 4.1 cents per km for a medium passenger BEV. According to [113], no battery replacement is expected before 375000 km distance theoretically, at least 250000 km in practice. Therefore, in this study, no battery replacement fee is applied to lifetime final cost for consumers. Considering the only difference in this study for the three structures is the gearbox, the lifetime vehicle maintenance cost is estimated to be the same, because the required maintenance for gearbox is infrequent, usually every 100000km for transmission oil change, comparing to the frequency of changing tyres, brakes, electronics and regular inspection. It only makes up very small part of the whole maintenance cost. Furthermore, some manufacturers guarantee their CVT products do not need any maintenance anymore [117].

All powertrain components received a manufacturer's mark-up of 50% in addition to a dealer's mark-up of 16.3% [111]. The final post-retail selling price on the market will be

approximately 1.7 times [118] as the pre-retail price calculated by data in Table 6-5, except the final battery pack retail price.

The required battery capacity is reduced due to the relative less energy consumed by two-speed DCT and CVT based BEV in particular testing cycles. Refer to the target performance and vehicle specifications listed in the Tables 4-1 and 4-2, the manufacturing and daily-use cost of SR, two-speed DCT and simplified CVT (Simulation) based BEVs are presented in the Tables 6-5. Again, it must be stressed that all the CVT relevant data is based on the simulation result. It still needs further experiment validation.

Table 6-5: Manufacturing Cost, Recommended Retail Price and Maintenance Cost

Vehicle Component Cost ($ USD)	SR based BEV	Two speeds DCT based BEV	Simplified CVT based BEV
Battery Manufacturing	$ 10944	$ 9968	$ 9936
BMS, Power Electronic, etc.	$ 6512	$ 5931	$ 5912
Battery Pack Final Cost (Incl. Margin and Warranty)	$ 21888	$ 19936	$ 19872
Transmission (125 kw)	$ 0	$ 1090	$ 1562
Motor	$ 5000	$ 5000	$ 5000
Total Powertrain Pre-Retail	$ 26888	$ 26026	$ 26434
Total Powertrain Post-Retail (1.7 retail makeup apply to	$ 30388	$ 30289	$ 31027

motor and transmission)			
Glider [118]	$ 17314	$ 17314	$ 17314
Recommended Retail Price	$ 47702	$ 47603	$ 48341
Vehicle Maintenance Cost (300000 km)	$ 12300	$ 12300	$ 12300
Battery Replacement Cost	$ 0	$ 0	$ 0
Electricity Cost in lifetime	$ 19241	$ 17525	$ 17468
Total Balance	$ 79243	$ 77428	$ 78109

CHAPTER 7 : BLENDED BRAKING SYSTEM ON MULTI-SPEED BEV

7.1 INTRODUCTION

Regenerative braking extends the mileage of electric vehicles by recapturing the vehicle's kinetic energy during braking, rather than dissipating it as heat. The motor supplied braking torque is applied to the wheels in an entirely different way compared to hydraulic friction braking systems. Drag torque and response delay may be introduced by transmitting the braking torque from the motor through a multi-speed transmission, axles, and differential to the wheels. Additionally, because the motor is usually only connected to one shaft and the available torque is limited, the traditional friction brake is still necessary for supplementary braking, creating a blended braking system. Complicated effects such as wheel slip and locking, vehicle body bounce and braking distance variation, will inevitability impact on the performance and safety of braking.

This chapter proposes a blended braking strategy with a manual selection function to achieve the balance between braking performance and energy recovery ability, but with safety ensured by an automatic overriding control strategy. Firstly, the energy lost in conventional friction braking in typical cycles is reported, to indicate the maximum potential gains from regenerative braking. Then, strengths and weaknesses of blended braking in a two-speed DCT based front-drive BEV are discussed. One advantage examined is the transfer of the load to the motor-connected front axle during braking,

while the torque interruption in gear shifting presents a disadvantage. Different strategies are designed to either recapture maximum braking energy, or achieve the best braking performance, or to compromise between energy recovery and braking performance. Then, a simulation model is established to analyse the details of braking force distribution, wheel slip, and kinetic energy recovery rates in various test conditions.

7.2 MAXIMUM KINETIC ENERGY RECOVERY

In EVs, regenerative braking captures the drop in the vehicle's kinetic energy, which in traditional ICE vehicles is lost as heat in friction brakes. However, the different working principles and the potential safety risks have been barriers to large-scale commercialization. To assess whether it is worth the extra cost of additional equipment and R&D to achieve a blended braking system for EVs, one must know the potential gain, i.e. how much energy is consumed by braking.

Fig.7-1 shows the distributions of energy consumption in several typical driving cycles for a medium size passenger Battery Electric Vehicle (BEV), without regenerative braking. The results are based on the integral of driving energy consumption and energy lost in friction braking with respect to time. The dynamic energy consumption in the driving of specification Table 4-1, i.e. rolling, aerodynamic drag and acceleration, is calculated by Eq.78, which is the product of vehicle dynamic resistance and travel distance per computational step size. According to the target speed profile of cycles, the dynamic friction braking force is achieved in Simulink model. For city or hybrid cycles, as shown in Fig.7-1, the energy wasted in braking is vary large, e.g. 39% in the

California Unified Cycle (LA-92) and 35% in Urban Driving Dynamometer Schedules (UDDS). In fact, the energy wasted can easily go over 50% during peak commuting times in congested cities, or in a long distance-downhill, is shown in Fig.7-2. Even in the highway cycle Highway Fuel Economy Testing (HWFET), with less acceleration and deceleration events, the braking loss is still a significant 15%. Though not all of the kinetic energy during braking can be recaptured, as shown in Fig.7-3, these figures show the great potential for a regenerative braking system (RBS) to extend driving range, thus saving energy use cost.

$$\Delta E_{driving} = (mgC_R \cos\varphi + mg\sin\varphi + C_D Au^2/21.15 + \delta m d_u/d_t) \times \Delta x \quad (82)$$

where C_R is the rolling resistance coefficient, φ represents the slope angles, C_D is the aerodynamic drag coefficient, A is the front area, u is vehicle velocity in km/h, δm is the equivalent mass in acceleration including the rotational components. Δx represents the travel distance per computational step size in Simulink model.
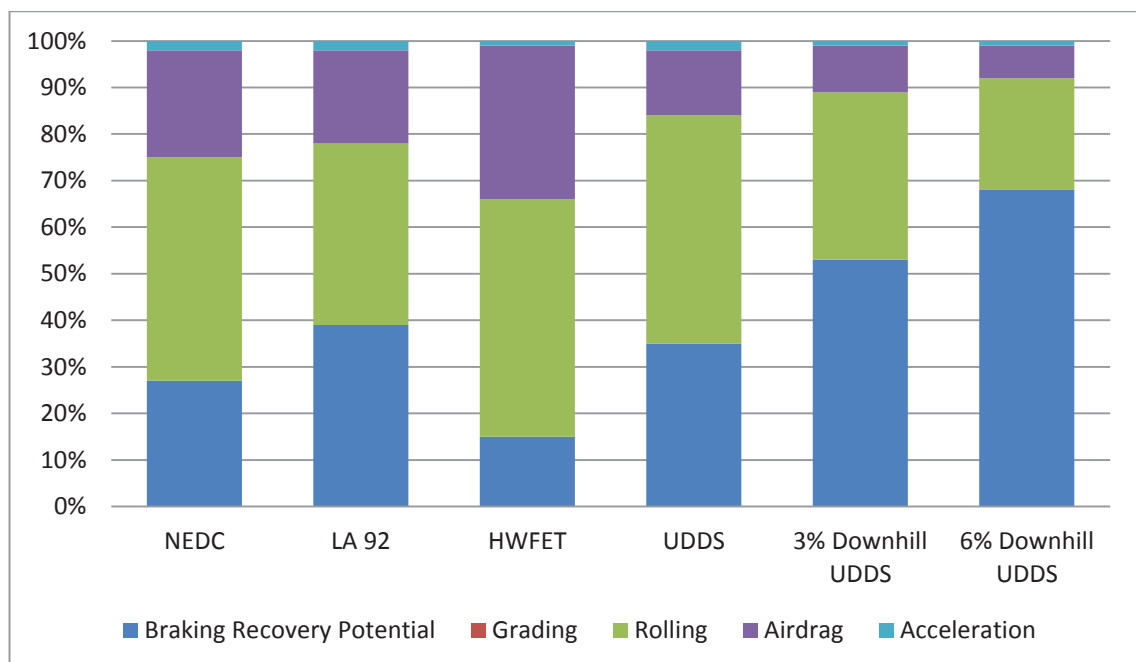
Figure 7-1: Energy Consumption Distribution in Driving Cycles
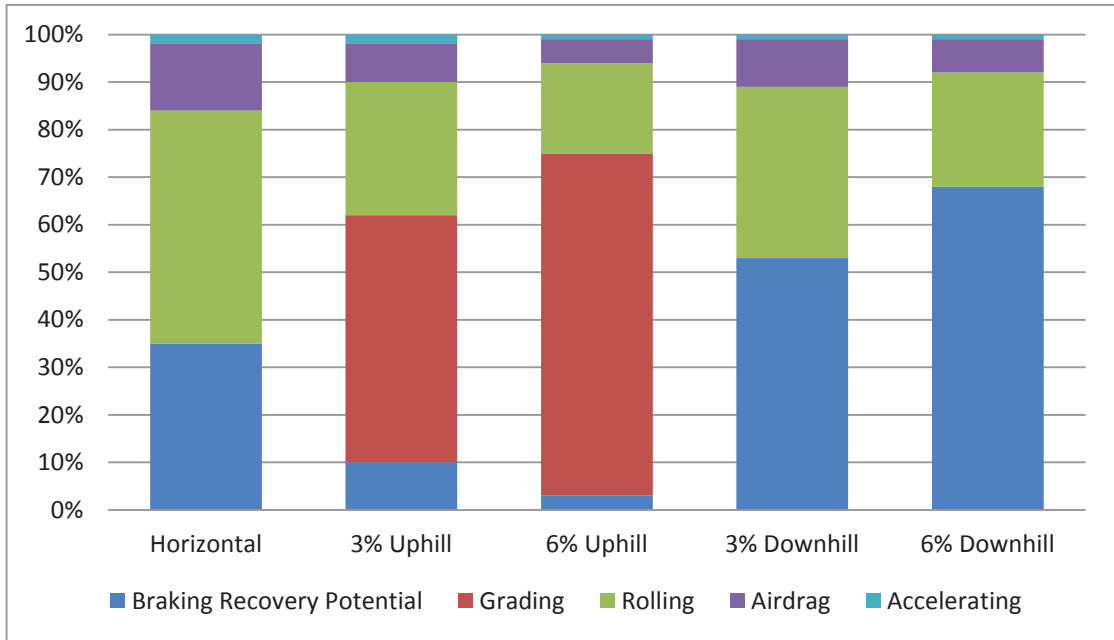
Figure 7-2: Energy Consumption Distribution in UDDS at different slope
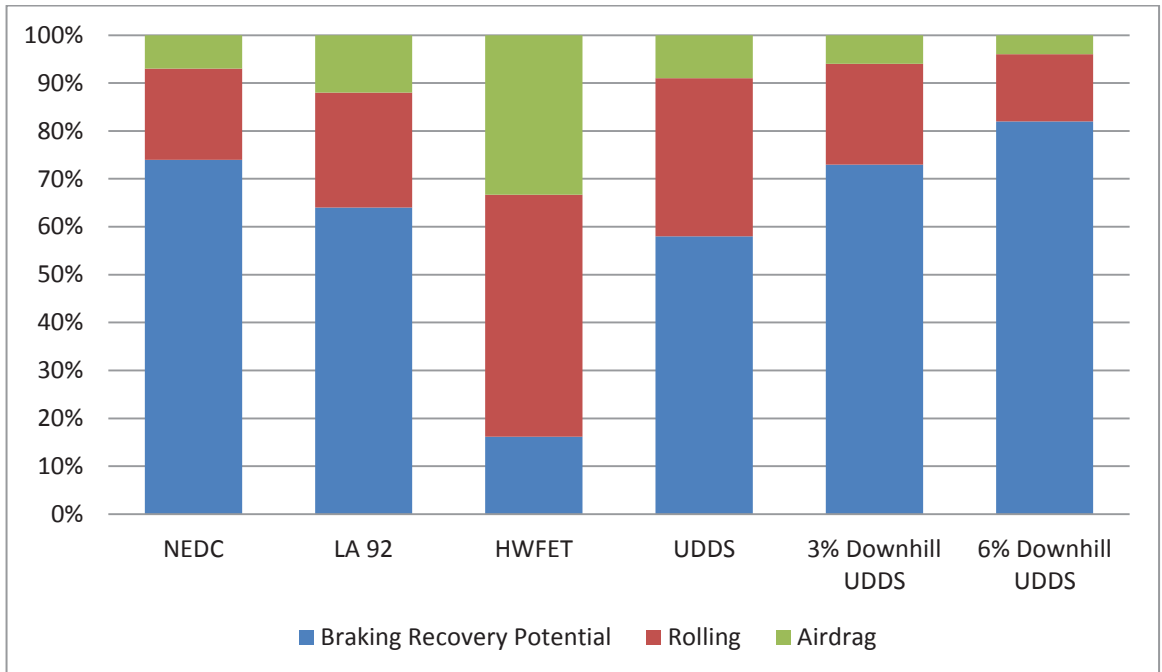
Figure 7-3: Energy Consumption Distribution in Driving Cycles during braking

Referring to Fig.4-20, for any given speed profile, the VCU calculates the required driving and braking torques and the power from the battery. The total required braking torque is apportioned in the 'Brake Torque Distribution' block into three command paths, to the front (axle) motor brake, the front friction brake, and the rear friction brake, according to the selected strategy. The regenerative braking torque is limited by the motor's maximum torque ability, which is a function of speed, and by the maximum charging current capability of the battery, which is a function of its state of charge. The motor torque goes through a multi-speed transmission, before being applied to the driven front axle. In the alternate torque command path, mechanical friction braking is directly applied to the wheels, front or rear, via a hydraulic system.

The advantages and details of a two-speed DCT-based BEV have been introduced in Ref [119]. Here, only topics relating to braking in this new DCT structure are examined. Fig.7-4a depicts the two-speed DCT-based powertrain topology, and Fig.7-4b shows the powertrain's installation on the test bench used in this study. The test rig incorporates a high rotational inertia provided by four railway wheels to mimic the linear inertia of a moving vehicle.
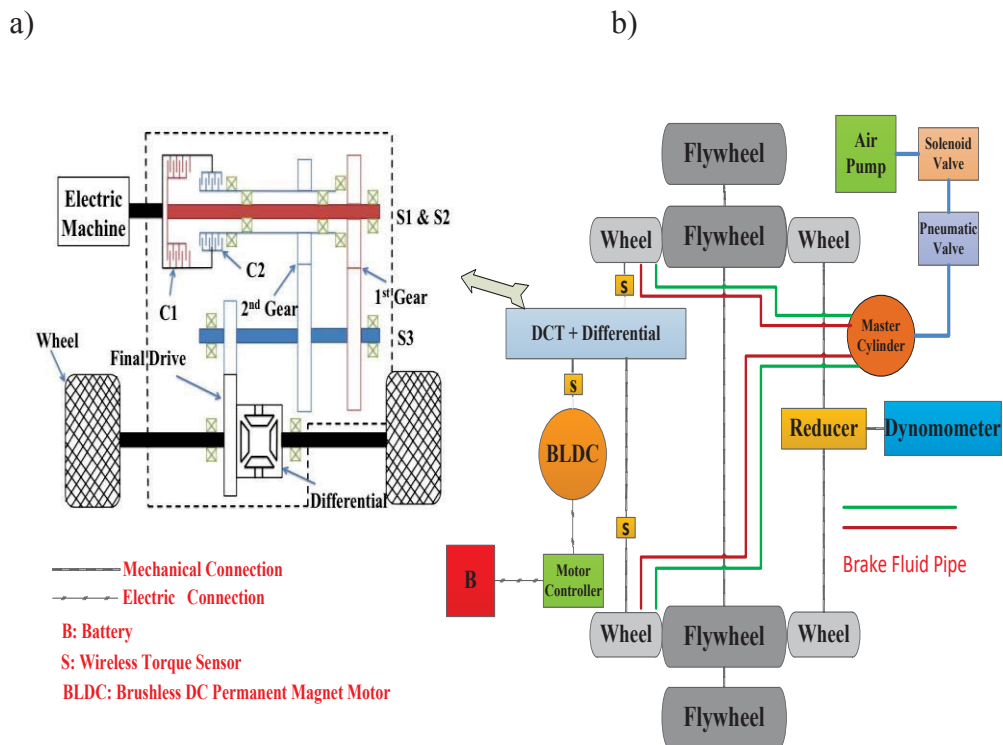
Figure 7-4: Schematic diagrams of: a) the Two-Speed DCT-based BEV powertrain

topology; and b) the test bench.

The benefits of using front wheel drive in traditional ICE vehicles carry over to BEVs, such as lower cost, simpler design, control and manufacture, and greater boot space. Furthermore, for BEVs, there is an additional advantage that regenerative braking has more significant energy recovery potential on the front axle compared to the rear axle due to load transfer. The dynamic added weight on the front axle when braking or on the rear axle when accelerating is expressed:

$$\Delta Weight = amh_g/w \qquad\qquad (83)$$

where a is the vehicle longitudinal acceleration, h_g is the height of the centre of mass, w is the wheelbase length and m is the total vehicle mass [120]. Fig.7-5 gives the ratio of

the normal forces on the front and rear wheels at different deceleration rates of specification Table 4-1.
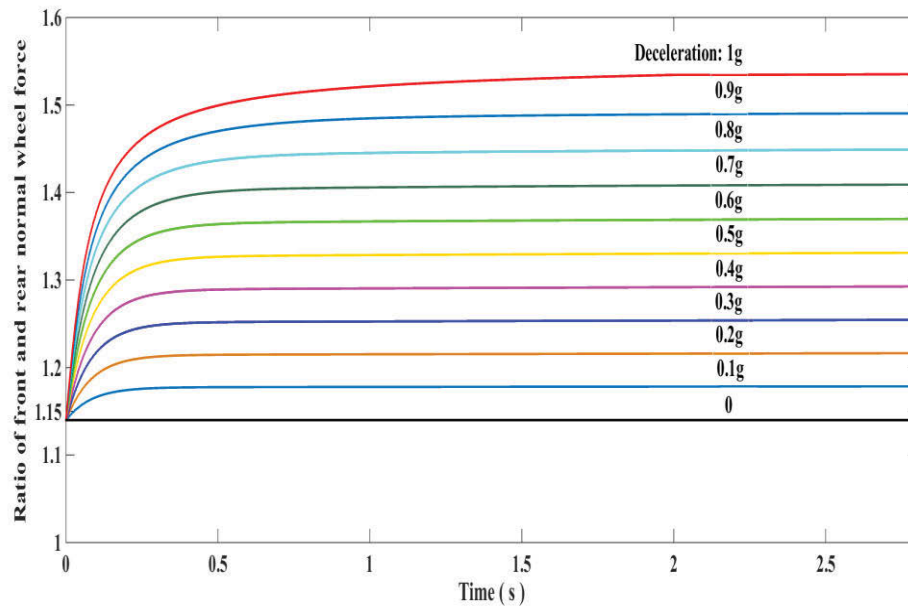
Figure 7-5: Ratio of the normal loads on the front and rear wheels during braking for a typical city vehicle chassis

The ratio increases from 1.15 at a constant speed to approximately 1.54 at 1 g (9.81 ms^{-2}) deceleration. The normal wheel load determines the maximum available friction force given the friction coefficient µ between a particular road and tyre, according to:

$$F_{friction} = \mu F_{normal} \qquad\qquad (84)$$

Thus, the additional normal load on the front axle during braking enables greater regenerative braking from a front-mounted motor.

7.3 BRAKING REGULATIONS AND PROPOSED TESTING MANOEUVRES

In addition to the braking stability and performance testing procedures implemented in conventional vehicles, a BEV that is equipped with a non-hydraulic RBS needs specialized testing to isolate any potential system failures. For example, with the regenerated energy typically being deposited in the battery, any effect on the RBS from the battery being full charged must be tested.

In Europe, general safety requirements for new vehicles are legislated in Regulation (EC) No 661/2009 [121]. Specific requirements for braking systems are legislated by one or other of the following UNECE Regulations depending on the vehicle type and mass, the first Regulation applying to cars (category M1 being passenger vehicles of up to 8 passenger seats with maximum laden mass less than 3.5 tonnes):

- ECE Regulation 13H for light passenger vehicles (M1) and optionally light goods vehicles (N1) [122]
- ECE Regulation 13 for virtually all other vehicles [123]

ECE 13H and 13 divide the types of regenerative braking systems into three categories and describe the testing procedures in great detail [122],[52]:

- Category A: The electric regenerative system is not part of the ("service" or main) braking system. Typically, the function and the braking feeling feedback to the driver are similar to engine braking in ICE vehicles.

- Category B Non-Phased: The electric regenerative system is part of the braking system, and regeneration commences or is increased when the brake is applied. The electric regenerative force starts to be developed at the same time as or slightly after the conventional friction brakes. This is also described as a parallel blended braking system.

- Category B Phased: The electric regenerative system is part of the braking system and the regenerative force can be developed ahead of any braking from the conventional friction brakes. This is also known as a serial blended braking system. This system allows the maximum amount of regenerative energy to be recovered.

Whichever the type of regenerative braking system, ECE 13H and 13 have the compulsory requirement of granting any ABS an overriding priority to control braking. Similar procedures are presented in the United States National Highway Traffic Safety Administration [124].

To demonstrate compliance with the aforementioned regulations, the following specially designed manoeuvres [52] and typical driving cycles are selected to test blended braking systems on BEV:

- Single straight line braking with piecewise braking force;
- The cooperation of ABS, Electronic Braking Force Distribution (EBD) and RBS;
- Load varying braking;
- Gear shift during braking;
- NEDC, UDDS, HWFET, LA-92 and JP1015 [125–129];

7.4 REGENERATIVE BRAKING CAPABILITY

Compared to hydraulic braking systems (HBS), the available regenerative braking torque is restricted by many factors, including the maximum available motor torque (which is a function of motor speed), the transmission gear ratios, and the maximum acceptable battery current. Therefore, the HBS must be ready to automatically compensate for any unexpected electric braking absence or diminishment, at any time. Furthermore, the HBS must be ready to adjust its braking output torque to an appropriate level to meet the driver's deceleration demand when the driving conditions change, for example if the vehicle hits a patch of ice.

The available regenerative braking force on the front wheels, shown in Fig.7-6, is restricted by the motor peak output torque, the speed, and the gear ratio. As we can see from Eq.86, the maximum braking force from the motor of specification table 3-1 is limited to approximately 5 kN when the vehicle runs in 2nd gear. Even when the vehicle runs in 1st gear with a bigger torque amplification ratio, shown in Eq.85, the available maximum motor braking force is only 8 kN because the peak motor torque can only be supplied up to a certain speed, namely 2500 rpm for the motor of the specification of table 3-1. These maximum torques are only available during the starting period until each gear's 'turning point', given by Eq.87 and Eq.88, above which the maximum available braking torque drops as shown by the top operating boundary curves of Fig.3-4. For this reason, mechanical braking is still necessary for BEVs, in addition to the safety concerns.

For mild or moderate braking in the normal speed range, the required braking force can be supplied by the motor alone. However, under heavy braking or for the vehicle cruising at high speed, the motor has to cooperate with mechanical friction braking to stop the vehicle jointly.

$$Brake_{\text{max\_1}}: T_{max} i_1 / r = 300 \times 8.45/0.3125 \ N = 8112 \ N \qquad (85)$$

$$Brake_{\text{max\_2}}: T_{max} i_2 / r = 300 \times 5.36/0.3125 \ N = 5146 \ N \qquad (86)$$

$$Turning \ point \ v \ in \ 1^{st} \ gear: \frac{2500 \times 2 \times pi \times 0.3125 \times 3.6}{8.45 \times 60} = 35 \ km \qquad (87)$$

$$Turning \ point \ v \ in \ 2^{nd} \ gear: \frac{2500 \times 2 \times pi \times 0.3125 \times 3.6}{5.36 \times 60} = 55 \ km \qquad (88)$$
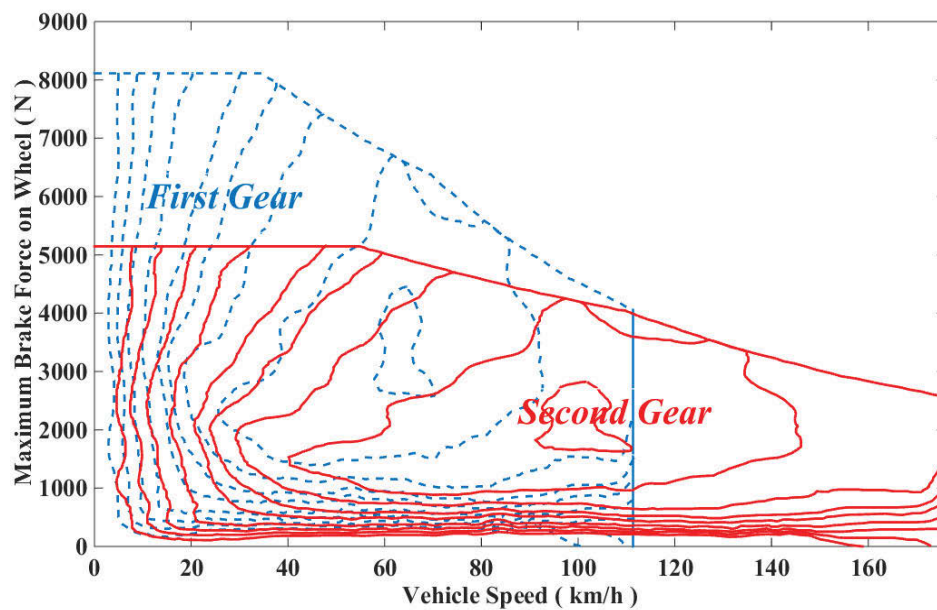
Figure 7-6: Available operating region of the motor braking force on the front wheels in different gears, also showing contours of motor efficiency.

7.5 STABILITY AND CONTROLLABILITY IN BRAKING

Backward-sloping colour lines in Fig.7-7 are the lines of constant total braking force, corresponding to the indicated deceleration values (as multiples of g). Eq.89 and Eq.90 give the maximum available friction force for front and rear tyres as a function of the road-tire friction coefficient.

$$F_{bf} = \mu mg(L_b + zh_g)/L \qquad (89)$$

$$F_{br} = \mu mg(L_a - zh_g)/L \qquad (90)$$

where F_{bf} and F_{br} are the dynamic maximum friction force on front and rear wheels during decelerating based on load transfer. L_a and L_b are the distances from wheel centre to the centre of mass. The total maximum friction force is

$$Maximum\ (F_{bf} + F_{br}) = \mu mg \qquad (91)$$
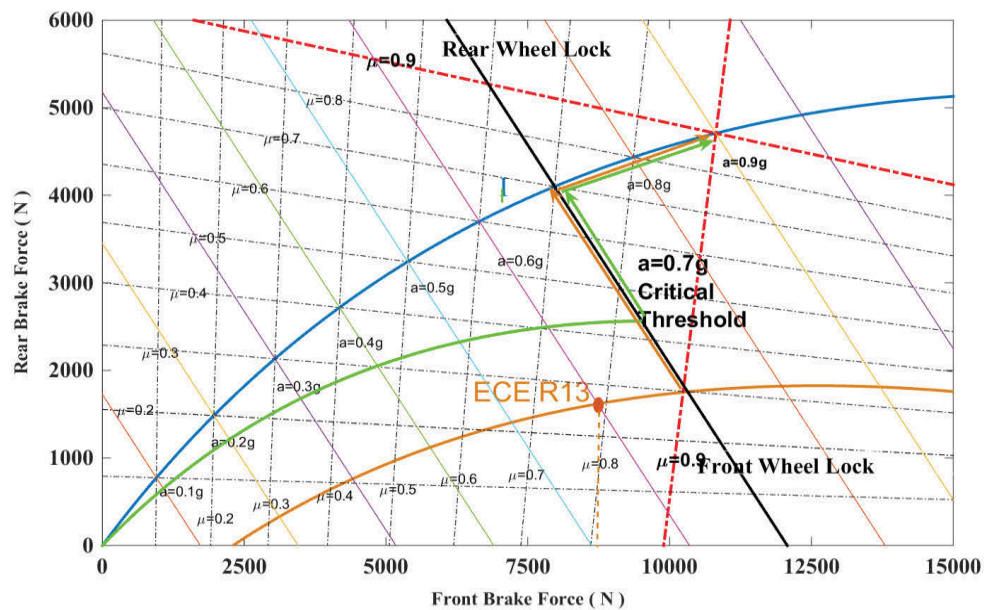
Figure 7-7: Braking force distribution on front and rear wheels for the vehicle of

specification

The vertical and horizontal black dash-dot lines represent the maximum available friction force based on different friction factors μ and the vehicle specification in Table 4-1. In other words, if the braking force applied to the wheels exceeds the critical threshold on a particular μ road, the wheel will lock. Generally, μ is less than 1.2, which means the maximum deceleration should be lower than 1.2g to avoid wheel locking, although the deceleration can go over 3g by improving vehicle aerodynamics structure and driving on a specially designed road, as is the case in Formula 1 racing. In this study, considering the various road conditions and tyre types used by the majority of passenger vehicles, which together determine the friction factor, the maximum μ is set to 0.9 for safety at the cost of wasting some braking capability. The two red dash-dot bolt lines in Fig.7-7 are the braking force limitations of the front and rear wheels in this study. For some special low μ road conditions such as wet and snow, the wheel locking risk generated by hard braking will be handled by ABS.

The solid blue line I joins the operating points of maximum total force for varying friction coefficient. If the front/rear wheel braking force distribution ratios always follow this blue curve, known as 'Ideal' braking force distribution ratio, the vehicle will make the maximum utilization of road-tyre friction force and ensure the most stability and controllability in braking. For all load conditions, UNECE Regulations demand that the adhesion coefficient utilization curve of the rear axle must not be higher than the curve for the front axle [130,131]. In regard to Fig.7-7, this means that the force distribution curve should always be lower than the ideal curve.

There are lots of braking related regulations and directives from worldwide governments and organizations, but regulations in most countries are very similar to ensure that road vehicles are designed and constructed to decelerate safely and efficiently under all conditions of operation. The European UN Regulation 13-H is recognized as a valid type-approval standard in all EU and many non-EU countries, with members of the 1958 Agreement including Japan, USA, Canada, Australia, Korea, China, India, and Malaysia. It requires that, for all states of loading, two-axle vehicles that are not equipped with ABS, the rate of braking must meet the requirement of Eq.92

$$z = a/g > 0.1 + 0.85(\mu - 0.2) \qquad (92)$$

Although for the weight of the vehicle assumed in the specification of Table 4-1, UN Regulation 13-H actually applies, in which the 0.85 factor in Eq.11 is replaced by 0.70, we will adopt the more demanding 0.85 factor of Regulation 13 assuming a greater margin of safety is desired. The distribution of braking forces is given by Eq.93 and Eq.94, which is shown by the golden curve in Fig.7-7.

$$F_{bf} = \left(L_b + zh_g\right)(z + 0.07)g/0.85L \qquad (93)$$

$$F_{br} = mgz - F_{bf} \qquad (94)$$

In summary, the area, restricted by solid blue 'Ideal braking force distribution' curve, red dash-dot 'maximum available friction braking force on front wheels' curve, golden ECE R13-H regulation curve, and horizontal axis, indicates the range of available braking force distribution ratios of the front and rear wheels.

7.6 SAFETY (MOTOR PRIORITY) STRATEGY

Braking safety, including stopping distance, stability and controllability, is always the top priority and is likely to be tested by bad weather and road conditions. The motion of a wheel in a normal driving vehicle consists of two parts, namely rolling and sliding, which causes a difference between the speeds of the vehicle and the wheel. In the longitudinal direction, if the force applied to the wheel by brake callipers exceeds the maximum available friction force between the tires and ground, as shown in Eq.95, then the relative motion between the tires and road will change from a mix of sliding and rolling to pure sliding. This phenomenon is known as 'wheel lock'. Specific to the blended braking system, it occurs when the total braking force from the motor and callipers exceeds the friction force from the ground:

$$f_{regen} + f_{caliper} > f_{brake\_friction} = mg\mu \qquad (95)$$

The wheel slip ratio is defined as the ratio of difference between the rotational speed of the wheel and the translational velocity of the wheel center:

$$\lambda = \Delta v/v = \left(\omega r_{dyn} - v\right)/v \qquad (96)$$

ω is the wheel rotation speed and r_{dyn} represents the dynamic radius of the wheel, which is determined indirectly by measuring the travel distance per rotation circle. λ is a value from 0 to 1 representing the motion of the wheel from freely rolling to lock. The solid blue curve in Fig.7-8 shows the dependence of the friction factor μ on the longitudinal slip ratio λ on dry asphalt pavement. The μ drops significantly when the

vehicle travels on a wet or snow-covered road, which is presented by solid and dashed green curves. Moreover, a steering angle causes the friction factor to fall as well.
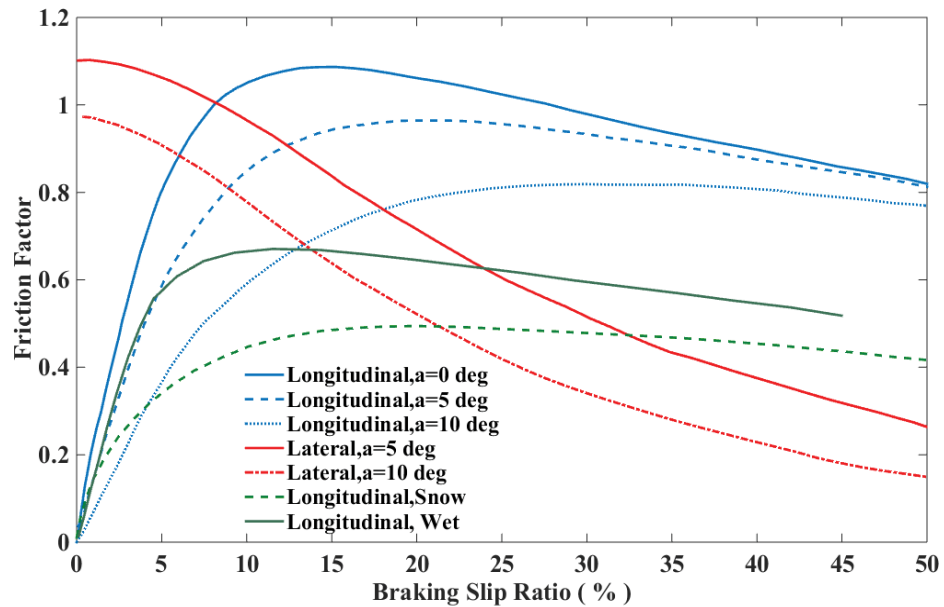
Figure 7-8: The influence of slip ratio, steering angle ("a" in degrees) and road condition on friction factor [132]

The force in the lateral direction of the road-tire contact surface directly affects the direction controllability of the vehicle. A locked wheel cannot generate lateral force to offset the sideslip trend, when cornering or unintentionally steering during an emergency brake, resulting in unnecessary under-steering and uncontrollable over-steering. As shown in Fig.7-8, the lateral friction factor falls dramatically with increased longitudinal braking slip ratio. For example, for a wheel with 5° steering angle and 20% longitudinal slip ratio, the lateral friction factor only equals half that of pure straight driving. When the longitudinal slip ratio hits 100% (wheel lock), steering input has no result on yaw motion because the front tires are saturated, and no lateral force can be

generated. If it happens to the front wheel, the vehicle will lose steering ability. However, there is no directional instability because whenever the lateral movement of the front wheels occurs, a self-correcting moment due to the inertial force of the vehicle about the yaw centre of the rear axle will be developed [40]. Consequently, it tends to bring the vehicle back to a straight line path. In contrast, if the rear wheels are locked, they lose their capability to generate the required side forces and the rear end might start to slide sideways, losing directional stability. The omitted red arrows on the rear wheel and front wheels, in the 'Over-steering' and 'Under-steering' Fig.7-9 schematics, indicate the locked wheels and lost lateral force. The black arrows show the potential movement directions.

The best 'Safety' strategy should properly distribute braking force to each wheel, keeping their operating points below the maximum front and rear road friction curves (Red dash-dot bolt lines in Fig.7-7). All wheels will lock simultaneously if using this strategy for maximum braking.

The critical threshold of deceleration rate in an emergency brake is set as 0.7g in this study. Therefore, if the strategy is manually set to 'Safety', or if the deceleration rate goes over this threshold value in other strategies, then the braking force must be ideally distributed to the front and rear wheels, i.e. on the blue curve I in Fig.7-7. To recapture as much braking energy as possible, 'Safety (Motor Priority)' strategy is proposed, in which the motor takes responsibility for supplying the required front torque until reaching its maximum ability. The principle and details of this strategy are presented in Fig.7-10. Of course, any wheel lock occurrence would be detected and avoided by ABS.

Non-ideal braking force distribution strategies result in asynchronous wheel locking time, which can cause over-steering or under-steering.
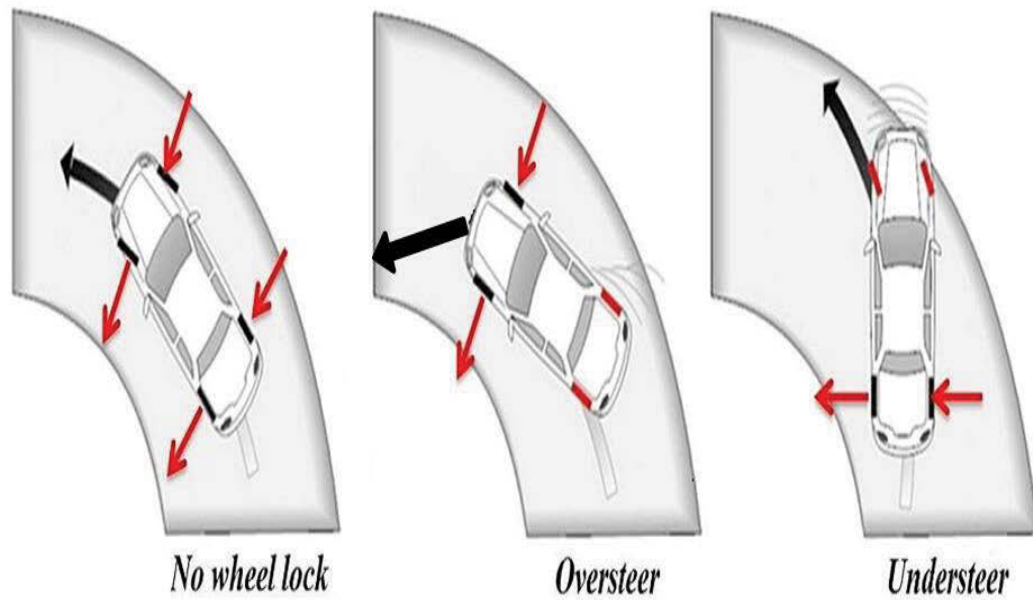
Figure 7-9: Schematic over-steering and under-steering when wheels lock, shown in red. Red arrows show lateral forces on unlocked wheels.
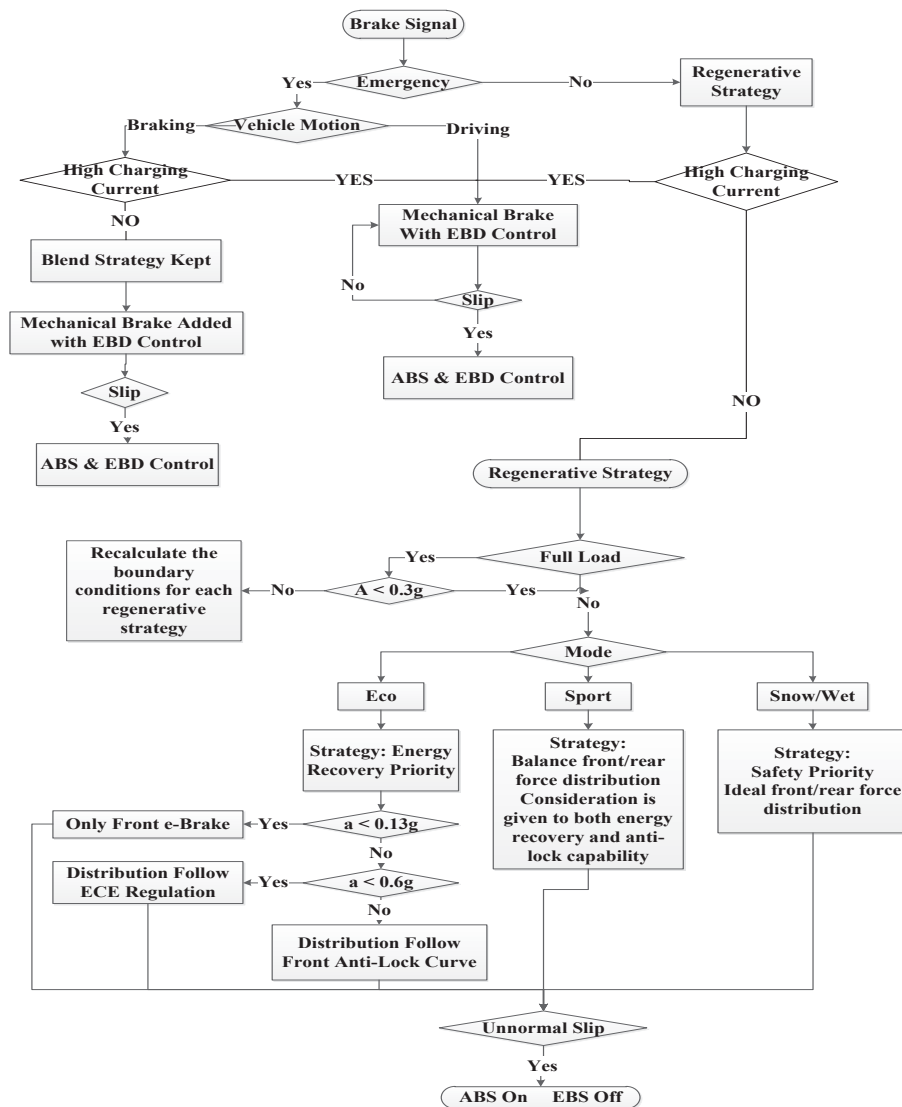
Figure 7-10: The Cooperation of RBS, EBD and ABS

7.7 ECO STRATEGY

To maximize the recovery of braking energy, only the front electric brake is utilized while deceleration remains below the critical intersection point, which is determined by the horizontal axis and ECE R13-H regulation curve. After that, the ratio of front and rear axle braking force follows the ECE regulation curve, the golden one in Fig.7-7,

until the deceleration triggers the emergency situation-0.7g. Then, the distribution strategy jumps to the 'Safety (Motor Priority)'.

7.8 SPORT STRATEGY

Aggressive driving is desired when the driver intentionally selects this strategy. Although, motor failure caused by the frequent and fast changed torque requirements should be avoided in any strategy, high acceleration and deceleration and more frequent start-stops may still increase the possibility of motor failure. This requires that the sudden absence of motor braking force will not affect the braking safety performance; the demanded motor torque never exceeds the motor ability, regardless of the motor speed and gear ratio in this strategy. The available electric brake varies according to the motor speed and gear ratio for a full pedal brake. The minimum available electric force in a full pedal brake ($Regen_{min}$) appears at the highest motor speed with the minimum gear ratio, which is 8000 rpm and 5.36 respectively in the specification of Table 4-1. To ensure this critical value is always lower than the required electric brake, the ratio of minimum full pedal electric brake force and the theoretical maximum brake force (mu equals 1) is defined as the ratio of regenerative/total required brake:

$$\frac{Regen_{min}}{Friction_{max}} = \frac{\frac{T_{min} \times i_{g2}}{r}}{m \times g \times mu} = \frac{\frac{150 \times 5.36}{0.3125}}{1800 \times 9.81 * 0.9} = 15.8\,\% \qquad (\,97\,)$$

Compared to the Eco strategy when electric braking has the priority and mechanical braking works as a supplement, the mechanical braking torque, and the motor supplied braking torque act jointly all the time in Sport strategy. Based on the braking force distribution in Safety strategy, the additional 15.8% of total required braking force

which is applied to the front axle, comes from the motor. Consequently, if motor works well, the friction and electric braking force will increase continuously and smoothly without any braking source alternation, at a fixed ratio. If the motor is out of order, the mechanical braking will work alone with an 'Ideal' front/rear distribution ratio to guarantee a stable and controllable deceleration.

7.9 MOTOR FAULT INSURANCE STRATEGY

Generally, electromagnetic equipment is considered to be not as robust as a hydraulic system. Specific to the blended braking system, motor downtime is a very dangerous situation, whether caused by IGBT failure or temperature protection. Especially during continuous downhill braking, high current may cause motor overheating and trigger a protection mechanism, especially when the cooling system is out of order. It is not common but is a serious event. A fail-safe provision of hydraulic braking should be activated immediately when electric braking torque is limited or a 'torque error' is detected. Including consideration of motor overload and failure redundancy, a fail-safe mechanism for the motor is presented in Fig.7-11.
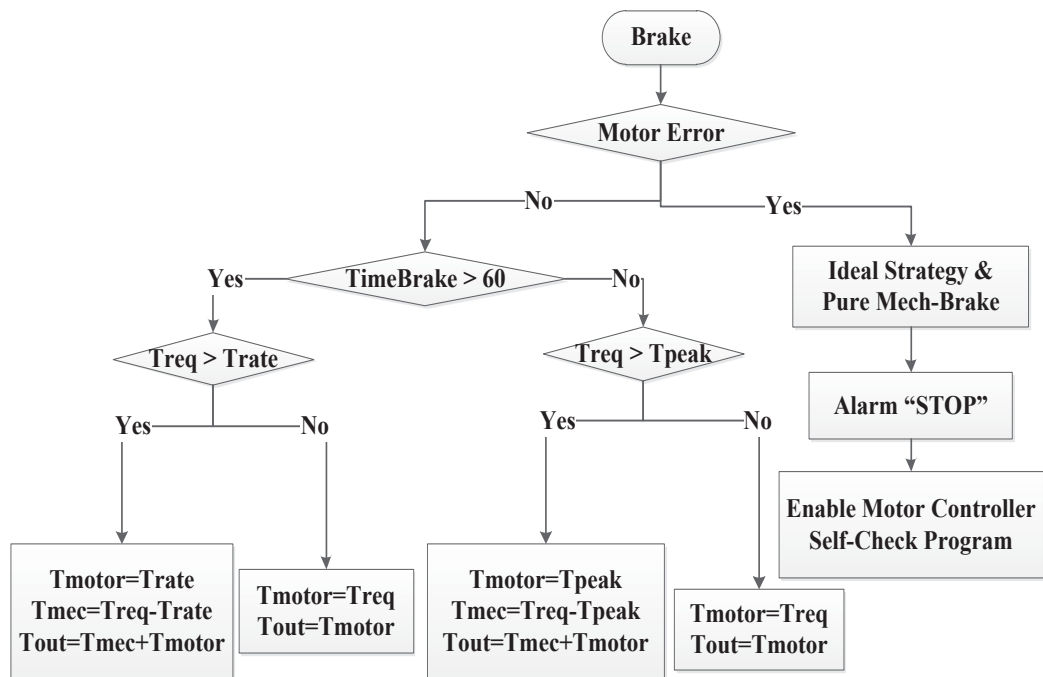
Figure 7-11: Motor control & fail-safe strategy

CHAPTER 8 :   BRAKING PERFORMANCE ANALYSIS OF THREE BLENDED BRAKING STRATEGIES

8.1 INTRODUCTION

The goal of automotive braking system design, whether for conventional or blended systems, is to achieve a comfortable and reliable deceleration at the request of the driver. In addition, the vehicle must be brought to a stop as soon as possible in an emergency situation, while maintaining dynamic stability and controllability.   This chapter is divided into four parts to test the performance of three different blended braking strategies in simulation: a) single straight line braking; b) the cooperation of regenerative braking, ABS, and EBD; c) gear shifting during a blended braking; d) braking performance in several typical cycles.

8.2 SINGLE STRAIGHT LINE BRAKING

In this testing profile, the vehicle begins to decelerate from 100 km/h to 92.8 km/h in 2 seconds, then, slows down to 60.4 km/h in 3 seconds, and finally brakes to a full stop in the next 2 seconds. The deceleration increases from 0.1g (Mild Braking) to 0.3g (Moderate Braking) to 0.9g (Emergency Braking) in three stages. Fig. 8-1 shows the braking forces and wheel slip versus time for the different strategies introduced in

Chapter 7 and Fig.8-1 plots the trajectory of the distribution of braking forces to the axles for each strategy.
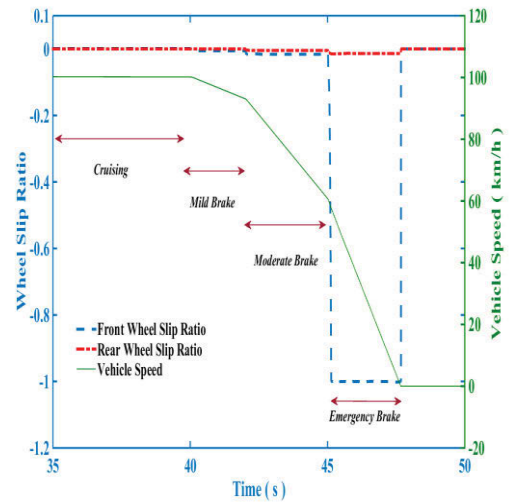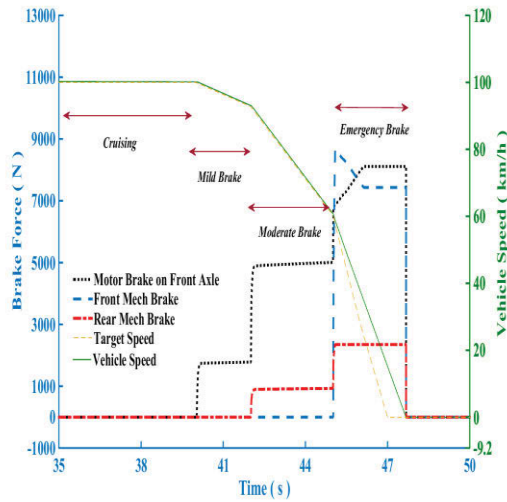
(a) Braking force distribution in Eco strategy   (b) Slip ratio in front & rear wheels for (a)
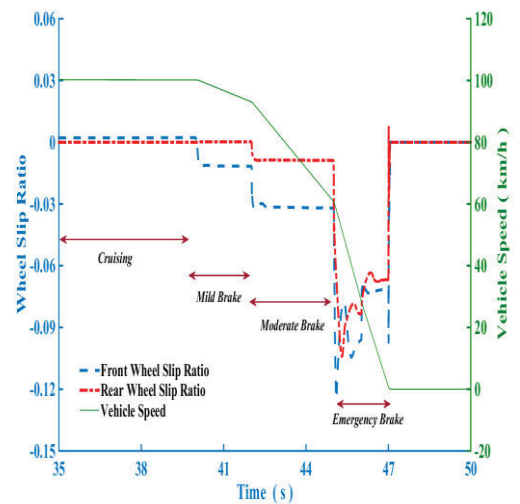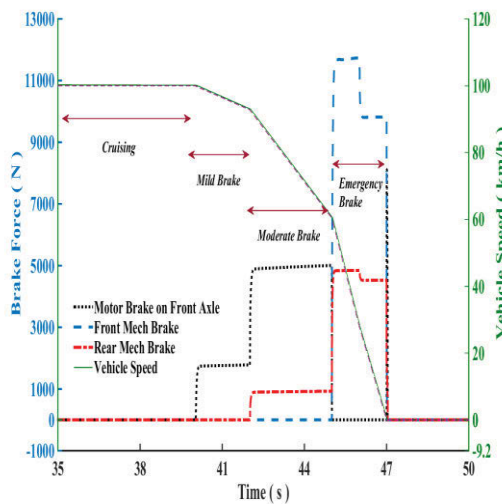
(c) Braking force distribution in Eco & Safety strategy (d) Slip ratio in wheels for (c)
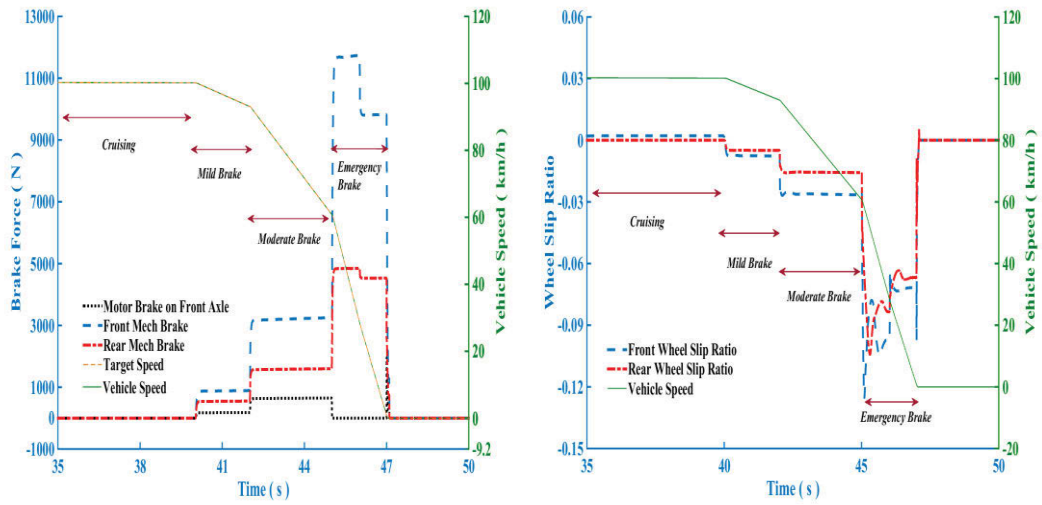
(e) Braking force distribution in Sport & Safety strategy (f) Slip ratio in wheels for (e)
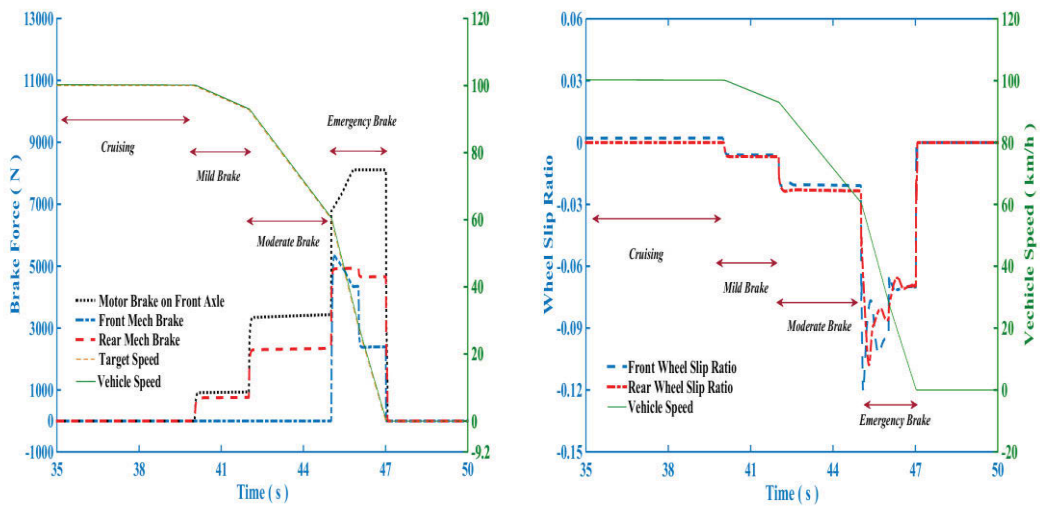
(g) Braking force distribution in Safety (Motor Priority) strategy (h) Slip ratio in wheels

Figure 8-1: Straight line braking force distribution and wheel slip ratios for: (a) and (b) Eco strategy; (c) and (d) Eco & Safety strategy; (e) and (f) Sport & Safety strategy; and (g) and (h) Safety strategy.

As shown in Fig.8-1 (a) and (b), the Eco strategy distributes the required braking force to the front axle as much as possible under the limitation of laws and regulations. Most of the front braking force is supplied by the motor, which is represented by the black dotted curve. During mild braking, all the required braking force is provided by the front-wheel regenerative brake. During moderate braking, front electric braking and rear friction braking, which is represented by the red dash-dot curve, share the increased braking force demand. Finally, during emergency braking, front friction braking (blue dash curve) increases sharply to compensate for the insufficient front braking force, due to the output torque limitation of the motor. It is apparent from Fig.8-2 that the purple curve strategy should be switched to the safety strategy, red hexagram curve, to avoid any wheel locking when the front or rear braking force goes over the 'wheel lock' line.

Therefore, if the strategy is not already chosen as 'Safety', the strategy should be automatically switched to 'Safety' when emergency braking occurs. The braking force distribution ratios of 'Eco' and 'Sport', represented by star and triangle curves in Fig.8-2, are automatically switched to 'safety' when deceleration gets close to 0.7g. As a result, both of them have satisfactory braking performance, as demonstrated by the actual speed following the target speed in Fig.8-1 (c) and (e). No braking force comes from the front friction brake in the 'Eco & Safety' strategy before emergency braking arises, after which the distribution ratio is switched to the 'Sport & Safety' strategy.

The electric brake supplies braking torque as much as possible until reaching its limitation in 'Safety (Motor Priority)' strategy, then, compensation is made by hydraulic friction braking on the front wheels to meet the driver's deceleration demand.
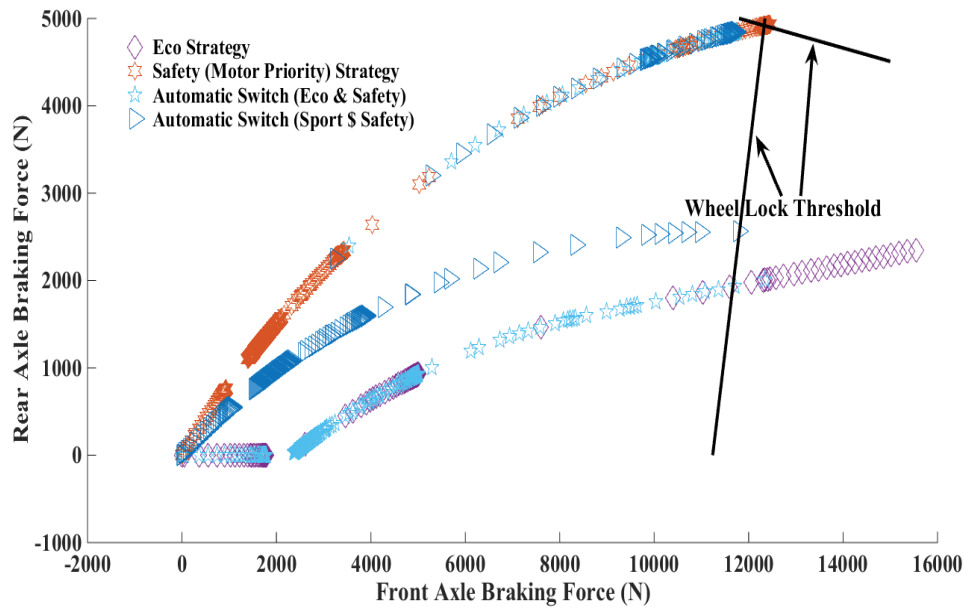
Figure 8-2: Front/Rear braking force distribution ratios for different strategies

Comparing these four strategies, the safety performance of 'Eco' (no switching) strategy is the worst. It cannot stop the vehicle in a satisfactory distance in an emergency case due to the wheel locking, although it can recover the most kinetic energy. Because the 'Safety (Motor Priority)' strategy always guarantees front and rear wheels lock simultaneously, it has the best safety performance and doesn't need to take the risk of strategy switching failure, like 'Eco & Safety' or 'Sport & Safety'. Furthermore, it has a higher utilization rate of electric braking than 'Sport & Safety', because the electric brake is strictly restricted to a certain level. The 'Eco & Safety' strategy has the highest energy recovery rate and an excellent decelerating stability. However, the potential risk of failure in switching between two strategies demands extra attention.

8.3 THE COOPERATION OF ABS, EBD AND RBS

In traditional ICE vehicles, to ensure the maximum braking force is available and to avoid wheel slipping, driver assistance systems are integrated into the vehicle such as ABS and EBD. The implementation relies on the hydraulic accumulators and actuators to work corporately with a complex relationship. In brief, the EBD supplies appropriate forces to help vehicle running on the initially intended path while the ABS stands by ready to prevent any wheel lock. However, with an RBS seeking braking energy recovery, the strategies and intervention time of hydraulic brake systems may change.

Deceleration rates varying braking and Split Mu braking show big challenges for blended braking strategy design. In this chapter, the safety-oriented cooperation of RBS, ABS and EBD is analysed and proposed, without going into the details of ABS or EBD.

8.3.1 RBS with EBD

When the deceleration intention is detected from the brake pedal in RBS, the motor begins to apply braking torque to the front wheels; meanwhile, pressure is established in the rear hydraulic actuator to decelerate the rear wheels. The braking force variation on the front and rear wheels, which is usually implemented by tuning the hydraulic accumulator and actuators, now can be provided by the motor from the viewpoint of energy recovery.

Fig.8-3 shows how the additional load affects braking performance and how a shorter stopping distance is achieved by RBS & EBD acting jointly. The variations of braking force distribution for normal load and added load with/without EBD are demonstrated

by bar indicators. According to Fig.8-3, EBD should distribute more braking force on the front wheel to offset the load transfer and avoid rear wheels locking. In contrast, when the vehicle is loaded with passengers or goods in back rows, EBD automatically detects and redistributes more braking force on the rear wheels to utilize the increased available friction force, as demonstrated in Fig.8-3-2A. However, the original distribution ratio is kept as the previous one from the viewpoint of energy recovery in this study, instead of increasing rear braking force and reducing the front braking force immediately, at the cost of a longer stop distance (Fig.8-3-2B). However, this only happens in mild braking (a<0.3g). Stopping distance retrieves the top concern when a stronger braking intention is detected (a>0.3g). The braking force distribution is rebalanced to take full advantage of load transfer. Rear mechanical braking force is increased, at the same time, reducing front mechanical braking and keeping motor braking, or reducing motor braking if there is no mechanical brake on the front wheels. The rebalance and detection procedures are described in the flowchart (Fig.7-10).
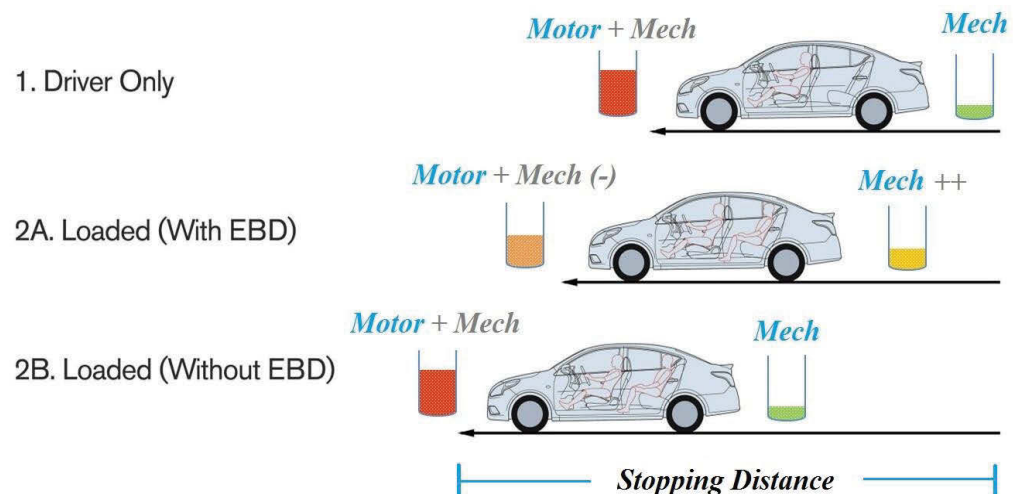
Figure 8-3: RBS Cooperating with EBD

8.3.2 RBS with ABS

ABS becomes involved when emergency braking is activated. ABS reduces the pressure in the hydraulic brake actuator of the wheel that is tending to lock.

However, there are two different preconditions for the blended braking system when ABS operates:

1. Emergency braking starts from driving
2. Emergency braking starts from an existing braking event

In case 1, emergency braking usually needs a large amount of force. Using RBS alone would generate high instantaneous current in the motor, which can't be taken by the battery. Given HBS has higher reliability, hydraulic ABS is given the top priority, which means motor braking does not participate in emergency braking in this situation.

In case 2, there is already some level of regenerative braking before the braking turns to strong. With respect to safety, keeping the existing regenerative braking and using mechanical braking to supply the rest of required braking force is the best choice.
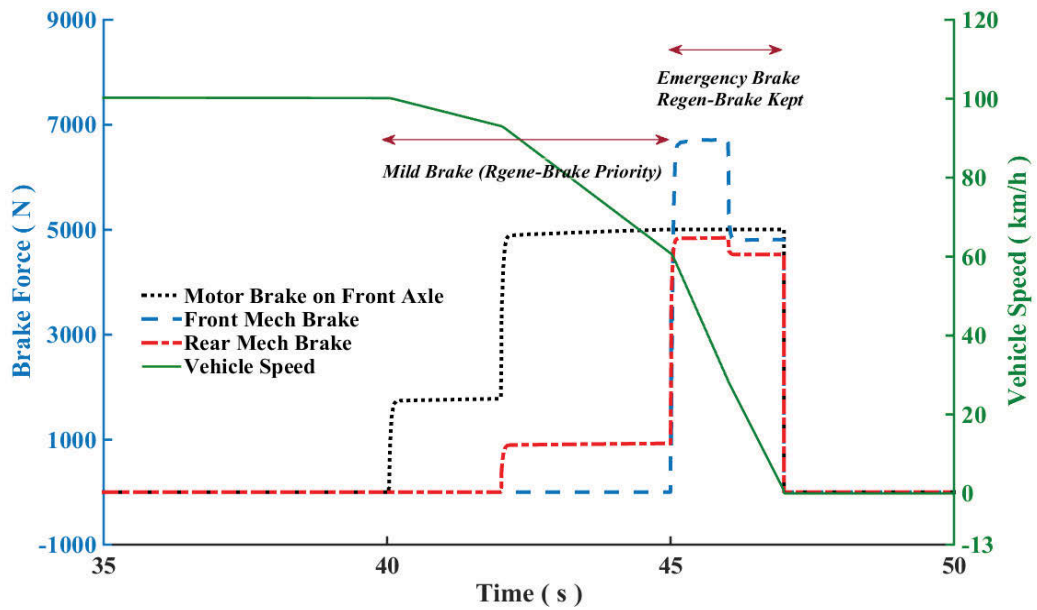
Figure 8-4: Emergency braking force distribution when motor torque is kept

The detail of this strategy and the testing result is included in Fig.7-10 and Fig.8-4.

8.4 GEAR SHIFTING DURING BRAKING

Unlike the conventional HBS, in which the braking force goes from the brake pedal to the master cylinder, hydraulic actuator, and callipers, then, directly to the wheels, electric braking goes through transmissions and differentials, then acts on the driven half shafts, which are connected to each wheel. On the one hand, regenerative braking from the motor may be insufficient when the vehicle is running at high speed with smaller gear ratio, as shown in Fig.7-6. On the other hand, the torque interruption introduced by gear shifting can result in a serious potential safety issue, especially for emergency braking. Although the interruption, also known as 'shifting torque hole' (Fig.8-5), is very short in DCT, it can still be felt and can send the wrong message to the

drivers, which may cause them to take unnecessary corrective measures. Theoretically, there are two potential solutions:

1. Lock out the shifting function and use the mechanical brake to supply the rest of the required braking force;
2. Use mechanical braking to provide the reduced torque during shifting, but reinstate the motor braking torque after shifting.

Obviously, the second solution can recapture more braking energy by giving regenerative braking more opportunities to participate. However, it also needs a more complicated control algorithm and a higher precision in the monitoring of HBS and RBS. When the shifting requirement occurs in emergency braking, considering the safety risk and energy recovery potential from emergency braking over a short period, 1st solution is the favoured choice for market products. However, when the shifting requirement occurs in a long-downhill road with a moderate braking, a downshifting should be allowed to increase the energy recovery rate.
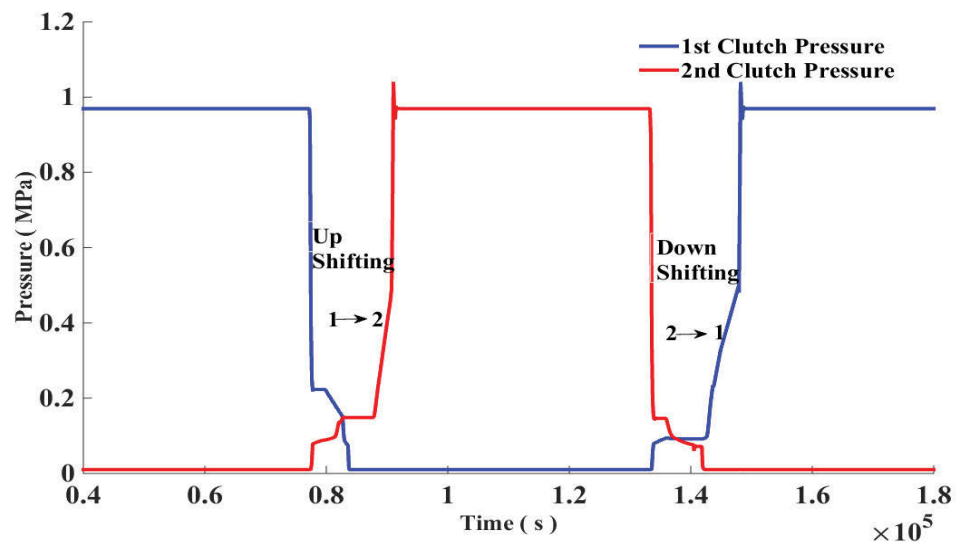
Figure 8-5: Clutch pressure variation during shifting

8.5 BRAKING IN TYPICAL CYCLES

The following chart, Fig.8-6, demonstrates the braking force distribution on the front (friction & regenerative braking) and rear wheels in different strategies. The various distribution ratios result in some fluctuations of total braking force for strategies in each driving cycle.

For the 'Eco' strategy, the required braking force in NEDC, HWFET and JP1015 never exceeds the threshold of ECE R-13 regulation, so all the braking force is supplied by the motor. The two US city cycles, UDDS, and LA-92, have a more aggressive braking event, and both need rear friction braking to meet the requirement of ECE R-13.

The 'Sport' strategy deliberately limits the motor's braking ability to a safe and low level, as described in Chapter 7. Consequently, front and rear mechanical friction brake account for most of the braking, rather than regenerative braking, in all driving cycles.

The motor has the priority and sufficient ability in the 'Safety (Motor Priority)' strategy to meet the front axle braking force requirement, causing a higher utilization rate of regenerative braking. Meanwhile, the lowest likelihood of wheel locking is guaranteed by the 'Ideal' braking force distribution ratio. Friction braking on the front wheels plays no role in typical driving cycle deceleration in this strategy, because the motor has the sufficient ability to meet the total front axle braking force requirement.

Summarizing the strategies' performance, 'Eco' is the winner for energy recovery, although it has an earlier wheel lock threshold and a higher risk of insufficient motor braking torque. 'Sport' mode can keep the vehicle decelerating as demanded, no matter what the motor speed and gear number, or even a motor fault happens. However, the braking energy recovery rate is the lowest. 'Safety (Motor Priority)' has an excellent braking performance regarding the wheel locking, and at the same time, has a satisfactory energy recovery rate.
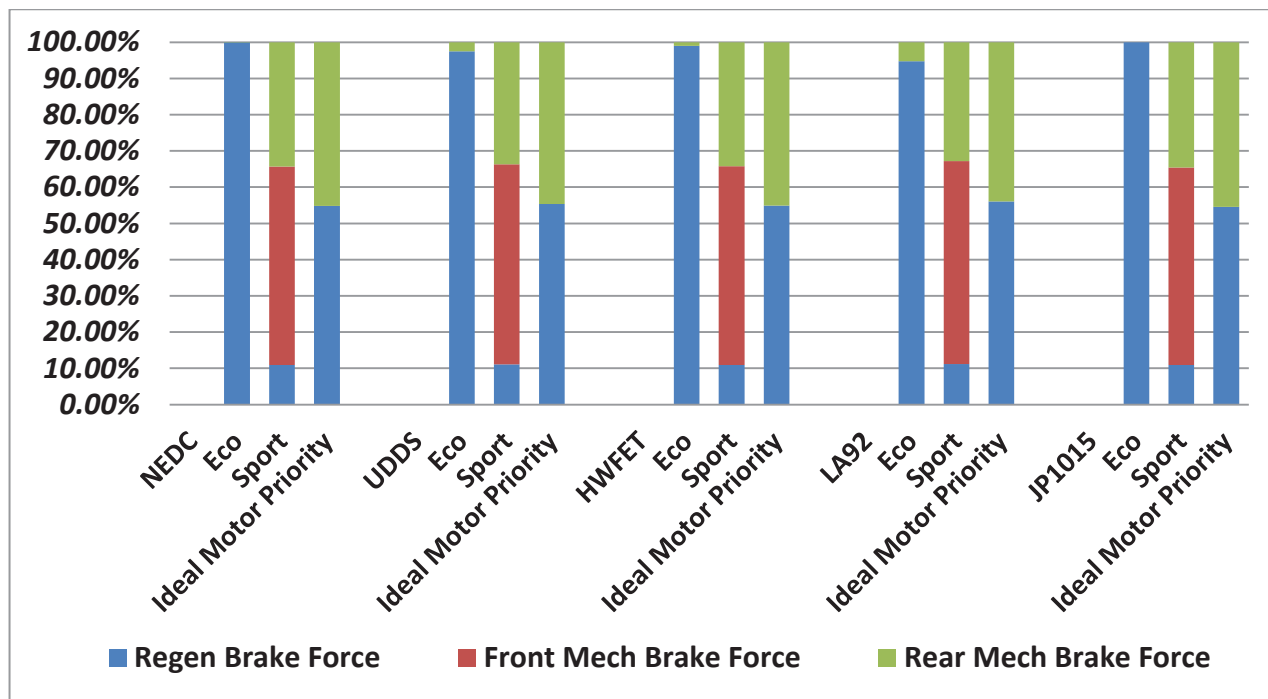
Figure 8-6: Braking force distribution for strategies in driving cycles

Eq.98 is used to evaluate the braking energy recovery potential of strategies. Fig.8-7 presents the comparison of potential braking energy recovery rates in driving cycles.

$$Energy\ Recovery\ Rate = \frac{Regenerative\ Braking\ Energy}{Total\ Braking\ Energy} \qquad (\ 98\ )$$
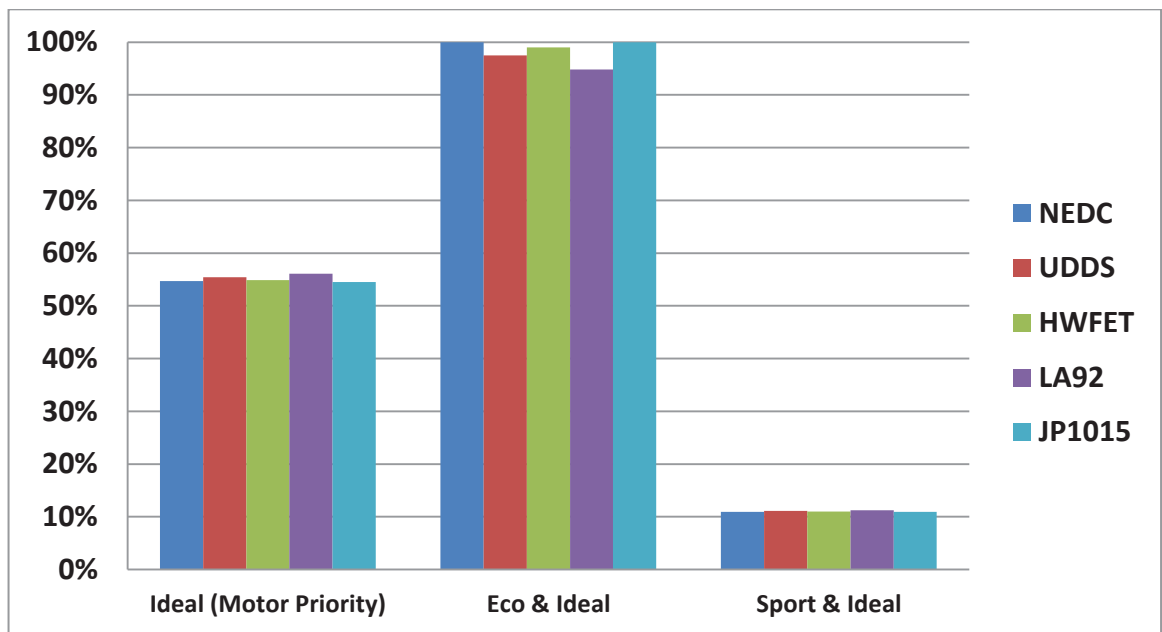
Figure 8-7: Braking energy recovery rate of strategies in each cycle

In the industry, battery energy recovery rate is widely accepted as the evaluation criterion of the regenerative braking system. The rate is defined as the ratio of the battery input energy from braking and the battery output energy for driving:

$$Q_{re} = \frac{E\_bat_{IN}}{E\_bat_{OUT}} \qquad (\ 99\ )$$

Table 8-1 shows a comparison of energy recovery rates for different driving cycles. Comparing the driving cycles, in columns, one observes that more energy can be recaptured in aggressive city cycles, UDDS, and LA-92, than others. JP1015 has the highest recovery rate. On the contrary, the recovery rate of HWFET is the lowest one.

Table 8-1: Energy recovery rates in term of driving cycles, plus wheel lock risk, with + indicating a higher risk

Energy Recovery Rates	NEDC	UDDS	HWFET	LA-92	JP1015	Wheel Lock Risk
Safety (Motor Priority)	12.4%	16.4%	8.6%	15.0%	17.8%	0
Eco & Safety	25.3%	30.4%	16.0%	24.6%	32.9%	++
Sport & Safety	2.4%	3.1%	1.8%	3.6%	3.6%	+

Comparing the strategies, in rows, safety risk is included to demonstrate a general evaluation of wheel locking possibility. 'Safety (Motor Priority)' is the baseline and has the highest avoidance of wheels lock. The highest energy recovery rate is achieved in 'Eco' because the required braking force rarely reaches the threshold of ECE R-13(H) regulation in all testing cycles. In other words, braking is supplied by the motor alone for most of the time. However, as more braking force is distributed to the front axle, the front wheels' locking point will arise earlier. Safety-oriented Sports strategy results in much lower energy recovery rate, all under 4%, due to the fixed ratio of front friction and regenerative braking.

CHAPTER 9 : EXPERIMENTAL RESULTS AND COST SAVING ANALYSIS OF REGENERATIVE BRAKING

9.1 INTRODUCTION

In this chapter, the performance of the 'Eco' blended braking strategy has been experimentally verified in driving cycles by an integrated powertrain testing bench in the Lab. The results show that the motor, especially for BEV, has sufficient ability to meet the braking requirement in the daily use. Specifically, 23.3% and 14.1% energy recovery rates, for NEDC and HWFET respectively, were achieved by the powertrain with regenerative braking in 'Eco' mode in experimental testing. These figures were approximately 10% below the calculated values, representing a good agreement between the simulation and the measurements.

Initial manufacture and daily-use cost savings by RBS were analysed and compared to evaluate the three strategies. The outcomes show the vehicle equipped with RBS can achieve a longer driving range per charge, a lower 'fuel' cost and a lower battery pack price with the same target driving range, and lower maintenance cost. In term of vehicle lifetime, savings of approximately US$10k in 'Eco', US$4-5k in 'Safety (Motor Priority)' and US$1-2k in 'Sport' are expected respectively, considering that friction braking is always required in all strategies for emergency braking.

9.2 REGENERATIVE BRAKING IN NEDC AND HWFET

The maximum decelerations in different driving cycles are presented in Table 9-1. The highest deceleration, 2.2 m/s^2 = 0.22g appearing in the LA-92 cycle, is far from the wheel-lock deceleration thresholds, represented by the two red dotted curves in Fig.7-7. Therefore, RBS can theoretically meet all the braking force requirements. Aiming at studying the energy recovery maximum potential and testing the motor braking safety performance, 'Eco' strategies are selected in these two cycles to be experimentally validated.

Table 9-1: Maximum deceleration in typical driving cycles

	NEDC	UDDS	JP-1015	HWFET	LA 92
Max Deceleration (g)	0.1	0.093	0.067	0.14	0.22

As shown in Fig.9-1, the vehicle can be decelerated and stopped as required by regenerative motor braking alone in both cycles. The negative current generated by the motor (acting as a generator) never exceeds 90 Amps. Therefore, according to the specifications of 72 Ah battery [133], which has a maximum charging current of more than 180 Amps, this charging current can be quickly absorbed.

a)

b)
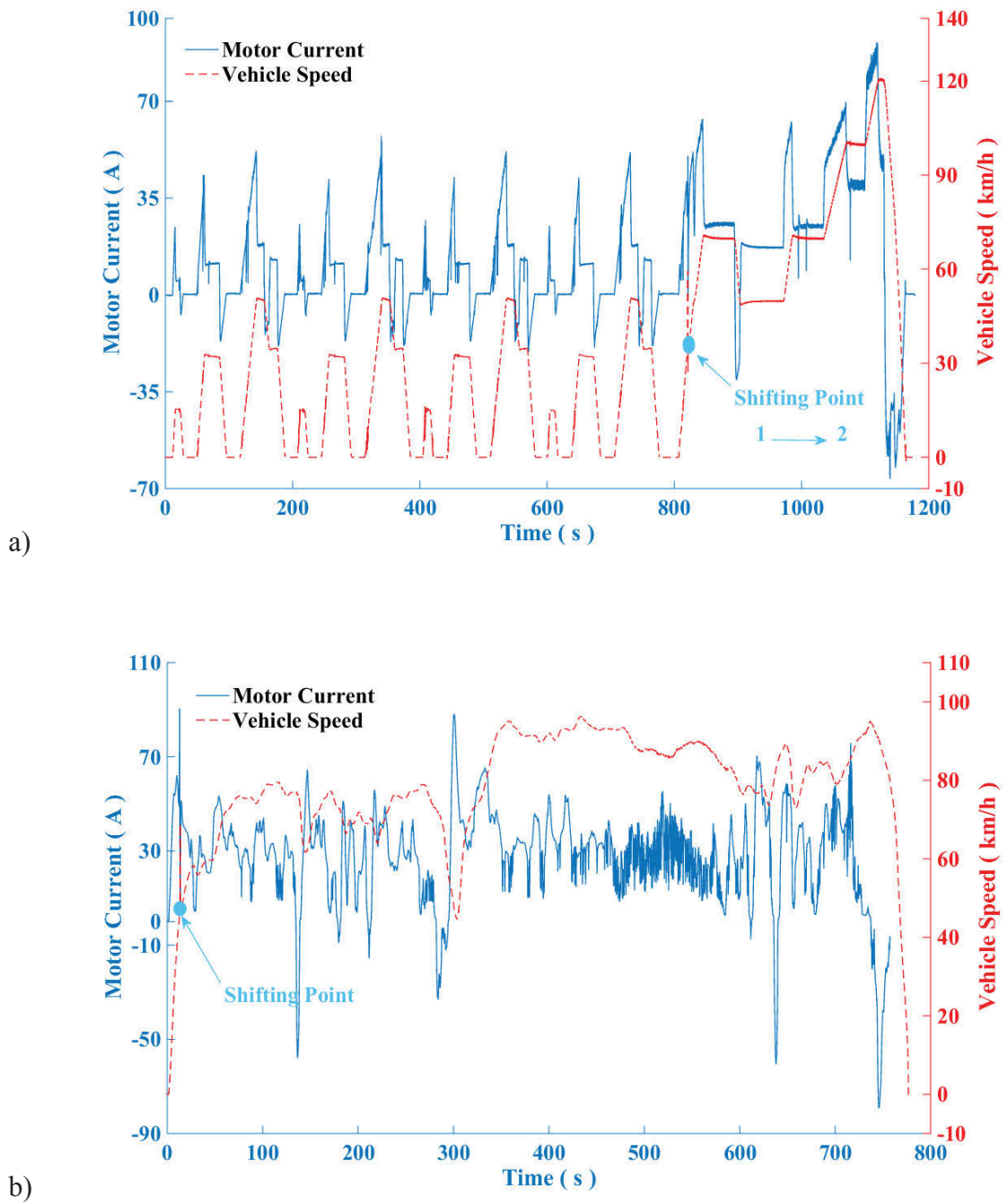
Figure 9-1: Motor current and vehicle speed for 'Eco' mode in: a) NEDC and b)

HWFET cycles

Fig.9-2 & Fig.9-3 compare the SOC for the powertrain with and without the

regenerative braking in one NEDC or HWFET cycle. We can see that the motor has

sufficient ability to meet the requirements of normal braking in daily use. Significant

benefits, 23.3% and 14.1% energy recovery rates for NEDC and HWFET respectively,

are achieved by the inclusion of regenerative braking in the 'Eco' strategy experimental

testing.

a)   b)
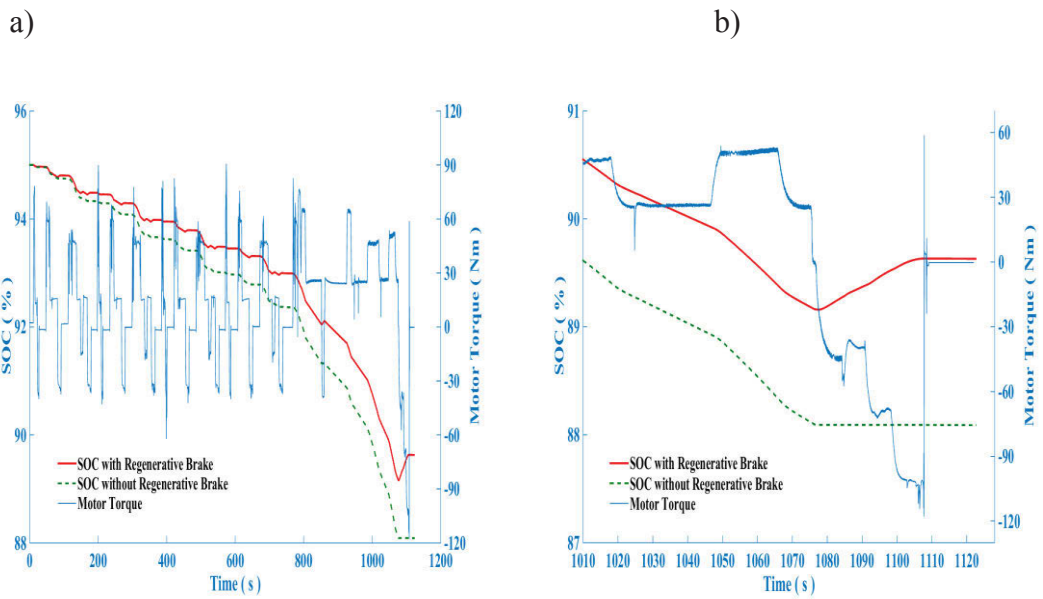
Figure 9-2: SOC and motor torque in NEDC cycle for 'Eco" mode over: a) the full

cycle; and b) the final 100 s
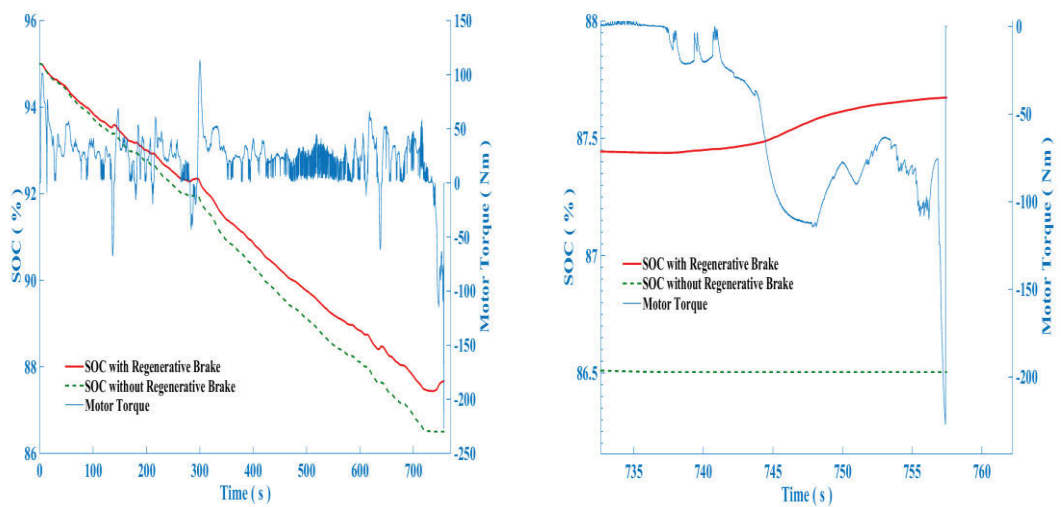
Figure 9-3: SOC and motor torque in HWFET cycle for 'Eco' mode over: a) the full

cycle; and b) the final 25 s

9.3 ENERGY RECOVERY AND COST SAVING ANALYSIS

9.3.1 The cost saving in braking energy recovery

According to the test results in chapter 9.2 and the battery specification in Table 4-1, the

recaptured braking energy in one NEDC and one HWFET cycle by 'Eco' strategy is

calculated and shown in Table.9-2. The measured battery energy recovery rates were

approximately 10% below the simulated rates given in Fig.8-6, which can be considered

as a good agreement.

Table 9-2: Recovered braking energy and mileage per NEDC and HWFET cycle

	NEDC	HWFET
Consumed energy (with no regenerative braking)	1888 Watt-Hour	2326 Watt-Hour
Recaptured energy	440 Watt-Hour	328 Watt-Hour
Mileage per cycle (MPC)	11.0 km	16.5 km
Consumed energy per km (CPK)	171.6 Wh/km	141.0 Wh/km
Braking energy recovered per km (RPK)	40 Wh/km	19.9 Wh/km
Battery energy recovery rate Q_{re}	23.3%	14.1%

A combined driving cycle is still used in this testing, referring to Eq.74, to simulate the daily driving of commuters. The reasonable consumed and recaptured braking energy per km of a combined driving, i.e. $CPK_{Combined}$ and $RPK_{Combined}$, are shown in Eq.100 and Eq.101, comparing to $120\ Wh/km$ in an average cycle and ranging from $100 - 160\ Wh/km$ for individual cycles [134].

$$CPK_{Combined} = \frac{1}{\frac{0.57}{CPK_{HWFET}} + \frac{0.43}{CPK_{NEDC}}} = \frac{1}{\frac{0.57}{141.0} + \frac{0.43}{171.6}} \quad (100)$$

$$= 152.7\ Wh/km$$

$$RPK_{Combined} = \frac{1}{\frac{0.57}{RPK_{HWFET}} + \frac{0.43}{RPK_{NEDC}}} = \frac{1}{\frac{0.57}{19.9} + \frac{0.43}{40}} \quad (101)$$

$$= 25.4\ Wh/km$$

The total mileage per charge for EV without regenerative braking is:

$$Range_{without\_Regen} = \frac{C_B \times V_B}{CPK_{Combined}} = \frac{72 * 380}{152.7} = 179.2\ km \quad (102)$$

The total mileage per charge with regenerative braking is:

$$Range_{with\_Regen} = \frac{C_B \times V_B}{CPK_{Combined} - RPK_{Combined}} = \frac{72 * 380}{152.7 - 25.4} \quad (103)$$

$$= 215\ km$$

Therefore, the rate of extended mileage per charge with the same battery for vehicle equipped with regenerative braking is:

$$Extended_{Mileage_{Rate}} = \frac{Range_{with\_Regen} - Range_{without\_Regen}}{Range_{without\_Regen}} \qquad (104)$$

$$= 20.0\%$$

In terms of battery capacity, the reduced requirement for the same travel distance, 188 km, is:

$$C_{reduced} = Range_{without\_Regen} \times RPK_{Combined} = 188 \times 25.4 \qquad (105)$$

$$= 4.8 \; kWh$$

The energy consumed per 100 km with and without regenerative braking respectively are:

$$No \; Regen: 152.7 \; \times 100 = 15.27 \; kWh \qquad (106)$$

$$Regen: (152.7 - 25.4) \times 100 = 12.73 \; kWh \qquad (107)$$

Fig.9-4 clearly demonstrates the braking energy recovery benefit, regarding to the driving range improvement and energy consuming minimizing. Top left three points, representing BEV with regenerative braking, have a longer driving range per charge and lower energy consuming rates (kW·h/100 km), comparing to the bottom right three points without energy recovering. Specific to cycles, highway cycle has the best performance, and city cycle consumes more energy. This graph also validates the effectiveness of representing two different kinds cycles for combined cycle.
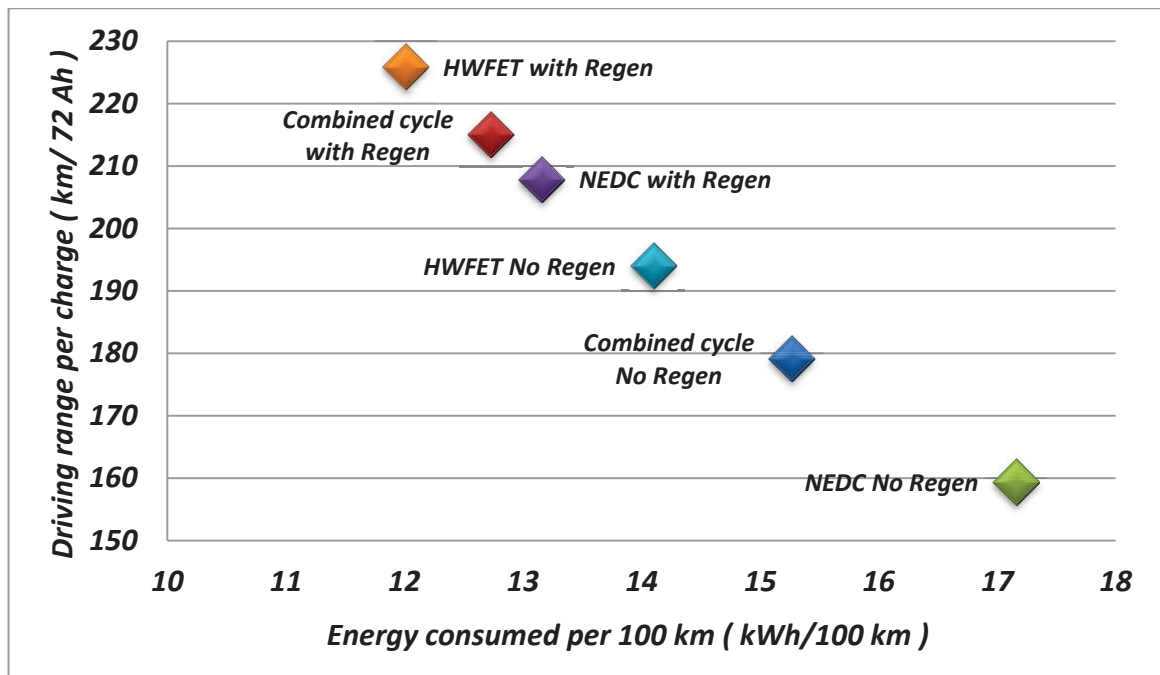
Figure 9-4: Driving range and energy utilization benefit of braking energy recovering

A typical passenger vehicle will travel a lifetime mileage of 250000 km according to [108] or 208000 km according to the product of the typical annual average travel of 18240 km per year [135] times the typical 11.4 years average vehicle life [136]. Considering that the powertrain of an EV is more reliable and simpler than that of the traditional vehicle, having a more robust motor and no gearbox or a simple 2-3 speeds gearbox, 250000 km lifetime mileage is taken in this study. Additionally, the charging efficiency with Level 2 standard voltage is 81% [109], as a result of the same 90% efficiency for both plug-in charger and lithium-ion battery charge/discharge [110]. The total expected electricity energy saved by regenerative braking with 'Eco' strategy in the whole life cycle is:

$$E_{save} = 25.4 * \frac{250000}{0.81} Wh = 7840 \; kWh \tag{108}$$

Since the limited electrical energy in the battery can be replenished by regenerative braking, significant cost saving can be obtained by reducing the required capacity of this expensive power source.

The estimated battery charge/discharge cycles in vehicle lifetime span with deep (80%) / swallow (45%) depth of discharge (DOD) are calculated in Eq.28 and Eq.29:

$$No \; Regen \begin{cases} LifeCycle_{50\%DOD} = \dfrac{250000/100 \times 15.27}{72 \times 380/1000} \times \dfrac{1}{50\%} = 2791 \\ LifeCycle_{80\%DOD} = \dfrac{250000/100 \times 15.27}{40 \times 380/1000} \times \dfrac{1}{80\%} = 1744 \end{cases} \tag{109}$$

$$With \; Regen \begin{cases} LifeCycle_{50\%DOD} = \dfrac{250000/100 \times 12.73}{40 \times 380/1000} \times \dfrac{1}{50\%} = 2326 \\ LifeCycle_{80\%DOD} = \dfrac{250000/100 \times 12.73}{40 \times 380/1000} \times \dfrac{1}{80\%} = 1454 \end{cases} \tag{110}$$

The reduced charging/discharging cycles in different DOD by regenerative braking are:

$$\begin{cases} LifeCycleSave_{50\%DOD} = 2791 - 2326 = 465 \\ LifeCycleSave_{80\%DOD} = 1744 - 1454 = 290 \end{cases} \tag{111}$$

The lifetime cycles of a typical li-ion battery are 3200 and 18000 for deep and swallow DOD respectively at room temperature (25°C) [137]. However, the lifetime cycles are not only related to DOD, also subjected to operating temperature and chemical materials. With the increasing working temperature, higher DOD and discharging rate, the life

cycles declines to lower than 1000 [138–140]. Additionally, considering the 5-8 years battery calendar year life span[138,141,142], it is inevitable for battery EV to replace the battery pack at least one time during the whole vehicle life. There is no doubt that regenerative braking can improve the battery life in terms of cycles/calendar year aging, however, the reduced charging/discharging cycles are not enough to save a whole battery pack.

In summary, according to the battery component and electricity cost shown in Table 9-3, the costs saving in electricity fee and battery pack by 'Eco' strategy are:

$$Electricity_{save} = 7840 \times 0.3 = 2352 \ (USD) \tag{112}$$

$$BatteryPack_{save} = 800 \times 4.8 = 3840 \ (USD) \tag{113}$$

9.3.2 The cost saving in braking equipment maintenance

Comparing to the mechanical parts in traditional vehicles, electrical components such as traction motors require little maintenance. The estimated overall maintenance costs for a BEV is approximately 70% of an equivalent ICE vehicle [116]. Specific to the RBS, the unique advantage is the durability and high-temperature resistance compared to a friction braking system. Whatever the materials selected for brake disk and pad, wear and deformation are inevitable, and failure is a fatality risk. Motor electric braking eliminates all these potential risks by directly applying negative torque on rotating shafts.

Depending on the vehicle type, brake pad materials, driving routes and operating environment, the average pad life varies from 28400 km to 33800 km [143]. Considering that emergency braking produces more wear than usual, ten brake pad replacements for the whole 250000 km vehicle life is regarded as a reasonable assumption in this study.

The cost of brake pads and rotors, which are presented in the following table, can be obtained from quotes on the web [144,145]. The rotors can last 2-3 sets of pads before needing replacement. The share of friction braking and motor braking for 'Sport' and 'Safety (Motor Priority)' strategies are roughly 15/85 and 50/50, based on Fig.8-7 and Eq.97, which are used to calculate the required brake pads/rotors and cost respectively. Additionally, one extra pair of brake pads is added to each blended braking strategy for emergency braking.

Table 9-3: Friction brake applications and pedal replacement cost (US$)

	Friction brake only	'Eco'	'Safety (Motor Priority)'	'Sport'
Number of replaced pads	10	1	6	9
Pads cost with labor (8 sets, two axles, $ USD)	$ 350	$ 350	$ 350	$ 350
Lifetime pads replacement cost	$ 3500	$ 350	$ 2100	$ 3150
Rotors cost with labour (4 sets, two axles)	$ 210	$ 210	$ 210	$ 210

Number of replaced rotors	4	0	2	3
Lifetime rotor replacement cost	$ 480-1200	0	$ 240-600	$ 360-900

Finally the total cost of electricity fees and brake system maintenance based on different braking architectures and strategies are demonstrated in Table.9-4:

Table 9-4: Blended braking system related EV lifetime cost saving summary (US$)

	Friction Brake Only	'Eco'	'Safety (Motor Priority)'	'Sport'
Electricity Fee	$ 14139	$ 11787	$ 12963 (Approx.)	$ 13786 (Approx.)
Battery Pack	$ 21888	$ 18048	$ 19968 (Approx.)	$ 21312 (Approx.)
Brake Pads	$ 3500	$ 350	$ 2100	$ 3150
Brake Rotors	$ 840	0	$ 420	$ 630
Total	$ 40367	$ 30185	$ 35451	$ 38878

The effectiveness of 'Eco & Safety' strategy is validated in both city and highway cycles in this experiment, expect rare emergency braking. Therefore, the 'Eco & Safety' strategy' can be used to evaluate the economic benefit of regenerative braking in daily commuting, comparing to conventional friction braking. The economic benefit of different blended braking strategies is shown in Fig.9-5, regarding to 'fuel' cost and mechanical maintenance cost. As shown in Fig.9-5, more than one fourth of total cost, including brake system maintenance and electricity, can be saved by energy recovering

in 'Eco & Safety' strategy. The figures for 'Safety (Motor Priority)' and 'Sport & Safety' are 12% and 4% respectively.
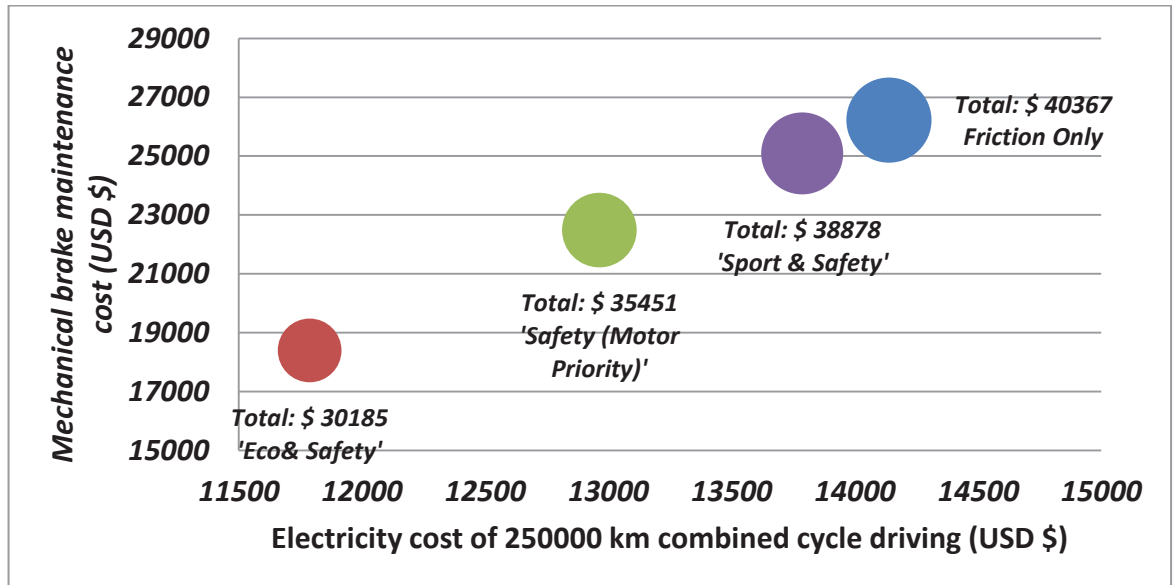
Figure 9-5: Lifetime fuel and maintenance cost of BEV in different braking strategies

CHAPTER 10 : THESIS CONCLUSIONS

This thesis proposes two redesigned multi-speed transmission systems, two-speed DCT and CVT without torque converter, as alternatives for widely used fixed ratio SR on BEVs. The structures and principles of two-speed DCT and simplified CVT are detailed to demonstrate how these can be integrated with the motor and how the traditional DCT and CVT transmissions can be simplified.

Gear ratios for different transmissions are determined to meet the performance requirements and make the most of the existing equipment. Based on the motor characteristics and the requirements of smooth shifting and energy saving, two customized shifting schedules are designed for two-speed DCT and simplified CVT. A comprehensive vehicle model is built in the Matlab/Simulink to calculate the motor efficiency improvement and saved battery energy. A detailed comparison of simulation results among SR, two-speed DCT and simplified CVT equipped BEVs, in urban and highway testing cycles, are presented that both two-speed DCT and simplified CVT have a significant improvement on economy performance relative to single speed transmission. At the same time, better dynamic performance is attained, e.g. faster acceleration time and higher top speed.

The performance of SR and two-speed DCT on BEVs was experimentally verified in an integrated powertrain testing bench in the Lab. Thanks to the additional relatively smaller ratio in 2nd gear, comparing to the SR, motor equipped with two-speed DCT is more likely to run in the high efficiency area and consume less energy. The

improvement varies with driving cycles. For the city cycles, e.g. ECE, frequent start-stop situations do not give much chance for the 2nd gear in two-speed DCT to participate. However, the 2nd gear plays a major role in highway situation, e.g. HWFET, 14% battery energy is saved in each cycle.

Initial manufacturing and the daily-use cost is analysed to estimate whether the multi-speed transmission is worthwhile for customers, considering the saved energy and increased transmission cost. The outcomes show that two-speed DCT based BEV has the lowest retail price, thanks to the minimized battery capacity requirement, though the gearbox is more expensive. Due to CVT being the most expensive one of these three candidates, the CVT based BEV costs a little bit more than SR based BEV. However, the small retail price difference obviously signals that it is a smart choice to add a multi-speed transmission system to BEVs. From the viewpoint of a lifetime costing, thousands of dollars saving is expected by minimizing electricity consumption.

The significant kinetic energy recovery potential in daily driving was reported. The structure and advantage of front driven BEV, especially for braking energy recovery, were discussed in detail. The factors, which restrict blended braking, were analysed to determine the available regenerative braking from the motor, the ratio of motor and friction braking and the ratio of front and rear braking. Then, three blended braking strategies, 'Eco', 'Sport' and 'Safety (Motor Priority)' with their characteristics, were proposed, the latter optimizing braking energy recovery and improving braking performance simultaneously. A 'motor fault insurance' strategy was developed to avoid any unexpected and potentially fatal errors in the motor braking system.

Several braking testing manoeuvres were used in this thesis to test the possible safety issues, which may be caused by redistributing the braking force between the front/rear axles in a mechanical/regenerative braking system. The feasible solutions were analysed and included in the specially designed algorithms. In a straight line braking test, the details of the braking force distribution between the front and rear wheels from the motor and hydraulic system are given in figures. A cooperation algorithm of RBS, EBD and ABS was proposed to provide safe, efficient blended braking. The possible braking torque interruption risk introduced by gear shifting is avoided by this specially designed strategy. The shares of front/rear friction braking and regenerative motor braking in strategies for typical driving cycles were presented in charts. Consequently, the braking energy recovery rates for different driving cycles were calculated.

The performance of the 'Eco' blended braking strategy has been experimentally verified in driving cycles by an integrated powertrain testing bench in the Lab. Thanks to the powerful motor and relatively small required braking force, most of the braking events were covered by regenerative motor braking alone in both city and highway cycles. In other words, the motor, especially for BEV, has sufficient ability to meet the braking requirements in daily use. Specifically, 23.3% and 14.1% energy recovery rates, for NEDC and HWFET respectively, were achieved by the powertrain with regenerative braking in 'Eco' mode in experimental testing. These figures were approximately 10% below the calculated values, representing a good agreement between the simulation and the measurements.

Initial manufacture and daily-use cost savings by RBS were analysed and compared to evaluate the three strategies. The outcomes show that a vehicle equipped with RBS can

achieve a longer driving range per charge, a lower 'fuel' cost and a lower battery pack price with the same target driving range, and lower maintenance cost. In terms of vehicle lifetime, savings of approximately US$10k in 'Eco', US$4-5k in 'Safety (Motor Priority)' and US$1-2k in 'Sport' are expected respectively, considering that friction braking is always required in all strategies for emergency braking.

In summary, both two-speed DCT and simplified CVT not only improve BEVs' dynamic performance with little additional initial cost but also save customer's money in the long term. The improvement achieved in this thesis is greater than for most 2, 3, even 4 speeds transmissions, which were designed for BEVs, proposed in the previous reference, while offering a simple structure and acceptable price. Furthermore, the two-speed DCT equipped BEV saves more money in the long term, but the simplified CVT equipped BEV can offer a better driving experience, no matter in accelerating, climbing or shifting. Additionally, the three blended braking strategies not only improve braking performance, enabling adaptive braking force control, shorter stopping distance when the load is changing, and seamless transfer within RBS, EBD and ABS, but they also save customer's money.

Further Research

Although two-speed transmission showed a satisfied result in dynamic and economic, other options, e.g. 3 or 4 speeds transmissions should be investigated, considering they can further decouple the launch, top speed, and economic driving requirements for the vehicle from the motor speed and torque range, which are likely to improve the overall operating performance of the vehicle.

The benefits may include:

1. Further improved motor efficiency over the vehicle driving range

2. Higher maximum vehicle speed and available torque

The disadvantages may include:

1. Increased weight from additional components

2. Poorer transmission efficiency

3. Higher manufacturing costs

Additionally, the application of hybrid energy storage systems (HESS) should be considered in the future study, where super-capacitors supplement the conventional battery pack to both maximize the recovery of brake energy and to improve battery life span. The capability of high C rate discharging and charging in HESS provides an important addition to hybrid electric vehicles in general and electric vehicles in particular.

APPENDIX A: WIRELESS TORQUE SENSOR

Table.A1 shows the specifications of selected torque sensors, which are used on the driving shafts to measure the torsional torque.

Table A1: ATi 2000 series wireless torque sensor specifications

SYSTEM	
Bandwidth	DC to 1100 Hz
filtered output	DC to 100 Hz
Integral Non-Linearity	+/- .10%
Repeatability	+/- .05%
Maximum Error	<.25% Full Scale
RECEIVER	
Power	12 Volts DC
Output	+/- 2 Volts
Display	3 Digit Backlit LCD
Output Ripple	< 2 mV (Filtered) < 15 mV (Wide Band)
Induction Power Supply	500kHz Induction Power
MINIATURE CRYSTALLED TRANSMITTERS	
Power	9 Volts or Induction Power
Acceleration Limit	32,000g Static (125g Dynamic, DC -1 kHz)
Zero Drift	0.02% / Deg C
Span Drift	0.02% / Deg C

Operating Temperature Range	-40 to 140 Deg C

Table A2 and A3 show the raw data from torque sensor calibration process, which are used to calculate the relationship of displayed voltage and actual torque applied on the shaft.

Table A2: Calibration data of torque sensors on transmission output shaft

Weight (kg)	Length of Bar (m)	Angle (°)	Voltage (v)
Front Axle Long Shaft			
Bar+Hook	2	8.0	-0.5
10	2	5	-1.86
20	2	2.0	-3.23
30	2	-1	-4.6
40	2	-5.5	-5.96
50	2	-10.5	-7.24
Front Axle Short Shaft			
Bar+Hook	2	3	-0.38
10	2	0.3	-1.37
20	2	-2.0	-2.38
30	2	-4.5	-3.35
40	2	-7.0	-4.33
50	2	-9.5	-5.29

Table A3: Correspondence between torque and display voltage

Torque (Nm)	Display Voltage (V)
Front Axle Long Shaft	
195.3	1.36
391.8	2.73
588.0	4.1
780.4	5.46
963.6	6.74
Front Axle Short Shaft	
196.0	0.99
391.8	2.00
586.2	2.97
778.2	3.95
966.6	4.91
Motor Input Shaft	
10	0.07
20	0.13
30	0.23
40	0.27
50	0.34
60	0.4
70	0.47

80	0.54
90	0.61
100	0.68
120	0.82
140	0.96
160	1.09
180	1.24
200	1.38
220	1.52
240	1.66
260	1.8
280	1.94
300	2.09

APPENDIX B: DCT TEMPERATURE VARIATION TESTING

Table.B1 shows the temperature variation of each gear in two-speed DCT during a 120 minutes constant input speed testing. Results showed that 2nd gear had a higher overall and average operating temperature than 1st gear, due to the relative higher rotation speed.

Table B1: Two-speed DCT components temperature variation of 1st gear

Time	Vehicle Speed km/h	Motor Speed rpm	Motor Temp ℃	MCU Temp ℃	GearBox Temp ℃	SOC	Bearing Temp ℃
9:40	0	0	26	25	22	95	24
9:45	69.7	4997	51	27	29	90.8	30
9:50	69.4	4984	62	30	36.7	87	35
9:55	72.1	5136	69	33	44.6	82.9	39
10:00	74.0	5291	73	36	51	79.1	43
10:05	74.5	5332	77	38	55.9	74.9	46
10:10	74.6	5345	79	38	58.7	70.9	49
10:15	75.4	5391	81	39	61.2	66.9	51
10:20	72.1	5151	82	40	63.6	62.8	53
10:25	72.1	5168	83	40	65.3	59.6	54
10:30	72.2	5174	84	40	66.4	55.7	54
10:35	72.7	5196	84	40	66.7	51.9	55

10:40	73.3	5259	84	41	67.6	47.7	55
10:45	73.7	5278	84	41	68.1	44.1	55
10:50	73.7	5287	84	41	68.6	40.8	56
10:55	73.8	5293	84	41	69.1	36.9	56
11:00	73.7	5284	84	42	69.4	33.3	56
11:05	73.7	5286	85	42	70	29.2	56
11:10	74	5280	85	42	70	25.6	56
11:15	73.9	5275	85	42	70.4	21.5	56
11:20	73.8	5287	85	42	70.7	17.4	56
11:25	73.6	5278	86	43	71.1	14.1	56
11:30	73.6	5278	86	43	71.4	10.4	56
11:35	73.6	5277	87	43	71.6	6.5	56
11:40	73.6	5271	87	43	71.8	2.9	56

Table B2: Two-speed DCT components temperature variation of 2nd gear

Time	Vehicle Speed km/h	Motor Speed rpm	Motor Temp ℃	MCU Temp ℃	GearBox Temp ℃	SOC	Bearing Temp ℃
1:45	0	0	31	29	30.5	95	28
1:50	87.3	3978	50	30	33.1	90.9	35
1:55	96.3	4364	61	34	43.3	85.2	41
2:00	100.2	4574	67	36	50.5	79.7	46
2:05	109.2	4955	73	38	56.6	73.7	49
2:12	124	5760	79	40	62.9	65.1	55
2:15	129.1	5856	84	38	67.5	61.2	58
2:21	123	5590	82	37	73.4	55.2	60
2:25	123.8	5600	81	37	76.2	52	62
2:30	124.3	5640	82	37	79.5	47.4	63
2:35	124.8	5671	82	37	84.1	41.9	66
2:40	125.1	5671	83	37	86.1	37.7	62
2:45	125.3	5679	83	37	87.6	31.9	67
2:50	125.2	5695	84	38	90.3	27.3	69
2:55	125.9	5702	84	38	93.1	22.7	70
3:00	125.7	5690	84	38	95.7	17.9	70
3:05	125.7	5697	85	38	97.9	13.1	72
3:10	126.4	5750	85	38	99.9	8.1	73
3:15	126.1	5719	85	39	101.1	3.2	72

Bibliography

[1]   Australia Goverment. Post-2020 emissions reduction target Report of the UNFCCC Taskforce. 2015.

[2]   Australian Greenhouse Office. Global Warming Cool it! A home guide to reducing energy costs and greenhouse gases 2006.

[3]   United States Environmental Protection Agency. Progress Cleaning the Air and Improving People's Health n.d.

[4]   DeCicco J, Fung F. Global warming on the road: the climate impact of America's automobiles. Environ Def 2006:33.

[5]   Shafiee S, Topal E. When will fossil fuel reserves be diminished? Energy Policy 2009;37:181–9. doi:10.1016/j.enpol.2008.08.016.

[6]   Organization of the Petroleum Exporting Countries. World oil outlook. vol. 4. 2014. doi:10.1190/1.1439163.

[7]   Xue XD, Cheng KWE, Cheung NC. Selection of Electric Motor Drives for Electric Vehicles. Power Eng Conf 2008 AUPEC '08 Australas Univ 2008:1–6.

[8]   West JGW. DC, induction, reluctance and PM motors for electric vehicles. Power Eng J 1994;8:77–88. doi:10.1049/pe:19940203.

[9]   Vagati A, Pellegrino G, Guglielmi P. Comparison between SPM and IPM motor drives for EV application. Electr Mach (ICEM), 2010 XIX Int Conf 2010:1–6.

doi:10.1109/ICELMACH.2010.5607911.

[10] Mishra P, Saha S, Ikkurti HP. Selection of propulsion motor and suitable gear ratio for driving electric vehicle on Indian city roads. Energy Effic Technol Sustain (ICEETS), 2013 Int Conf 2013:692–8. doi:10.1109/ICEETS.2013.6533469.

[11] Li Y, Liu M, Lau J, Zhang B. A novel method to determine the motor efficiency under variable speed operations and partial load conditions. Appl Energy 2015;144:234–40. doi:http://dx.doi.org/10.1016/j.apenergy.2015.01.064.

[12] Roberts S. Multispeed transmission for electric vehicles. ATZ Worldw 2012;114:8–11. doi:10.1007/s38311-012-0162-4.

[13] Di Nicola F, Sorniotti A, Holdstock T, Viotto F, Bertolotto S. Optimization of a multiple-mpeed transmission for downsizing the motor of a fully electric vehicle. SAE Int J Alt Power 2012;1:134–43. doi:10.4271/2012-01-0630.

[14] Sorniotti A, Subramanyan S, Turner A, Cavallino C, Viotto F, Bertolotto S. Selection of the Optimal Gearbox Layout for an Electric Vehicle 2011;4:1267–80. doi:10.4271/2011-01-0946.

[15] Morozov A, Humphries K, Zou T, Martins S, Angeles J. Design and Optimization of a Drivetrain with Two-speed Transmission for Electric Delivery Step Van. IEEE Int. Electr. Veh. Conf. IEVC 2014, Florence, Italy, 2014.

[16] Wu G, Zhang X, Dong Z. Impacts of Two-Speed Gearbox on Electric Vehicle's

Fuel Economy and Performance 2013. doi:10.4271/2013-01-0349.

[17]   Jun-Qiang X, Guang-Ming X, Yan Z. Application of automatic manual transmission technology in pure electric bus. 2008 IEEE Veh Power Propuls Conf VPPC 2008 2008:5–8. doi:10.1109/VPPC.2008.4677583.

[18]   Birch S. Clutchless four-speed EV transmission debuts - SAE International. SAE Int 2012. http://articles.sae.org/10669/ (accessed April 23, 2016).

[19]   Matthes B. Dual Clutch Transmissions - Lessons Learned and Future Potential 2005. doi:10.4271/2005-01-1021.

[20]   Walker PD, Abdul Rahman S, Zhu B, Zhang N. Modelling, simulations, and optimisation of electric vehicles for analysis of transmission ratio selection. Adv Mech Eng 2013;2013. doi:10.1155/2013/340435.

[21]   Walker PD, Abdul Rahman S, Zhang N, Zhan W, Lin Y, Zhu B. Modelling and Simulation of a Two Speed Electric Vehicle. In: Subic A, Wellnitz J, Leary M, Koopmans L, editors., Berlin, Heidelberg: Springer Berlin Heidelberg; 2012, p. 193–8. doi:10.1007/978-3-642-24145-1_25.

[22]   Patel D, Ely J, Overson M. CVT Drive Research Study 2005. doi:10.4271/2005-01-1459.

[23]   Srivastava N, Haque I. A review on belt and chain continuously variable transmissions (CVT): Dynamics and control. Mech Mach Theory 2009;44:19–41. doi:10.1016/j.mechmachtheory.2008.06.007.

[24] Mäder KM. Continuously Variable Transmission : Benchmark , Status & Potentials. 2005.

[25] Lee, H; Kim H. Improvement of fuel economy by shift speed control for a metal belt continuously variable. Proc Inst Mech Eng PART D J Automob Eng 2012;216:741–9.

[26] Ren Q, Crolla D a., Morris a. Effect of transmission design on Electric Vehicle (EV) performance. 5th IEEE Veh Power Propuls Conf VPPC '09 2009;4:1260–5. doi:10.1109/VPPC.2009.5289707.

[27] Bottiglione F, De Pinto S, Mantriota G, Sorniotti A. Energy consumption of a battery electric vehicle with infinitely variable transmission. Energies 2014;7:8317–37. doi:10.3390/en7128317.

[28] Bonsen B, Steinbuch M, Veenhuizen P a. CVT ratio control strategy optimization. 2005 IEEE Veh Power Propuls Conf 2005:227–31. doi:10.1109/VPPC.2005.1554561.

[29] Galvagno E, Velardocchia M, Vigliani a. Analysis and simulation of a torque assist automated manual transmission. Mech Syst Signal Process 2011;25:1877–86. doi:10.1016/j.ymssp.2010.12.014.

[30] R P G Heath. Seamless AMT offers efficient alternative to CVT. JSAE Annu Congr 2007:4.

[31] Yang Y, Jiang Q ZB and WJ. A study on the optimal-power shift schedule for

electric vehicle. Automob Technol 2011;3:1–5.

[32] Hayashi K, Shimizu Y, Dote Y, Takayama A, Hirako A. Neuro fuzzy transmission control for automobile with variable loads. IEEE Trans Control Syst Technol 1995;3:49–53. doi:10.1109/87.370709.

[33] Xiusheng C, Yongdao S, Qiang G, Xi L. Shift control for dry dual clutch transmission of pure electric vehicle. Transp Mech Electr Eng (TMEE), 2011 Int Conf 2011:854–7. doi:10.1109/TMEE.2011.6199336.

[34] Hong S, Ahn S, Kim B, Lee H, Kim H. Shift control of a 2-speed dual clutch transmission for electric vehicle. 2012 IEEE Veh Power Propuls Conf 2012:1202–5. doi:10.1109/VPPC.2012.6422510.

[35] Walker PD, Zhang N, Zhu B, Rahman SA. Dynamics and control of gear shifts in a two speed electric vehicle. 2012.

[36] Han J, Park Y. Cooperative regenerative braking control for front-wheel-drive hybrid electric vehicle based on adaptive regenerative brake torque optimization using under-steer index. Int J Automot Technol 2014;15:989–1000. doi:10.1007/s12239-014-0104-9.

[37] Zhou Z, Mi C, Zhang G. Integrated control of electromechanical braking and regenerative braking in plug-in hybrid electric vehicles Zhiguang Zhou Guixiang Zhang. Int J Veh Des 2012;58:223–39.

[38] Lv C, Zhang J, Li Y, Yuan Y. Novel control algorithm of braking energy

regeneration system for an electric vehicle during safety-critical driving maneuvers. Energy Convers Manag 2015;106:520–9. doi:10.1016/j.enconman.2015.09.062.

[39] Li L, Zhang Y, Yang C, Yan B, Marina Martinez C. Model predictive control-based efficient energy recovery control strategy for regenerative braking system of hybrid electric bus. Energy Convers Manag 2016;111:299–314. doi:10.1016/j.enconman.2015.12.077.

[40] Mehrdad Ehsani, Yimin Gao, Ali E. Modern electric, hybrid electric and fuel cell vehicles: fundamentals, theory, and design. 2nd ed. 2009.

[41] Haataja M, Leinonen T. On the Distribution of Braking Forces in Road Braking 2000. doi:10.4271/2000-01-3413.

[42] Hano S, Hakiai M. New Challenges for Brake and Modulation Systems in Hybrid Electric Vehicles (HEVs) and Electric Vehicles (EVs) 2011.

[43] Ko J, Lee G, Ko S, Ahn S, Kim H, Choi S, et al. Co-operative Control of Regenerative Braking using a Front Electronic Wedge Brake and a Rear Electronic Mechanical Brake Considering the Road Friction Characteristic 2012. doi:10.4271/2012-01-1798.

[44] Antanaitis DB. Effect of Regenerative Braking on Foundation Brake Performance. SAE Int J Passeng Cars – Mech Syst 2010;3:14–30. doi:10.4271/2010-01-1681.

[45] Walker AM, Lampérth MU, Wilkins S. On Friction Braking Demand with Regenerative Braking 2002. doi:10.4271/2002-01-2581.

[46] Gao Y, Chen L, Ehsani M. Investigation of the Effectiveness of Regenerative Braking for EV and HEV 1999. doi:10.4271/1999-01-2910.

[47] Hartley J, Day A, Campean I, McLellan RG, Richmond J. Braking System for a Full Electric Vehicle with Regenerative Braking 2010. doi:10.4271/2010-01-1680.

[48] Zhang J, Lv C, Yue X, Qiu M, Gou J, He C. Development of the Electrically-Controlled Regenerative Braking System for Electrified Passenger Vehicle 2013. doi:10.4271/2013-01-1463.

[49] von Albrichsfeld C, Karner J. Brake System for Hybrid and Electric Vehicles 2009. doi:10.4271/2009-01-1217.

[50] Gao Y, Ehsani M. Electronic Braking System of EV And HEV---Integration of Regenerative Braking, Automatic Braking Force Control and ABS 2001. doi:10.4271/2001-01-2478.

[51] Rosenberger M, Uhlig RA, Koch T, Lienkamp M. Combining Regenerative Braking and Anti-Lock Braking for Enhanced Braking Performance and Efficiency 2012. doi:10.4271/2012-01-0234.

[52] Oleksowicz SA, Burnham KJ, Southgate A, McCoy C, Waite G, Hardwick G, et al. Regenerative braking strategies, vehicle safety and stability control systems:

critical use-case proposals. Veh Syst Dyn 2013;51:684–99. doi:10.1080/00423114.2013.767462.

[53] Krueger E, Kidston K, Busack A. Reducing Disturbances Caused by Reductions in Regenerative Brake Torque 2011. doi:10.4271/2011-01-0972.

[54] Ruan J, Walker P. An Optimal Regenerative Braking Energy Recovery System for Two-Speed Dual Clutch Transmission-Based Electric Vehicles 2014. doi:10.4271/2014-01-1740.

[55] Infantini MB, Britto JFFH, Perondi E. Model of an ABS pneumatic regenerative braking system 2005. doi:10.4271/2005-01-4033.

[56] Conlon B, Kidston K. Electric vehicle with regenerative and anti-lock braking, 1997.

[57] Zhu ZQ, Howe D. Electrical Machines and Drives for Electric, Hybrid, and Fuel Cell Vehicles. Proc IEEE 2007;95:746–65. doi:10.1109/JPROC.2006.892482.

[58] Ehsani M, Rahman KM, Toliyat HA. Propulsion system design of electric and hybrid vehicles. IEEE Trans Ind Electron 1997;44:19–27. doi:10.1109/41.557495.

[59] Tiecheng W, Ping Z, Qianfan Z, Shukang C. Design characteristics of the induction motor used for hybrid electric vehicle. 2004 12th Symp Electromagn Launch Technol 2004 2004:523–7. doi:10.1109/ELT.2004.1398136.

[60] Cho DH, Jung HK, Member S, Lee CG. Induction motor design for electric vehicle using a niching genetic algorithm. IEEE Trans I A 2001;37:994–9.

doi:10.1109/28.936389.

[61]   Fonseca A. New Modeling Methodology For Induction Machine Efficiency Mapping For Hybrid Vehicle n.d.:776–81.

[62]   Torrey DA. Switched reluctance generators and their control. IEEE Trans Ind Electron 2002;49:3–14. doi:10.1109/41.982243.

[63]   Mueller M. Electronic control of switched reluctance machines [Book Review]. Power Eng J 2002;16:222.

[64]   Uddin MN, Radwan TS, Rahman MA. Performance of interior permanent magnet motor drive over wide speed range. IEEE Trans Energy Convers 2002;17:79–84. doi:10.1109/60.986441.

[65]   Wang SL, Chueh TY. Research of permanent magnetic brushless motor on epoxy resin with Taguchi method. Consum Electron Commun Networks (CECNet), 2012 2nd Int Conf 2012:3423–4. doi:10.1109/CECNet.2012.6201996.

[66]   Chen YS, Zhu ZQ. Investigation of Magnetic Drag Torque in Permanent Magnet Brushless Motors. IEEE Trans Magn 2007;43:2507–9. doi:10.1109/TMAG.2007.893768.

[67]   Zeraoulia M, Benbouzid MEH, Diallo D. Electric Motor Drive Selection Issues for HEV Propulsion Systems: A Comparative Study. IEEE Trans,Vehicular Technol 2006;55:1756–64. doi:10.1109/TVT.2006.878719.

[68]   Merwerth J. THE HYBRID-SYNCHRONOUS MACHINE OF THE NEW

BMW i3 & i8. 2014.

[69] Technologies U. PowerPhase ® 125 Traction System. 2002.

[70] Combustion Engines Information | Engineering360 n.d. http://www.globalspec.com/learnmore/motion_controls/engines_components/ind ustrial_engines (accessed May 19, 2016).

[71] Shin JW, Kim JO, Choi JY, Oh SH. Design of 2-speed transmission for electric commercial vehicle. Int J Automot Technol 2014;15:145–50. doi:10.1007/s12239-014-0016-8.

[72] Walker PD, Zhang N, Tamba R. Control of gear shifts in dual clutch transmission powertrains. Mech Syst Signal Process 2011;25:1923–36. doi:http://dx.doi.org/10.1016/j.ymssp.2010.08.018.

[73] Goetz M, Levesley MC, Crolla DA. Integrated Powertrain Control of Gearshifts On Twin Clutch Transmissions 2004. doi:10.4271/2004-01-1637.

[74] Zhu B, Zhang N, Walker P, Zhan W, Zhou X, Ruan J. Two-Speed DCT Electric Powertrain Shifting Control and Rig Testing. Adv Mech Eng 2013;2013:1–10. doi:10.1155/2013/323917.

[75] Roser H, Walker PD, Nong Zhang. IMECE2013-64139. Proc. ASME 2013 Int. Mech. Eng. Congr. Expo. IMECE2013, 2013, p. 1–7.

[76] Walker PD, Zhang N. Modelling of dual clutch transmission equipped powertrains for shift transient simulations. Mech Mach Theory 2013;60:47–59.

doi:10.1016/j.mechmachtheory.2012.09.007.

[77] British Standards Institute. Gears — Thermal capacity — Part 1: Rating gear drives with thermal equilibrium at 95 °C sump temperature. ISO 2001;ISO/TR 141.

[78] Dawson PH. Windage loss in larger high-speed gears. Arch Proc Inst Mech Eng Part A Power Process Eng 1983-1988 (Vols 197-202) 2006;198:51–9. doi:10.1243/PIME_PROC_1984_198_007_02.

[79] Eastwick CN, Johnson G. Gear Windage: A Review. J Mech Des 2006;130. doi:10.1115/1.2829983.

[80] Changenet C, Velex P. A model for the prediction of churning losses in geared transmissions—preliminary results. J Mech Des 2006;129. doi:10.1115/1.2403727.

[81] Yang L, Li H, Ma B. Prediction model of no-load power loss for a DSG transmission. Automob Technol 2013;5. doi:10.3969/j.issn.1000-3703.2013.05.010.

[82] Harris TA, Michael N K. Roller bearings analysis. 5th ed. CRC Press; 2006.

[83] Heingartner P, Mba D. Determining power losses in the helical gear mesh. ASME 2003 Int. Des. Eng. Tech. Conf. Comput. Inf. Eng. Conf., 2003, p. 965–940. doi:10.1115/DETC2003/PTG-48118.

[84] Changenet C, Oviedo-Marlot X, Velex P. Power Loss Predictions in Geared

Transmissions Using Thermal Networks-Applications to a Six-Speed Manual Gearbox. J Mech Des 2005;128:618–25.

[85] Herrmann Schlichting, Gersten K. Boundary-Layer Theory. 8th ed. Springer-Verlag Berlin Heidelberg; 2000.

[86] The performance of a turbulent-lubricated sliding bearing subject to centrifugal effect. Trans Jpn Soc Mech Eng Ser C 2003;49:1753–61.

[87] Kato Y, Murasugi T, Hirano H, Shibayama T. Fuel economy improvement through tribological analysis of the wet clutches and brakes of an automatic transmission. JSAE Conv Proc 1993;934:57–60.

[88] Kitabayashi H, Li CY, Hiraki H. Analysis of the Various Factors Affecting Drag Torque in Multiple-Plate Wet Clutches 2003. doi:10.4271/2003-01-1973.

[89] Li H, Jing Q, Ma B. Proceedings of the FISITA 2012 World Automotive Congress: Volume 5: Advanced Transmission System and Driveline, Berlin, Heidelberg: Springer Berlin Heidelberg; 2013, p. 21–30. doi:10.1007/978-3-642-33744-4_3.

[90] Shihua Y, Zengxiong P, Chongbo J. Experimental Research and Mathematical Model of Drag Torque in Single-plate Wet Clutch. CHINESE J Mech Eng 2010;23:1–8. doi:10.3901/CJME.2010.

[91] Simmons RA, Shaver GM, Tyner WE, Garimella S V. A benefit-cost assessment of new vehicle technologies and fuel economy in the U.S. market. Appl Energy

n.d. doi:http://dx.doi.org/10.1016/j.apenergy.2015.01.068.

[92] Veenhuizen P a, Bonsen B, Klaassen TWGL, Albers PHWM. Pushbelt CVT efficiency improvement potential of servo-electromechanical actuation and slip control 2004:1–7.

[93] van der Sluis F, van Dongen T, van Spijk G-J, van der velde A, van Heeswijk A. Efficiency Optimization of the Pushbelt CVT 2007. doi:10.4271/2007-01-1457.

[94] Saito T, Miyamoto K. Prediction of CVT Transmission Efficiency by Metal V-Belt and Pulley Behavior with Feedback Control 2010. doi:10.4271/2010-01-0855.

[95] XTRONIC CVT | NISSAN | TECHNOLOGICAL DEVELOPMENT ACTIVITIES n.d. http://www.nissan-global.com/EN/TECHNOLOGY/OVERVIEW/cvt.html (accessed May 19, 2016).

[96] Naotoshi O. Development of New Generation CVT with Auxiliary Gear Box 2016. doi:10.4271/2016-01-1109.

[97] Asl HA, Azad NL, McPhee J. Math-based torque converter modelling to evaluate damping characteristics and reverse flow mode operation. Int J Veh Syst Model Test 2014;9:36. doi:10.1504/IJVSMT.2014.059155.

[98] Kano S, Terasaka Y, Yano K. Prediction of Torque Converter Characteristics. vol. 50. 2004.

[99] D. L. Robinette, J. M. Schweitzer, D. G. Maddock, C. L. Anderson, J. R. Blough

and MAJ. Development of a Dimensionless Model for Predicting the Onset of Cavitation in Torque Converters. New Adv. Veh. Technol. Automot. Eng., 2012, p. 333–58. doi:10.5772/45793.

[100] Saito T. Transmission Efficiency Prediction of a Metal Pushing V-belt CVT with Implementation of Control Logic. SIMULIA Cust. Conf., 2010, p. 1–12.

[101] Zhu B, Zhang N, Walker P, Zhou X, Zhan W, Wei Y, et al. Gear shift schedule design for multi-speed pure electric vehicles. Proc Inst Mech Eng Part D J Automob Eng 2014;229:70–82. doi:10.1177/0954407014521395.

[102] Liu Y, Qin D, Jiang H, Liu C, Zhang Y, Lei Z. Shift schedule optimization for dual clutch transmissions. Veh Power Propuls Conf 2009 VPPC '09 IEEE 2009:1071–8. doi:10.1109/VPPC.2009.5289728.

[103] Q8Oils. Q8 Auto DCT Product data sheet. 2014.

[104] VolksWagon. DSG transmission oil and filter change : Volkswagen UK n.d. http://www.volkswagen.co.uk/owners/servicing/what-we-check-and-why/dsg-transmission-oil-and-filter-change#details (accessed July 14, 2015).

[105] Naunheimer H, Bertsche B, Ryborz J, Novak W. Overview of the Traffic – Vehicle – Transmission System. Automot. Transm. SE - 2, Springer Berlin Heidelberg; 2011, p. 28–72. doi:10.1007/978-3-642-16214-5_2.

[106] Francis van der Sluis, Noll E van der, Leeuw H de. Key Technologies of the Pushbelt CVT. Int J Automot Eng 2013;4:1–8.

[107] Berry IM. The effects of driving style and vehicle performance on the real world fuel consumption of US light duty vehicles. Massachusetts Institute of Technology, 2010.

[108] Lu S. Vehicle survivability and travel mileage Schedules. Natl Tech Inf Serv 2006:40.

[109] Saxena S, MacDonald J, Moura S. Charging ahead on the transition to electric vehicles with standard 120 V wall outlets. Appl Energy 2014;157:720–8. doi:10.1016/j.apenergy.2015.05.005.

[110] Bi Z, Song L, De Kleine R, Mi CC, Keoleian GA. Plug-in vs. wireless charging: life cycle energy and greenhouse gas emissions for an electric bus system. Appl Energy 2015;146:11–9. doi:10.1016/j.apenergy.2015.02.031.

[111] Laboratory ORN. Plug-in hybrid electric vehicle value proposition study. US Dep ENERGY 2010:218.

[112] Kinghorn R, Kua D. Forecast uptake and economic evaluation of electric vehicles in victoria. Melbourne: 2011.

[113] Cluzel C, Douglas C. Cost and performance of EV batteries: Final report for The Committee on Climate Change. 2012.

[114] Newbery D, Strbac G. What is the target battery cost at which Battery Electric Vehicles are socially cost competitive ? 2014.

[115] Commission AEM. ELECTRICITY PRICE TRENDS FINAL REPORT:

Possible future retail electricity price movements: 1 July 2012 to 30 June 2015. Sydney: 2013.

[116] Onat NC, Kucukvar M, Tatari O. Conventional, hybrid, plug-in hybrid or electric vehicles? State-based comparative carbon and energy footprint analysis in the United States. Appl Energy 2015;150:36–49. doi:10.1016/j.apenergy.2015.04.001.

[117] Subaru CVT - Why you should have it and when you shouldn't. n.d. http://www.manchestersubaru.com/cvt-transmission.htm (accessed July 14, 2015).

[118] Sharma R, Manzie C, Bessede M, Brear MJ, Crawford RH. Conventional, hybrid and electric vehicles for Australian driving conditions – Part 1: Technical and financial analysis. Transp Res Part C Emerg Technol 2012;25:238–49. doi:10.1016/j.trc.2012.06.003.

[119] Ruan J, Walker P, Zhang N. A comparative study energy consumption and costs of battery electric vehicle transmissions. Appl Energy 2016;165:119–34. doi:10.1016/j.apenergy.2015.12.081.

[120] Genta G, Morello L, editors. The Automotive Chassis: Vol. 2: System Design, Dordrecht: Springer Netherlands; 2009, p. 231–45. doi:10.1007/978-1-4020-8675-5_8.

[121] REGULATION (EC) No 661/2009 OF THE EUROPEAN PARLIAMENT AND OF THE COUNCIL of 13 July 2009. Off J Eur Union 2009:1–24.

[122] Regulation No. 13-H Uniform provisions concerning the approval of passenger cars with regard to braking. UNITED 2014:97.

[123] Regulation No. 13 Uniform provisions concerning the approval of vehicles of categories M, N and O with regard to brkaing 2002:1–194.

[124] National Highway Traffic Safety Administration Laboratory Test Procedure for 2005.

[125] Emission Test Cycles: ECE 15 + EUDC / NEDC n.d. https://www.dieselnet.com/standards/cycles/ece_eudc.php (accessed March 31, 2016).

[126] EPA U. EPA Urban Dynamometer Driving Schedule (UDDS) | Emission Standards Reference Guide | US EPA n.d. https://www3.epa.gov/otaq/standards/light-duty/udds.htm (accessed March 31, 2016).

[127] EmissionTest Cycles: EPA Highway Fuel Economy Test Cycle n.d. https://www.dieselnet.com/standards/cycles/hwfet.php (accessed March 31, 2016).

[128] EPA U. LA92 "Unified" Dynamometer Driving Schedule | Emission Standards Reference Guide | US EPA n.d. https://www3.epa.gov/otaq/standards/light-duty/la92.htm (accessed March 31, 2016).

[129] Emission Test Cycles: Japanese 10-15 Mode n.d.

https://www.dieselnet.com/standards/cycles/jp_10-15mode.php (accessed March 31, 2016).

[130] Hsu Y-HJ. Estimation and control of lateral tire forces using steering torque. STANFORD UNIVERSITY, 2009.

[131] Chu L, Yao L, Chen J, Chao L, Guo J, Zhang Y, et al. Integrative braking control system for electric vehicles. 2011 IEEE Veh Power Propuls Conf VPPC 2011 2011. doi:10.1109/VPPC.2011.6042995.

[132] Huinink H, Volk H, Becke M. Bremsenhandbuch: Grundlagen, Komponenten, Systeme, Fahrdynamik. In: Breuer B, Bill HK, editors., Wiesbaden: Vieweg+Teubner Verlag; 2012, p. 65–84. doi:10.1007/978-3-8348-2225-3_5.

[133] Energy V. 12.8 Volt Lithium-Iron-Phosphate Batteries n.d. https://www.victronenergy.com/upload/documents/Datasheet-12,8-Volt-lithium-iron-phosphate-batteries-EN.pdf.

[134] Björnsson L-H, Karlsson S. The potential for brake energy regeneration under Swedish conditions. Appl Energy 2016;168:75–84. doi:10.1016/j.apenergy.2016.01.051.

[135] U.S. Environmental Protection Agency. Greenhouse gas emissions from a typical passenger vehicle 2014:1–5.

[136] Transportation, U.S. Department BOTS. National Transportation Statistics 2015:1–470.

[137] Omar N, Monem MA, Firouz Y, Salminen J, Smekens J, Hegazy O, et al. Lithium iron phosphate based battery – Assessment of the aging parameters and development of cycle life model. Appl Energy 2014;113:1575–85. doi:http://dx.doi.org/10.1016/j.apenergy.2013.09.003.

[138] Swierczynski M, Stroe D-I, Stan A-I, Teodorescu R, Kaer SK. Lifetime Estimation of the Nanophosphate LiFePO4/C Battery Chemistry Used in Fully Electric Vehicles. IEEE Trans Ind Appl 2015;51:3453–61. doi:10.1109/TIA.2015.2405500.

[139] Omar N, Monem MA, Firouz Y, Salminen J, Smekens J, Hegazy O, et al. Lithium iron phosphate based battery – Assessment of the aging parameters and development of cycle life model. Appl Energy 2014;113:1575–85. doi:10.1016/j.apenergy.2013.09.003.

[140] Deshpande R, Verbrugge M, Cheng Y-T, Wang J, Liu P. Battery Cycle Life Prediction with Coupled Chemical Degradation and Fatigue Mechanics. J Electrochem Soc 2012;159:A1730–8. doi:10.1149/2.049210jes.

[141] Hu C, Jain G, Tamirisa P, Gorka T. Method for estimating capacity and predicting remaining useful life of lithium-ion battery. Appl Energy 2014;126:182–9. doi:10.1016/j.apenergy.2014.03.086.

[142] Saft. Lithium-ion battery life. 2014.

[143] Grochowicz J, Grabiec T. Potential for commonization of brake testing for globally marketed vehicles 2009. doi:10.4271/2009-01-3031.

[144] Brake pads replacement cost guide n.d. http://www.brakepadscostguide.com/ (accessed February 24, 2016).

[145] Brake pads cost guide: average brake pad replacement cost n.d. https://autoservicecosts.com/brake-pad-replacement-cost/ (accessed February 24, 2016).